APMED'12
ROGRAM

JAPMED' 12

BATUMI SHOTA RUSTAVELI STATE UNIVERSITY

12th Japanese-Mediterranean Workshop Applied Electromagnetic Engineering for Magnetic, Superconducting, Multifunctional and Nanomaterials

BOOK OF ABSTRACTS

17-20 JULY, 2023

Opening Welcoming Address

პატივცემულო Rector of the Batumi Shota Rustaveli State University Professor Merab Khalvashi, Minister of Education, Culture and Sport, Ms. Maia Khajishvili, Distinguished Colleagues and Dear Undergraduate and Graduate Students.

As *Honorary Chairman of the Executive Committee* it is my great pleasure to warmly welcome all of you to the *12th Japanese-Mediterranean Workshop on Applied Electromagnetic Engineering for Magnetic, Superconducting, Multifunctional and Nano Materials* a landmark in development of materials, advanced manufacturing and mechanical and electromagnetic engineering.

This Conference, held every two years, is jointly organized this year by my international *Project Center for Nanotechnology and Advanced Engineering*, the *Japan Society of Applied Electromagnetics and Mechanics*, the two high level American Universities *Texas A&M* and *University of Nevada Reno*, the *Faculty of Electrical Engineering and Electronics of the National Technical University of Athens*, the *Izmir Institute of Technology*, Turkey, the *Beijing Institute of Technology*, P.R. of China and the two leading Georgian Universities, the *Batumi Shota Rustaveli State University* and the *Georgian Technical University*.

The *JAPMED* has been originated in the late 90's from the previous, very successful, *1st and 2nd Japanese - Greek Joint Workshops*, held in Athens, Greece in May 1999 and Oita, Japan in May 2001, respectively. Subsequently, it was extended to further wide International participation and cooperation, with the 3rd Event hosted in Athens, Greece in May 2003, the 4th in Cairo, Egypt in September 2005, the 5th in Larnaca, Cyprus in September 2007, the 6th in Bucharest, Romania in July 2009, the 7th in Budapest, Hungary in July 2011, the 8th in Athens, Greece in June 2013, the 9th in Sofia, Bulgaria in July 2015, the 10th in Izmir, Turkey in July 2017, the 11th in Batumi, Georgia in July 2019, whilst the current 12th Conference, initially planned for July 2021, has been postponed until today due to the Pandemic COVID-19.

This Conference provides a forum for specialists from *Universities*, *Research Centers* and *Industry* of various Countries worldwide to establish cooperation, to share knowledge and experience and the cross-fertilization of new ideas and developments in the *design, analysis, new materials utilization and optimization techniques* in the broad areas of *electromagnetics and advanced manufacturing of advanced materials and their industrial sustainable applications*, in the modern technological sectors: *precision / ultraprecision engineering, nanotechnology, powder production* and *processing associated with high strain-rate phenomena, electricity* and *electronics, biomedical engineering, transportation, safety and defense, energy and environment*. Additional topics related to practical applications, operation, maintenance and sustainability are also highly encouraged.

From the very beginning, the *high- and low-temperature superconductivity* constituted the first preferential subject of the Conference, focusing on the recent progress in physics, mechanics, materials and applications of high- and low- temperature superconductors, with a projection to the emerging and future areas in science and technology.

Magnetic materials, such as *magneto-resistance and ferroelectric materials*, as well as *conventional ferromagnetic materials and electromagnetics*, constitute the second preferential subject, with results that appear to exhibit a breakthrough either conceptually or in the applications they generate.

The scope of the Conference has been further expanded over the years towards *advanced manufacturing* to include the modern advanced technological fields: *nanotechnology, precision / ultraprecision manufacturing, biomedical engineering and transport*, whilst, ten years ago, two additional topics have been included, namely: the *multifunctional materials*, in relation also to *computational mechanics*, i.e. the interests of the then International Institute for Multifunctional Materials for Energy Conversion (IIMEC) of the Texas A&M

University, and the *shock loading of materials and structures*, as a part of the that time established *Shockwaves Cluster*, involving cooperation between Greece, Russia, USA, Germany, Japan, China, Hungary, Ukraine, Turkey, Georgia and India. The purpose of this international cooperation is the strong belief that we have to enhance our efforts and cooperation towards these advanced technologies, which may greatly affect our lives in the future.

Since *sustainability* prevails in science, technology, industry and many other parts of human life, as a follow-up of my *Sustainability Award* for the *SIPS 2018 Mamalis International Symposium on Advanced Manufacturing of Advanced Materials and Structures with Sustainable Industrial Applications* in November 2018 in Rio de Janeiro, I have incorporated it in the JAPMED topics, with the aim to further enhancing our international collaboration.

Although the world financial crisis, the war in Ukraine and the Pandemic COVID-19 have highly affected the much higher expected participation in this Conference, my Georgian Colleagues and I will do our best to demonstrate the famous Georgian and Balkan hospitality, not sparing any effort to make your stay in this beautiful Country memorable. I am sure that your participation in this Conference is going to be an exciting experience with many benefits to all of us.

Finally, the last but not the least, as Founder of the JAPMED Conferences I have taken the initiative to dedicate this JAPMED'12 to my beloved, too clever and beautiful three years old Granddaughter LYDIA, being sure that she will suceed in her future scientific life. Unforturnately, due to travel difficulties, it was not possible to be present here, but she sends her Best Wishes and Regards to all of you.

Didi Madloba	Arigato	Xièxiè	Spaciba
Teşekkür Ederim	Danke Schön	Thank you	Ευχαριστώ

Academician Prof. Dr-ing, Dr.h.c. Prof.h.c. A.G. Mamalis

Honorary Chairman of the JAPMED'12

PROGRAM

PROGRAM OF THE TWELVE JAPANESE-MEDITERRANEAN WORKSHOP ON APPLIED ELECTROMAGNETIC ENGINEERING FOR MAGNETIC, SUPERCONDUCTING, MULTIFUNCTIONAL AND NANO MATERIALS (JAPMED'12)

MONDAY, JULY 17th

14:00 – 16:00 Registration

16:00 – 17:00 Opening Session

Chair: N. Gomidze

16:00 – 16:30 **Welcome Address:** Honorary Chairman of the JAPMED'12, Prof. A.G. Mamalis
Welcome Address: President of the JSAEM, Prof. Y. Ido
Welcome Address: Rector of the Batumi Shota Rustaveli State University, Prof. M. Khalvashi
Welcome Address: Government Chairman of the Ajara Autonomous Republic, Mr.T. Rizhvadze
Welcome Address: Minister of Education, Culture and Sport, Ms. M. Khajishvili
Welcome Address: President of European Academy of Arts and Sciences, Prof. P. Kervalishvili

16:30 – 17:00 **Plenary Presentation (108): Advanced Manufacturing: Principles and Industrial Sustainable Trends**
Academician Prof. Dr.-Ing. Dr.h.c. Prof.h.c. Athanasios G. Mamalis
Project Center for Nanotechnology and Advanced Engineering (PC-NAE), Athens, Greece
agmamalis@yahoo.com

17:00 – 17:30 Coffee Break/Lunch Break

17:30 – 19:00 Oral Session A: High Strain-Rate Phenomena / Impact to Shock Loading

Chair: J. Ramsden

17:30 – 18:00 **Keynote Presentation A1 (23): Explosion Syntheses of High Entropy Alloys in Fe-W-Al-Ti-Ni–B-C System**
N. Chikhradze[1,2,a], D. Tsverava[1,2,b], M. Chikhradze[2,3,c], G. Janikashvili[2]
[1] *G. Tsulukidze Mining Institute, 7, E. Mindeli Str., 0186, Tbilisi, Georgia,* [a]chikhradze@mining.org.ge
[2] *Georgian Technical University, 77, Kostava Str., 0160, Tbilisi, Georgia,* [b]datotsverava@gmail.com
[3] *F. Tavadze Institute of Metallurgy and Materials Science, 0186, Tbilisi, Georgia,* [c]m.chikhradze@gtu.ge

18:00 – 18:20 **A2 (34): Preparation of Corrugated Tubes for High Efficiency Heat Exchangers by Explosive Forming**
I. Zador[1,a] , A.Mamalis[2,b], A.Szalay[1,c],
[1] *KOGAT Ltd, Budapest, Hungary,* [a]istvan.zador@kogat.hu
[2] *Project Center for Nanotechnology and Advanced Engineering, NCSR "Demokritos", Greece,* [b]agmamalis@yahoo.com
[3*] Puraset *Water and Metall Solutions Ltd, Budapest, Hungary,* [c]andras.szalay@puraset.hu

18:20 – 18:40 **A3 (33): High Quality Splices for Superconductors**
A.Szalay[1,a], A.Mamalis[2,b], I.Zador[3,c]
[1]*Puraset Water and Metall Solutions Ltd, Budapest, Hungary,* [a]andras.szalay@puraset.hu
[2] *Project Center for Nanotechnology and Advanced Engineering, NCSR "Demokritos", Greece,* [b]agmamalis@yahoo.com
[3] *KOGAT Ltd, Budapest, Hungary,* [c]istvan.zador@kogat.hu

18:40 – 19:00 **A4 (119) Algorithmic Foundations of Optimization Using Finite Element Modeling of High-Speed Grinding Technology in Application to 3D Micro-Level Models**
A.Mamalis[1,a],V.Fedorovich[2], D.Romashov[2,b], Y.Ostroverkh[2]
[1] *Project Center for Nanotechnology and Advanced Engineering, NCSR "Demokritos", Athens, Greece,* [a]*agmamalis@yahoo.com*
[2] *Department of Integrated Engineering Techniques named after M.F. Semko, National Technical University "Kharkov Polytechnic Institute", Kharkov, Ukraine,* [b]*romashov86@ukr.net*

19:00 – 19:20 **A5 (113): Computer Simulations of Static Stress-Strain States for Long-Length Pressurized Pipes with External Protective Thin Nanoengineered Coating under Nonuniform Temperature Fields**
I.Nevliudov[1.a], A.Mamalis[2,b], Yu.Romashov[1,3,c]
[1]*Kharkiv National University of Radio Electronics, Ukraine, Kharkiv,* [a]*igor.nevliudov@nure.ua*
[2]*Project Center for Nanotechnology and Advanced Engineering, NCSR "Demokritos", Greece, Athens* [b]*agmamalis@yahoo.com*
[3]*V.N. Karazin Kharkiv National University, Ukraine, Kharkiv,* [c]*yurii.romashov@nure.ua*

TUESDAY, JULY 18th

09:00 – 11:30 Registration

09:00 – 10.30 Oral Session B: Electromagnetic Engineering
Chair: R. Turmanidze

09:00 – 09:30 **Keynote Presentation B1 (26): Reduction of Iron Loss on Laminated Stator Cores by Secondary Current Heating Method**
Yuji Tsuchida
Division of Electrical and Electronic Engineering, Oita University, Japan, tsuchida@oita-u.ac.jp

09:30 – 09:50 **B2 (103): Magnetic shielding materials for electric vehicles**
T. Damatopoulou[1,a], S. Angelopoulos[1,b], A. Ktena[2], P. Svec[3,c], A. Mamalis[4,d], E. Hristoforou[1,e]
[1] *Laboratory of Electronic Sensors, National TU of Athens, Zografou Campus, Athens 15780, Greece,* [a]*damatat5@central.ntua.gr,* [b]*spyrosag@central.ntua.gr* , [c]*hristoforou@ece.ntua.gr*
[2]*National Kapodistrian University of Athens, Greece*
[3]*Slovak Academy of Sciences, Bratislava, Slovakia,* [c]*peter.svec@savba.sk*
[4]*Project Center for Nanotechnology and Advanced Engineering (PC-NAE), NCSR Demokritos, Athens, 15310, Greece,* [d]*agmamalis@yahoo.com*

09:50 – 10:10 **B3 (102): Optimizing QE of CCD by Modifying Black Comet Detector**
J. Shainidze[a], N.Gomidze[b]
Batumi Shota Rustaveli State University, Batumi, Georgia, [a]*jaba.shainidze@bsu.edu.ge,* [b]*gomidze@bsu.edu.ge*

10:10 – 10:30 **B4 (41): Influence of Surface Roughness on the Amplitude of Giant Magnetoresistance Effect in Multilayered Thin Films**
A Melikadze[a], L. Kalandadze[b], N. Gomidze[c]
Batumi Shota Rustaveli State University, 6010 Batumi, Georgia
[a]*Aleksander.melikadze@gmail.com,* [b]*lali.kalandadze@bsu.edu.ge,* [c]*gomidze@bsu.edu.ge*

10:30– 11:00 Coffee Break

11:00 – 12:50 Oral Session C: Applications in Energy and Transportation

Chair: Y. Ido,

11:00 – 11:30 **Keynote Presentation C1 (35): Magnetic Field between Polar Hemispheres: Remarks on the Dislocation of Zones of a Constant Gradient and Force Factor**

A. Sandulyak, M. Polismakova, D. Sandulyak, A. Dwivedi*, C. Doumanidis, A. Sandulyak, V. Ershova.
[1]*MIREA — Russian Technological University, Moscow, Russia*
[2]*Guangdong Technion-Israel Institute of Technology, Shantou, China,*
[*]*anand.dwivedi@gtiit.edu.cn*

11:30 – 11:50 **C2 (45): Features of Magnetization of Ferromagnetic Composites: Role of Grain Chains on an Example of Granulated Media**

D. Sandulyak[1], A Sandulyak[1], M. Polismakova[1], A. Sandulyak[1], I. Solovev[1], A.Dwivedi[2*], C. Doumanidis[2]
[1]*MIREA — Russian Technological University, Moscow, Russia*
[2]*Guangdong Technion-Israel Institute of Technology, Shantou, China,*
[*]*anand.dwivedi@gtiit.edu.cn*

11:50 – 12:10 **C3 (116): Excitons and Biexcitons in Cylindrical Nanowires of Group II-IV Materials**

Z. Machavariani[1,3,a], R. Kezerashvili[2,b], T. Tchelidze[1,c]
[1] *Department of Exact and Natural Sciences, Tbilisi State University, 0179, Tbilisi, Georgia,* [a]*zaal.machavariani@tsu.ge*
[2] *Physics Department, New York City College of technology, The City University of New York, Brooklyn, New York 11201, USA,* [b]*rkezerashvili@citytech.cuny.edu*
[3]*Doctoral School, Kutaisi International University, Youth Avenue, 5th Lane, 4600 Kutaisi, Georgia,* [c]*tchelidze@tsu.ge*

12:10 – 12:30 **C4 (26): Can the Formation of Compensating Donors Be Suppressed in Modulated p-Dopped Gallium Oxide Quantum Wells?**

T. Tchelidze[1,a], Z. Machavariani[1,2,b] , E. Chikoidze [3]
[1] *Department of Exact and Natural Sciences, Tbilisi State University, 0179, Tbilisi, Georgia,* [a] *tchelidze@tsu.ge*
[2]*Doctoral School, Kutaisi International University, Youth Avenue, 5th Lane, 4600 Kutaisi, Georgia,* [b]zaal.machavariani@tsu.ge
[3] University Paris Saclay, Grp Etud Matiere Condensee GEMaC, UVSQ CNRS, 45 Ave des Etats Unis, F-78035 Versailles, France

12:30 – 12:50 **C5 (100): Materials and Devices for Spin-Qubit Quantum Computers**

G. Kervalishvili[1,a], R. Vardapetian[2,b]
[1]*Georgian Technical University, Tbilisi, Georgia,* [a]*gkerval@gmail.com*
[2]*European Centre for Knowledge and Technology Transfer Brussels, Belgium,*
[b]*rv.eurotex@gmail.com*

12:50 – 13:30 Lunch Break

13:30 – 15:20 Oral Session D: Sustainability: Principles and Applications

Chair: Y. Tsuchida,

13:30 – 14:00 **Keynote Presentation D1 (105): An Information Theoretical Analysis of the Spirit of the Age**

J. Ramsden[1*] A. Mamali[2], N.Athanassoulis[3]
[1]*Faculty of Medicine and Health Sciences, The University of Buckingham, England,*
[*]*jeremy.ramsden@buckingham.ac.uk*
[2] *Cass Business School Alumni, Athens, Greece*

[3] *Laboratory of Energy and Industrial Economics (LIEE), National Technical University of Athens, Greece*

14:00 – 14:20 **D2 (107): Health Hazards and Pollution Risk from Large Battery Energy Storage Systems**
J.Ramsden
Faculty of Medicine and Health Sciences, The University of Buckingham, England, jeremy.ramsden@buckingham.ac.uk

14:20 – 14:40 **D3 (109): Analysis of Possibilities the Current Situation for Using and Accumulating Green Energies in Georgia**
R.Turmanidze[1], N. Gomidze[2*], G.Popkhadze[1], L.Gomidze[3]
[1]*Georgian Technical University, Tbilisi, Georgia, inform@gtu.ge*
[*2]*Batumi Shota Rustaveli State University, Georgia, gomidze@bsu.edu.ge*
[3]*Department of Exact and Natural Sciences, Tbilisi State University, 0179, Tbilisi, Georgia*

14:40 – 15:00 **D4 (106): Discovering the Cause of Aerotoxic Syndrome: A Causal Calculus Approach**
J. J. Ramsden
Faculty of Medicine and Health Sciences, The University of Buckingham, England
jeremy.ramsden@buckingham.ac.uk

15:00 – 15:20 **D5 (111): An Overview of Life Cycle Assessment Criteria for Transportation Decision-Making**
N.T. Athanassoulis[*], A.Tsakanikas
Laboratory of Industrial & Energy Economics National Technical University of Athens,
[1]nathanas@*ce* [2]atsaka@central.ntua.gr

15:20 – 15:50 Coffee Break

15:50 – 18:30 Oral Session E: Composite, Ceramic and Magnetic Nanomaterials
Chair: A. Dwivedi

15:50 – 16:20 **Keynote Presentation E1 (17): Effect of Nanoadditives on the Properties of Partially Stabilized Zirconia**
A.Mamalis[1,a], E.Hevorkian[2,b], V.Nerubatskyi[3,c], M. Rucki[4,d] Z. Krzysiak[2], O.Morozova[3,e]
[1]*Project Center for Nanotechnology and Advanced Engineering, Athens, Greece,*
[a]*agmamalis@yahoo.com*
[2]*University of Life Sciences in Lublin, 13 Akademicka, Lublin 20-950, Poland,* [b]*cermet-u@mail.com*
[3]*Ukrainian State University of Railway Transport, Kharkiv, Ukraine,* [c]NVP9@i.ua, [e]*oksanabakan2012@gmail.com*
[4]*Kazimierz Pulaski University of Technology and Humanities in Radom, Poland,*
[d]*m.rucki@uthrad.pl*

16:20 – 16:40 **E2 (114): Effect of CrB2 Reinforcement on the Mechanical Properties of Ceramic Matrix Composites (CMCs) and Metal Matrix Composites (MMCs)**
M. Rucki[1,a], E.Hevorkyan[2,b], V.Mechnik[3,c], B. Ratov[4,d], S. Muratova[5,e]
[1] *Kazimierz Pulaski University of Technology and Humanities in Radom, Radom, Poland,*
[a]*m.rucki@uthrad.pl*
[2] *University of Life Sciences in Lublin, Lublin, Poland,* [b]*edsgev@gmail.com*
[3] *Bakul Institute for Superhard Materials, National Academy of Sciences of Ukraine, Kyiv, Ukraine,* [c]*vlad.me4nik@ukr.net*
[4] *Satpayev University, Almaty, Kazakhstan,* [d]*b.ratov@satbayev.university*
[5] *Caspian University, Almaty, Kazakhstan,* [e]*samal.muratova@cu.edu.kz*

16:40 – 17:00 **E3 (115): Peculiarities of Obtaining Nanostructured Materials Compacted by the Method of Hot Pressing Due to the Passage of Direct Electric Current**
A.Mamalis[1,a], E.Hevorkian[2,b], V. Nerubatskyi[3,c], Z. Krzysiak[2], O. Morozova[3,d], L. Chalko[4]
[1]*Project Center for Nanotechnology and Advanced Engineering, Athens, Greece,* [a]*agmamalis@yahoo.com*
[2]*University of Life Sciences in Lublin, 13 Akademicka, Lublin 20-950, Poland,* [b]*cermet-u@mail.com*,
[3]*Ukrainian State University of Railway Transport, Kharkiv, Ukraine,* [c]*nerubatskyi@kart.edu.ua*, [d]*oksanabakan2012@gmail.com*
[4]*Kazimierz Pulaski University of Technology and Humanities in Radom, Poland*

17:00 – 17:20 **E4 (12): Features of Magnetization of Ferromagnetic Composites: Role of Grain Chains on an Example of Granulated Media**
S. Petrosyan[a], A. Khachatryan[b]
Institute of Radiophysics and Electronics, NAS of Armenia, Ashtarak, Armenia, [a]stepan.petrosyan@rau.am, [b]ashot.khacahtryan@mail.ru

19:00 – 22:30 Conference Dinner

WEDNESDAY, JULY 19th

09:00 – 11:30 Registration

09:00 – 11.00 Oral Session F: Advanced Industrial Technologies
Chair: N. Chikhradze

09:00 – 09:30 **Keynote Presentation F1 (14): Thermal Conduction and Magnetic Properties of Magnetorheological Elastomers Dispersing Sendust Particles**
Y. Ido[1,a], Y. Hiroshima[1,b],Y. Iwamoto[1,c], Y. Hirota[2,d], S. Fujioka[2,e]
[*1] *Department of Electrical and Mechanical Engineering, "Nagoya Institute of Technology", Japan,* [a]*ido.yasushi@nitech.ac.jp,* [b]*y.hirosima.265@stn.nitech.ac.jp,* [c]*iwamoto.yuhiro@nitech.ac.jp*
[2] *Ferrotec Materials Technologies, Japan,* [d]*hirota-yst@ft-mt.co.jp,* [e]*fujioka-stm@ft-mt.co.jp*

09:30 – 09:50 **F2 (39): Rheological Properties of Thin-Film Permanent Magnet Elastomers in Stretch Deformation**
Y. Iwamoto[1*], T. Minakawa[1], Y. Ido[1], M. Kamezaki[2]
[1] *Department of Electrical and Mechanical Engineering, Nagoya Institute of Technology, Japan,* [*]*iwamoto.yuhiro@nitech.ac.jp*
[2] *Department of Electrical Engineering and Information Systems, Graduate School of Engineering, The University of Tokyo, Japan*

09:50 – 10:10 **F3 (7): Alternative design of a high torque density two-phase brushless direct current motor**
S. Abareshi[a], J. Faiz[b], M. Ghods[c]
School of Electrical and Computer Engineering, College of Engineering, University of Tehran, Tehran, Iran, [a]*saeed.abareshi@ut.ac.ir,* [b]*jfaiz@ut.ac.ir,* [c]*ghods-mehrage@ut.ac.ir*

10:10 – 10:30 **F4 (44): Fundamental Study of Haptic Sensor Utilizing Magnetic Compound Fluid Rubber Sensor for Investigation of Nuclear Facilities**
R. Ikeda[1], K. Shimada[2], H. Kikura[3]
[1] *Nuclear Engineering Course, Tokyo Institute of Technology, Japan,* *ikeda.r.ah@m.titech.ac.jp*
[2] *Faculty of Symbiotic Systems Sciences, Fukushima University, Japan,* *shimadakun@sss.fukushima-u.ac.jp*

[3] *Laboratory for Zero-Carbon Energy, Tokyo Institute of Technology, Japan,* kikura.h.aa@m.titech.ac.jp

10:30 – 10:50 **F5 (38): Experimental Study on Sealing Performance and Flow Characteristics of Magnetic Fluid in Extremely Tiny Clearance under Magnetic Field**
Y. Kato[1], M. Motozawa[2*], W. Rakpakdee[2], M. Fukuta[2]
[1] *Graduate School of Integrated Science and Technology, Shizuoka University, Shizuoka, Japan*
[2] *Faculty of Engineering, Shizuoka University, Shizuoka, Japan,*
[*] *motozawa.masaaki@shizuoka.ac.jp*

10:50 – 11:30 Coffee Break

11:30 – 13:00 Oral Session G: Material Synthesis, Measurements and Characterization
Chair: M.Motozawa

11:30 – 12:00 **Keynote Presentation G1 (108): The Concept of Obtaining Spintronic Nanostructures for Quantum Devices**
Paata J. Kervalishvili
Georgian Technical University, Tbilisi, Georgia, paata.kervalishvili@gtu.ge

12:00 – 12:20 **G2 (110): Barium Titanate Based Acoustic Sensing Elements**
N. Motsi[1,a], N. Siafakas[1], A.Mamalis[2,b], E.Hristoforou[1,c]
[1]*School of Electrical and Computer Engineering, National Technical University of Athens, Iroon Polytechniou 9, 15780 Zografou, Greece,* [a]*nefelimotsi@mail.ntua.gr*, [c]*hristoforou@ece.ntua.gr*
[2]*Project Center for Nanotechnology and Advanced Engineering (PC-NAE), NCSR Demokritos, Athens, 15310, Greece,*[b]*agmamalis@yahoo.com*

12:20 – 12:40 **G3 (9): Study of Silicon-Graphene Properties**
A. Bakhtiari [1*], T. Berberashvili [1], P. Kervalishvili [1], A. Bilbilashvili [2], Z. Kushitashvili [2]
[*1] *Georgian Technical University, Kostava str. 77, Tbilisi, Georgia,* [*]*bakhtiari.habib@gmail.com*
[2] *Institute of Micro and Nanoelectronics, Ilia Chavchavadze Ave. 13, Tbilisi, Georgia*

12:40 – 13:00 **G4 (10): Experimental Device for 2D Materials Preparation by Laser-Plasma Method**
A. Bakhtiari[1*], W. Maier[2], P. Kervalishvili[1]
[1] *Georgian Technical University, Kostava str. 77, Tbilisi, Georgia,*
[*]*bakhtiari.habib@gmail.com*
[2] *AE Solar GmbH, Messerschmittring 54, Konigsbrunn, Germany*

13:00 – 14:00 Lunch Break

14:00 – 15:00 Poster Session (P)
Chair: Y. Ido, P. Kervalishvili, N.Gomidze

P1 (15): Integrating IoT into Agricultural Operations Towards the Industry 4.0 and Sustainability
E. Symeonaki, H. Leligou, D. Tseles[*], T. Ganetsos, C. Drosos
Dept. of Industrial Design and Production Engineering, University of West Attica, Greece,
[*]*dtsel@uniwa.gr*

P2 (19): Development and Characteristics of Metal-Polymer Laminates
G. Baliashvili, T. Iashvili, S. Kvinikadze D. Tsverava , G. Abashidze, A. Vanishvili[*]
LEPL Grigol Tsulukidze Mining Institute., 7, E. Mindeli Str., 0186, Tbilisi, Georgia,
[*]*alexandre.vanishvili@gmail.com*

P3 (22): ZrO2 Nanopowders as Fillers of Epoxy Polymers
T. Hryhorenkoa*, Y. Kochergin, X. Meng
*Harbin Institute of Technology, China, *grigorencot@outlook.com*

P4 (27): On the Convergence of the Solution of Schrodinger Equation for Finite Difference Method
D. Kobaidze[1*], T. Gagnidze[1], T. Tchelidze[1], T. Davitashvili[1], H. Meladze[2]
[1]*Ivane Javakhishvili Tbilisi State University, Tbilisi, Georgia*
[2]*Muskhelishvili Institute of Computational Mathematics,*
[*]*adaviti.kobaidze708@ens.tsu.edu.ge*

P5 (29): Particle in Multi-Step Quantum Well
N. Basharuli,a, T. Tchelidze
Ivane Javakhishvili Tbilisi State University, Tbilisi, Georgia
anikabasharuli907@ens.tsu.edu.ge

P6 (30): Solving 1D Stationary Schrodinger Equation Numerically
L. Burdiladze[1*], T.Gagnidze[1], T. Tchelidze[1], T. Davitashvili[1], H. Meladze[2]
[1]*Ivane Javakhishvili Tbilisi State University, Tbilisi, Georgia,*
[*]*luka.burdiladze108@ens.tsu.edu.ge*
[2]*Muskhelishvili Institute of Computational Mathematics*

P7 (36): Modeling and Optimization of Properties of Ga2O3-Based Quantum Structures in Order to Achieve Hole Conductivity
T. Gagnidze[1,2,3*] , D. Kobaidze[1], L.Burdiladze[1],N. Basharuli[1], E. Chikoidze[4], T. Davitashvili[1], H. Meladze[5], T. Tchelidze[1]
[1]*Ivane Javakhishvili Tbilisi State University, Tbilisi, Georgia,* [*] *tornike.gagnidze@tsu.ge*
[2] *AndronikaShvili Institute of Physics, Tbilisi, Georgia*
[3] *Chavchanidze Institute of Cybernetics, Tbilisi, Georgia*
[4] *Groupe d'Etude de la Matiere Condensee (GEMaC), Universite de Versailles Saint Quentin en Y.-CNRS, Universite Paris-Saclay, 45 Av. des Etats-Unis, 78035, Versailles Cedex, France*
[5] *Muskhelishvili Institute of Computational Mathematics, Tbilisi, Georgia*

P8 (37): Proposal of a 3-D Stereolithography System Incorporating Magnetic Levitation Technique
T. Ohji*, K. Nishi, J. Yui, K. Amei
Faculty of Engineering, University of Toyama, 3190 Gofuku, Toyama 930-8555, Japan,
ohji@eng.u-toyama.ac.jp

P9 (104): To the Properties of Laser-Induced Plasma
D.Jakobia[1,a], P.Kervalishvili[2,b], N.Gomidze[1,c]
[1*] *Batumi Shota Rustaveli State University, 6010 Batumi, Georgia,*
[a]*david.935335@gmail.com,* [c]*gomidze@bsu.edu.ge*
[2] *Georgian Technical University, Kostava str. 77, Tbilisi, Georgia,*
[b]*paata.kervalishvili@gtu.ge*

P10 (112): Creation 3D Fluorescence Spectra of Wine
M.Khajishvili*, N.Gomidze, I.Jabnidze, K.Makharadze, L.Kalandadze, O.Nakashidze
[*] *Batumi Shota Rustaveli State University, 6010 Batumi, Georgia,*
miranda.khajishvili@bsu.edu.ge

P11 (118): Structural Properties of III-Nitrides Received by UV Stimulated Technology
Z.Kushitashvili*, A.Bibilashvili, A.Kurtanidze

[*] *LEPL Institute of Micro and Nanoelectronics, Ivane Javakhishvili Tbilisi State University, Tbilisi, Georgia, zurab_kush@yahoo.com*

P12(16): Smart Energy Management in the Context of Industry 4.0

N. Kyrtsilas, E. Symeonaki, D. Tseles[*], M. Papoutsidakis, C. Drosos
Dept. of Industrial Design and Production Engineering, University of West Attica, Greece, dtsel@uniwa.gr

P13 (120): On the effective dielectric permittivity of nanocomposite structures

O.Nakashidze, L Kalandadze[*], N.Gomidze, I.Jabnidze
Department of Physics, Batumi Shota Rustaveli State University, Georgia, lali.kalandadze@bsu.edu.ge

15:00 – 19:00 Excursion: BSU – Mtsvane Konckhi – Tsikhisdziri - BSU / Conference Photos

THURSDAY, JULY 20th

09:00 – 10.50 Oral Session H: Superconductivity

Chair: P. Kervalishvili

09:00 – 09:30 **Keynote Presentation H1 (32): Bulk MgB2 and MT-YBCO for Superconducting Bearings Working in Liquid Hydrogen**

T. Prikhna[1,a], M. Eisterer, A. Mamalis[3], V. Moshchil[1], B. Büchner[4], D. Lindackers[4], X. Obradors[5], T. Puig[5], F. Werfel[6], U. Flögel – Delor[6], V. Sverdun[1], A. Vakaliuk[6], S. Ponomarov[7], P. Sass[8]
[1]*V. Bakul Institute for Superhard Materials of the National Academy of Sciences of Ukraine,* [a]prikhna@ukr.net
[2] *Institute of Atomic and Subatomic Physics, TU Wien, Stadionallee 2, 1020 Vienna, Austria*
[3] *Project Centre for Nanotechnology and Advanced Engineering, NCSR "Demokritos", Athens, Greece*
[4]*Leibniz-Institut für Festkörper- und Werkstoffforschung Dresden e. V., Helmholtzstraße 20, 01069 Dresden, Germany*
[5]*Institute of Materials Science of Barcelona (ICMAB), CSIC, Spain*
[6]*Adelwitz Technologiezentrum GmbH (ATZ), Naundorfer Str. 29 04860 Torgau, Germany*
[7]*Institute of Semiconductor Physics of the National Academy of Sciences of Ukraine, 41, Nauky Ave., Kyiv 03028, Ukraine*
[8] *ScIDre – Scientific Instruments Dresden GmbH, Gutzkowstrasser 30, Dresden 01069, Germany*

09:30 – 09:50 **H2 (24): Production of Homogeneous Composite Press-Powders Based on ZrB2 and SiC for UHTCs**

G. Bokuchava[1], E. Sanaia[1], Z. Mestvirishvili[1,a], N. Jalagonia[1], T. Prikhna[2], T. Kuchukhidze[1], N. Darakhvelidze[1]
[1] *Ilia Vekua Sukhumi Institute of Physics and Technology. 7 Mindeli Str., Tbilisi, Georgia,* [a]*zviad.mst@gmail.com*,
[2] *V.Bakul Institute for Superhard materials, 2, Avtozavodskaya Str., Kiev, Ukraina*

09:50 – 10:10 **H3 (101): Functional Superconductor-Ferromagnet Nanostructures for Superconducting Electronics**

A. Sidorenko[1a,] V. Boian[1], E. Antropov[1], Yu. Savva[2], A. Lomakin[2], A. Vakhrushev[3]
[1*]*Institute of Electronic Engineering and Nanotechnologies named after D. Ghitu, Moldova, MD-2028, Chisinau, Academiei 3/3,* [a]*sidorenko.anatoli@gmail.com*
[2]*Orel State University named after I.S. Turgenev, Russia, 302026, Orel, Komsomolskaya, 95*

[3]*Udmurt Federal Research Center, Ural Branch of the Russian Academy of Sciences, ul. T. Baramzina, 34*

10:10 – 10:30 **H4 (31): Diffusion-Driven Local Ordering in Pt/Co Bilayers**

R. Pedan[a], P. Makushko, O. Dubikovskyi, A. Bodnaruk , A. Burmak, D.Makarov, I. Vladymyrskyi

[1] *Igor Sikorsky Kyiv Polytechnic Institute, Prospect Peremogy 37, Kyiv 03056, Ukraine.* [a]*roman1pedan@gmail.com*

[2] *Helmholtz-Zentrum Dresden-Rossendorf e.V., Institute of Ion Beam Physics and Materials Research, Bautzner Landstrasse 400, 01328 Dresden, Germany.*

[3] *V. Lashkaryov Institute of Semiconductor Physics, National Academy of Sciences of Ukraine, Prospect Nauky 41, Kyiv 03680, Ukraine.*

[4] *Institute of Physics, National Academy of Sciences of Ukraine, Prospect Nauky 46, Kyiv 03028, Ukraine.*

10:30 – 11:00 Coffee Break

11:00 – 12:00 Closing Session

Chair: A.G. Mamalis

Closing Remarks

Paper Submission

Best Poster

PLENARY PRESENTATION

ADVANCED MANUFACTURING: PRINCIPLES AND INDUSTRIAL SUSTAINABLE TRENDS

Academician Prof. Dr.-Ing. Dr.h.c. Prof.h.c. Athanasios G. Mamalis

Project Center for Nanotechnology and Advanced Engineering (PC-NAE), Athens, Greece

agmamalis@yahoo.com

Abstract

Some trends and developments in the important engineering topic from industrial, research and academic point of view: *advanced manufacturing of advanced materials from macro- to nanoscale* subjected to static, low speed / high speed / hypervelocity impact and shock loading, with sustainable industrial applications to net-shape manufacturing, bioengineering, transport, energy and environment, defense and safety, an outcome of the very extensive, over 55 years, work on these scientific and industrial areas performed by the author and his research international team, are briefly outlined in the present Plenary Lecture of the *12th Japanese / Mediterranean Joint Workshop on Applied Electromagnetic Engineering for Magnetic, Superconducting, Multifunctional and Nanomaterials, JAPMED'12*, held in Batumi, Georgia on July 2023.

The topics considered may be listed as:

- Mechanics (Structural plasticity, Low / High speed impact loading, Hypervelocity impact, Shockwaves loading)
- Precision / Ultraprecision manufacturing from macro-, micro- to nanoscale (Metal forming, Metal removal processing, Surface engineering / Wear, Non-conventional techniques)
- Nanotechnology / Nanomaterials manufacturing
- Ferrous and non-ferrous materials (Metals, Ceramics, Superhard, Polymers, Composites, Multifunctional), from macro- to nanoscale (Nanostructured materials, Nanoparticles, Nanocomposites)
- Powder production and processing technologies (High strain-rate phenomena and treatment under shock: Explosives, Electromagnetics, High temperature / high pressure techniques)
- Biomechanics / Biomedical engineering
- Transport / Crashworthiness of Vehicles: Passive and active safety for passengers and cargo (Surface transport: Automotive, Railway; Aeronautics: Aircraft, Helicopters)
- Energy (Superconductors, Semiconductors, Electromagnetics, Solar cells, Photovoltaics, Nuclear reactors)
- Environmental aspects (Impact on climate change: Nanotechnology; Automotive industry; Aeronautics industry)
- Safety (Detection of explosives and hazardous materials)
- Defense (Ballistics, Projectiles hitting targets, Shock loading)
- Industrial sustainability

KEYNOTE PRESENTATIONS

EXPLOSION SYNTHESES OF HIGH ENTROPY ALLOYS IN FE-W-AL-TI-NI–B-C SYSTEM

Nikoloz Chikhradze[1,2,a], Davit Tsverava[1,2,b], Mikheiil Chikhradze[2,3,c], George Janikashvili[2,d]

[1] G. Tsulukidze Mining Institute, 7, E. Mindeli Str., 0186, Tbilisi, Georgia,
[2] Georgian Technical University, 77, Kostava Str., 0160, Tbilisi, Georgia,
[3] F. Tavadze Institute of Metallurgy and Materials Science, 0186, Tbilisi, Georgia,
[a] chikhradze@mining.org.ge, [b]datotsverava@gmail.com, [c]m.chikhradze@gtu.ge, [d]g_janika@yahoo.com

According to the latest definitions [1], High-Entropy Alloys (HEAs) are the alloys where the concentration of basic (at least 5) elements varies between 5-35%. The HEA have higher mixing entropy than the conventional alloys and intermetallic compounds and form the stabile solid solutions with disordered structure [1, 2, 3, 4, 5, 6, 7]. In 2004, by two groups of J.W Yeh [1] and B. Kantor [4] were published important results about the unique and special properties of HEAs, in particular high hardness, wear-resistance, significantly high strength, structural stability, good corrosion and oxidation-resistance.

HEAs "exotic", core effects are: high configurational entropy; sluggish diffusion; lattice distortion and cocktail effect [8]. The "High Entropy effect" is the base for the formation of HEAs. The microstructure of HEA is often characterized with lattice distortion and nano-precipitates, which contributes to interesting mechanical properties [9].

Core effects endow the extraordinary properties of HEAs and stimulate the increasing interest for development of new generation materials for multifunctional applications.

At the current stage the volume of investigations towards high entropy materials is extended from single phase solid solution structure to multi-phase structures, containing solid solution phases, intermetallic compounds, oxides, borides and etc. [8, 9, 10, 11].

Promised direction in this field are the high-entropy composites, prepared based on the HEAs matrix-reinforced with hard ceramic compounds. Reinforcement of HEA matrix by Intermetallics and ceramic compounds are additional tools/and challenge to improve/or design new properties of HEA based composites. Accordance evaluation "HEA is still in earlier stages hence a detailed investigation is needed" [8]. Especially, It should be underlined that HEAs, as the composite materials, are less investigated and the studies in that direction are now quite intensive.

On the other hand, nanostructure materials expose completely unique physical and mechanical, chemical, optical and other properties, which provide the increasing interest towards those materials.

Accordingly, there is a huge potential to find new properties in the field of multi-component high-entropy nanostructure materials.

Therefore, the elaboration of new technologies for the production high entropy, nano-structured bulk alloys/nanocomposites is one of the challenge for scientific centers of materials science.

In the paper the Fe-W-Al-Ti-Ni–B-C system was selected for the investigations. Arguments for selection of composition was following: a) Wide possibilities to syntheses of intermetallics, borides, oxides, carbides and solid solutions with different structural modifications (TiB_2, TiC, B_4C, W_2B_5, WB_2 WB, WB_4 and other) b) Experience of authors and results (obtained in previous research) of sintering of nanocomposites by mechanical alloying (MA) and explosive compaction (EC) in comparably simple systems (Ti-Al-Ni, Ti-Al-B and Ti-Al-B-C) [12, 13, 14, 15]; c) Composition are very attractive for practical application (energy sector, defense, ballistics, machine building, chemical industries, anti-corrosion coatings, electronics, nuclear power plant and etc.).

Based to detailed literature data review, it can be concluded, that conventional technologies are not convenient to fabricate the bulk high entropy nanocomposites for the industrial applications. The analyses shows, that the explosive compaction technology is most attractive for the synthesis of high-entropy nanocomposites

In the study, the mechanical alloying (MA), followed by adiabatic explosive consolidation was considered for sintering of bulk high entropy nanocomposites in Fe-W-Al-Ti-Ni–B-C system.

Research methodology

The selection of percentage content of elements in blend were determined on the base of thermodynamic analysis and existing phase diagrams available in scientific databases. The principle of minimization of Gibbs free energy was used for phase equilibrium analysis in multi component systems.

For MA and nanopowder production, the high energetic "Fritsch" Planetary premium line mill and vibration mill "Retsch" was used. The time of the processing was varied in range: 1h; 2h; 5h; 15; 30h. 36h. The ratio of balls to blend was 10:1. The phase composition and particle sizes of the powders were controlled by X-ray diffraction system and SEM.

The selection of explosive loading parameters (ratio of blend and explosive, container size, etc) determined according to the mathematical and computer modeling using "LS DYNA" code. The stress-deformed condition of the reaction mixture under explosive loadings, were determined according to solutions of mathematical physics and elasticity theory and by the computer program created by authors.

For shock wave generation (explosive compaction experiments) the industrial explosives (Ammonite, Mixtures of Ammonite and Ammonium Nitrate, Powergel, Hexogen) are used in the experiments.

The explosive compaction were performed at the underground explosive chamber.

The MA nano blend was charged in Steel 3 alloy-tube container and at the first stage the pre-densification of the mixtures were performed by static press installation (intensity of loading P=500-1000 kg/cm^2). Cylindrical ampoule-containers were closed at both sides.

A cardboard box was filled with the powdered explosive and placed around the cylindrical sample container and detonated. The experiments were performed at room temperature. The shock wave pressure (loading intensity) were varied in range 3-20Gpa. The set conditions the explosive were detonated by electrical-detonator. High pressure developed by explosive and temperature initiate the syntheses and consolidate the nanopowder. The compacting process accompanied with the syntheses and resulting simultaneously obtaining the bulk high entropy alloys. The phase analyses and structure-property of bulks HEA compact samples were studied. The obtained results and discussions are presented in the paper.

References:

[1] Yeh J. et al, Nanostructured high entropy alloys with multiple principal elements: novel alloy design concepts and outcomes, Adv. Eng. Mater. V. 6., #5, 2004

[2] Michael C. Cao, Jien-Wei-Yeh, Peter K. Liaw, Youg Zhang, eBook: High-Entropy Alloys, Fundamentals and Applications, Springer, 2016

[3] High-Entropy Alloys, JOM, An official publication of The Minerals, Metals & Materials Society, Springer, November 2017

[4] Cantor B. et al., Materials Science and Engineering: A, 375-377, 213-218, 2004,

[5] He Q. F. et al, Design of High-Entropy Alloy: A Perspective from Nonideal Mixing, JOM, v.69., # 11, p. 2092-2098, 2017

[6] Wang et all., Microstructure and compressive properties of AlCrFeCoNi high entropy alloy, Materials Science and Engineering: A, v. 491, issue 1-2, p. 154—158, 2008, https://www.sciencedirect.com/science/article/pii/S0921509308001123

[7] Miracle D.B. et al, Exploration and Development of High Entropy Alloys for Structural Applications, Entropy, v.16. #1, p.494-525, 2014, http://www.mdpi.com/1099-4300/16/1/494

[8] Miracle D.B. High Entropy Alloys: A current Evaluation of Founding ideal Core Effects and Exploring "Nonlinear" Alloys, JOM, v.69., # 11, p. 2130-2136, 2017

[9] Li J. Combustion syntheses of High Entropy Materials and Thermoelectric Materials, Coimbra, 2017, http://www.ism.ac.ru/events/EPNM2016/presentations/16.pdf

[10] Weiping Chen et al. Alloying Behavior, microstructure and Mechanical properties of $FeNiCrCo_{0.3}Al_{0.7}$High Entropy Alloy, Materials and Design, v. 51 p. 854-860, 2013, https://www.sciencedirect.com/science/article/pii/S0261306913003841

[11] Prabakaras R. K. et al. Synthesis and Characteristization of High Entropy Alloy (CrMnFeNiCu) Reinforced AA6061 Aluminium Matrix Composite, Mechanics and Mechanical Engineering, Vol. 21, No. 2 (2017) 415–424

[12] M. Chikhradze, G. Oniashvili. "Theoretical and Experimental Investigations of Shock wave induced reactions in Ti-Al System"International Journal of Powder Metallurgy, 2008

[13] M. Chikhradze, F.D.S. Marquis, Synthesis of Energetic Composites in Ti-Al-B-C System by Adiabatic Explosive Compaction, Chapter · February 2017, DOI: 10.1007/978-3-319-52132-9_42, 2017

[14] M. Chikhradze et al., Investigation of Intermetallides, Obtained in Ti-Al-B System in Dynamic Conditions

[15] M. Chikhradze et al., Explosive Consolidation of Ultrafine Ni-Al-Ti Powder, Proceeding of 10th International Multidisciplinary Scientific GeoConference SGEM2010, v.1, p. 1167-1172, 2010

REDUCTION OF IRON LOSS ON LAMINATED STATOR CORES BY SECONDARY CURRENT HEATING METHOD

Yuji Tsuchida

Division of Electrical and Electronic Engineering, Oita University, Japan

tsuchida@oita-u.ac.jp

Abstract. In this paper, the "secondary current heating method," which has been proposed in the previous reports, was used to heat-treat the laminated stator cores of actual motors to reduce iron loss. To evaluate the magnetic properties of the laminated stator cores including the teeth, an inner core was installed inside the stator to form a closed magnetic path. The air gap between the stator and the inner core causes the B-H loops to be tilted compared to the one of the back yoke, though, it was found that the iron loss was reduced by about 30% in the laminated stator core after heat treatment.

1. Introduction

Residual stresses generated in the manufacturing processes of motor cores, such as punching, laminating, caulking, welding, winding, and press-fitting, are factors that degrade the magnetic properties of electrical steel sheets [1]. For this reason, all industrial motor cores used to undergo heat treatment (strain relief annealing) in a large electric furnace. In large electric furnaces, the heat treatment time is long (about 12 hours) and the running cost is high because of the atmosphere heating (indirect heating). Therefore, heat treatment is not currently used for industrial motors in Japan. However, it is an important issue to reduce the iron loss of industrial motor cores and achieve higher efficiency by some kind of treatment in order to realize a carbon neutral society.

Therefore, we have proposed a new heat treatment method for ring-shaped laminated cores of electrical steel sheets that are to be heated in a much shorter time than in a conventional large electric furnace to reduce the iron loss [2]. The new heat treatment method is named "Secondary Current Heating method," and it has been shown that the iron loss of ring-shaped laminated cores can be reduced by up to 14% in about 10 minutes [2]. The principle diagram of the Secondary Current Heating method is shown in Fig. 1. The magnetic flux change chained around the centre of the ring-shaped laminated cores generates a secondary current (induced current) in the object to be heated, enabling direct heating using the object itself as the heat source. This enables heat treatment in a shorter time than indirect heating in an electric furnace.

In this paper, we examine to apply the Secondary Current Heating method into heating actual motor laminated stator cores to reduce iron loss.

2. Secondary Current Heating Method

As shown in Fig. 1, the Secondary Current Heating device consists of a main yoke, an excitation coil, an auxiliary yoke, and a laminated stator core as the object to be heated. The auxiliary yoke and laminated stator cores are removable for installation in the actual manufacturing process. The excitation coil generates magnetic flux in the main yoke and the auxiliary yoke. Due to the alternating magnetic flux, time-varying magnetic fluxes intersect in the laminated stator cores surrounding the auxiliary yoke, generating an induced electromotive force. Since the back yoke section of the laminated stator cores is electrically short-circuited, a secondary current (induced current) flows. Fig. 2 shows the laminated stator core used in this paper. The stator core has an outer diameter of approximately 50 mm, an inner diameter of the teeth of approximately 30 mm, and a lamination thickness of approximately 26.5 mm. The number of teeth is 6. The stator cores are made from non-oriented electrical steel sheets with the 0.5 mm-thickness, laminated by punching and caulking. For the ring-shaped specimens reported so far, the target temperature was set at around 600 °C to minimize the heating time, but for the laminated stator cores, we aimed at a shorter heat treatment time above the recommended strain relief annealing temperature to further reduce the iron losses in the cores.

3. Magnetic properties of laminated stator cores and reduction of iron loss

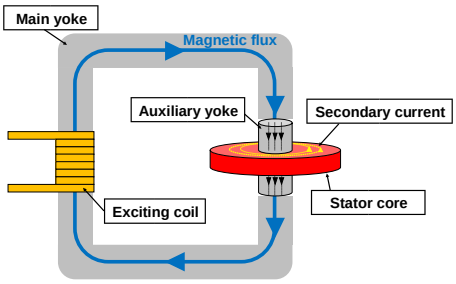

Fig. 1 Secondary Current Heating method

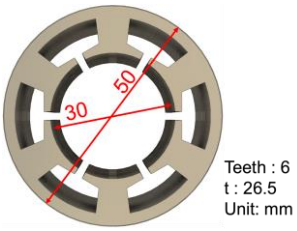

Fig. 2 Laminated stator core

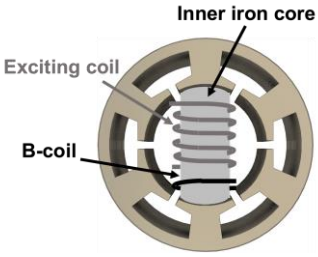

Fig. 3 Allocation of exciting coil and B-coil of stator cores

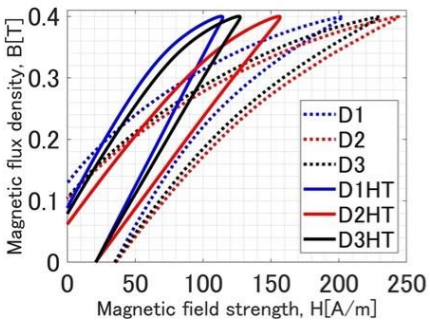

Fig. 4 B-H loops of stator core at frequency, 50 Hz at 0.4 T.

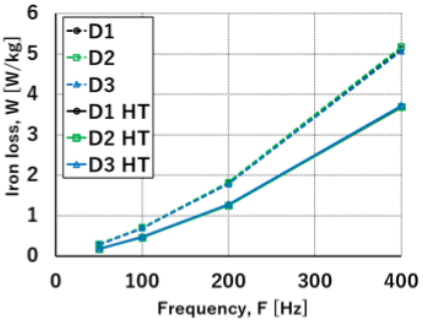

Fig. 5 Iron distribution of stator cores

In the measurement system on magnetic properties, the magnetic flux density B of the laminated stator cores is feedback-controlled by a PC to set the target value so that the magnetic properties and iron loss, which are different due to heat treatment, can be compared and evaluated under the same magnetic conditions. The B-H loops were derived from the excitation coil and B coil, and they were compared and evaluated. The iron losses were calculated from the B-H loops, and the usefulness of heat treatment using the Secondary Current Heating method was discussed.

Since the magnetic properties of the teeth contribute greatly to motor performance, the magnetic properties of the stator cores, including the teeth, were evaluated. As shown in Fig. 3, the excitation coil and B coil are wound around the inner core so that it can be easily installed in any pair of teeth. In our preliminary experiment, the B-H loops varied depending on the position where the inner core was installed. We investigated the reason, and found that the laminated stator cores used in this paper were for small power motors, so rolling direction was not taken into account during laminating, and the effect of magnetic anisotropy was found. Therefore, to ensure that the rolling direction of the laminated stator cores and the direction of the inner core installation were unique, measurements were performed by installing the inner core in three different ways: PositionD1, Position-D2, and Position-D3. The B-H loops measured with the inner core is shown in Fig. 4. The magnetic flux condition is 0.4 T. The dotted line is before heat treatment and the solid line is after heat treatment. Compared to the B-H loops measured on the back yokes, these B-H loops are significantly tilted. This is due to the gap between the stator cores and the inner core. However, the B-H loops including the teeth are also improved after proposed heat treatment, and it is possible to evaluate the magnetic properties of the entire laminated stator cores including the teeth by using the inner core. Fig. 5 shows the iron loss distributions. Compared to the back yoke section, the iron losses increase. Since the iron losses remain almost the same even when there is a gap in the magnetic path, the iron losses of the entire laminated stator cores, including the teeth section, is considered to be larger than that of the back yoke section. In any case, the iron losses of the entire laminated stator cores were found to be reduced by about 30% after heat treatment. Details and further discussions are to be presented in the full paper.

References:

[1] Schoppa A., et al., Influence of the manufacturing process on the magnetic properties of non-oriented electrical steels, *Journal of Magnetism and Magnetic Materials*, 2000, **215-216**, 74-78.

[2] Tsuchida Y., Yoshino N., and Enokizono M., Reduction of Iron Loss on Laminated Electrical Steel Sheet Cores by means of Secondary Current Heating Method, *IEEE Transactions on Magnetics*, 2017, **53**, 4 pages.

MAGNETIC FIELD BETWEEN POLAR HEMISPHERES: REMARKS ON THE DISLOCATION OF ZONES OF A CONSTANT GRADIENT AND FORCE FACTOR

Anna A. Sandulyak[1], Maria N. Polismakova[1], Darya A. Sandulyak[1], Anand P. Dwivedi[2,a], Charalampos C. Doumanidis[2], Alexander V. Sandulyak[1], Vera A. Ershova[1]

[1]MIREA — Russian Technological University, Moscow, Russia
[2]Guangdong Technion-Israel Institute of Technology, Shantou, China
[a]anand.dwivedi@gtiit.edu.cn

Abstract: To create an inhomogeneous magnetic field, in which there would be zones with a practically constant value of the magnetic gradient (MG) and / or magnetic force factor (MFF), an original solution was indicated: the use of an electromagnetic system with spherical poles. In this case, the coordinate dependences of MG and MFF in the interpolar region are extreme and the zones localized in the domain of the extrema are practically stable, referred to as the MG_{Const} and MFF_{Const} zones, with individual coordinates x_{extr} of their conditional centers and length Δx (with an allowable error changes in MG and MFF data within these zones). The data following from experimental studies is given on the dislocation of the indicated zones between the poles-hemispheres of diameter *D*, separated by different distances *b*; the values of x_{extr}/D and $\Delta x/D$ depend on *b/D*. It is shown that the dependencies x_{extr}/D on *b/D* obtained separately for the MG_{Const} and MFF_{Const} zones, demonstrating, like the dependencies $\Delta x/D$ on *b/D*, mutual similarity (up to a constant multiplier), obey power functions with exponents of 0.5 and 0.4, respectively. A closer (to the center-to-center line of pole-hemispheres) and more compact (in length) dislocation of the MFF_{Const} zones compared to the MG_{Const} zones was revealed: almost 1.3 times both in x_{extr}/D and in $\Delta x/D$.

Key words*:* Spherical pole pieces, magnetic parameters, gradient, force factor, zones of constancy of parameters, inhomogeneous magnetic field.

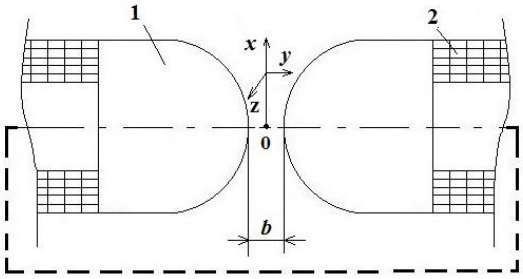

Fig. 1. Illustration of the use of spherical pole pieces in an electromagnetic system, which allow creating local zones of almost constant values of the magnetic gradient and magnetic force factor; 1 - pole piece, 2 - winding of the electromagnetic system

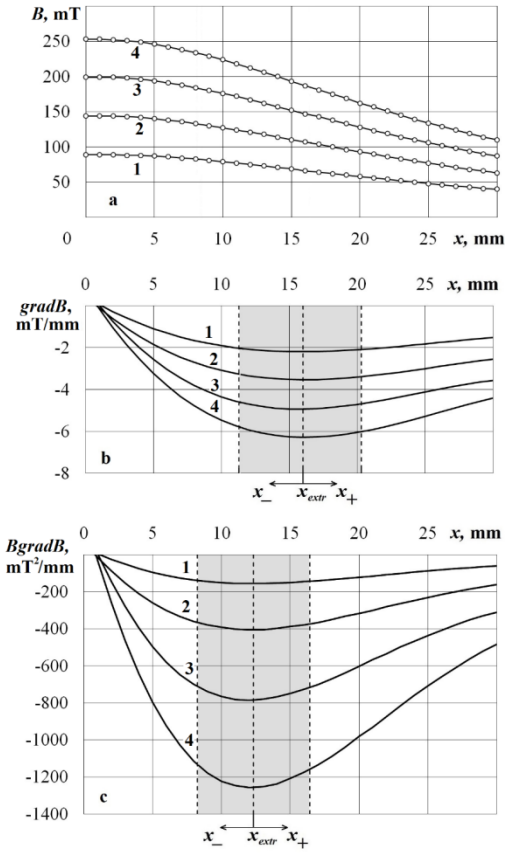

Fig. 2. An example of coordinate magnetic characteristics between hemispherical poles with a diameter *D* = 100 mm and a distance *b* = 13 mm: *a*) winding for induction (points - experiment, line - approximation by a polynomial of the fourth degree), *b*) extreme for MG, *c*) extreme for MFF; 1 - *Iω* = 3000 A, 2 - 6000, 3 - 12000, 4 - 22500; the MG_{Const} and MFF_{Const} zones are dimmed.

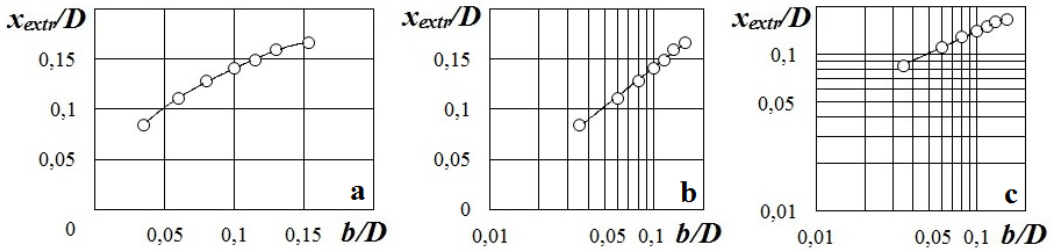

Fig.3. Influence of the relative distance *b/D* between the polar hemispheres on the relative coordinate x_{extr}/D of the conditional center of the zone MG_{Const}; *a*) in conventional coordinates, *b* and *c*) respectively in semi-logarithmic and logarithmic coordinates.

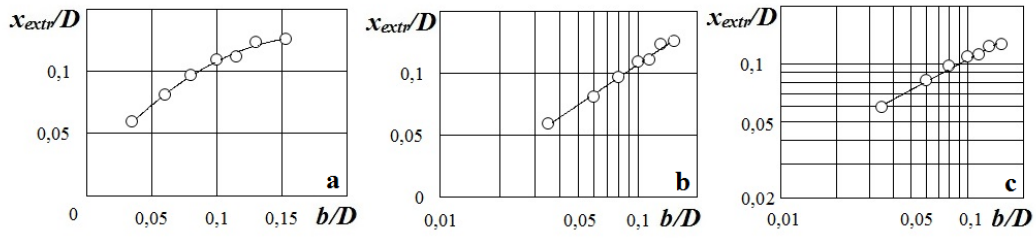

Fig. 4. The same as in Fig.3, but for the conditional center of the zone MFF_{Const}.

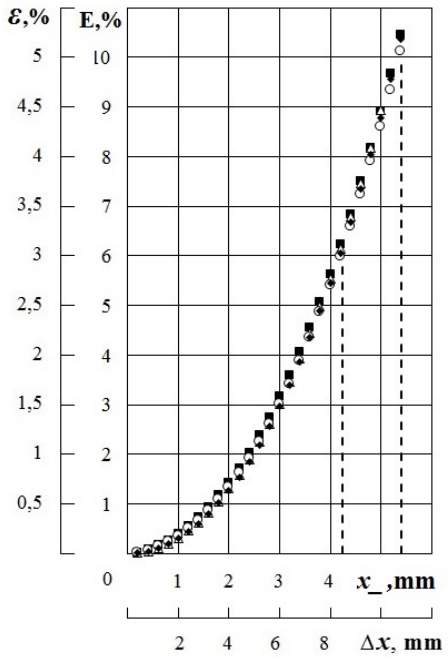

Fig.5. Obtained from the data of Fig. 2b and relations (4), (6) dependence of the indices *E* and *ε* on the step-by-step displacement *x_* in the half-zone MG_{Const} and the length $\Delta x \cong 2x\_$ of the zone; ♦ - *Iω* = 3000 A, ○ - 6000, Δ - 12000, ■ - 22500.

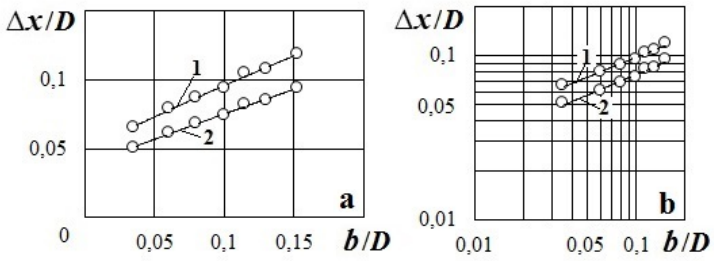

Fig.6. Influence of the relative distance *b/D* between the polar hemispheres on the relative length $\Delta x/D$ of the zone MG_{Const}: when the current data deviates from the average values up to 5% (line 1) and up to 3% (line 2); *a*) and *b*) in ordinary and logarithmic coordinates.

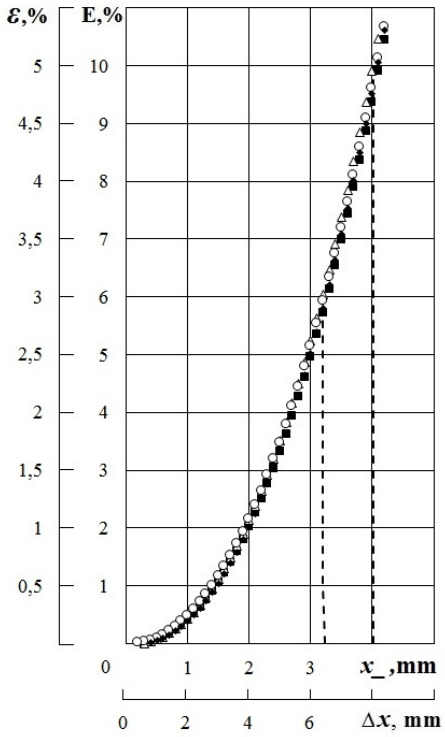

Fig.7. Obtained from the data in Fig. 2c and relations (5), (8) dependence of the indices *E* and *ε* on the step-by-step displacement *x_* in the MFF$_{Const}$ half zone and the length $\Delta x \cong 2x\_$ of the zone; ♦ – Iω = 3000 A, ○ – 6000, Δ – 12000, ■ – 22500.

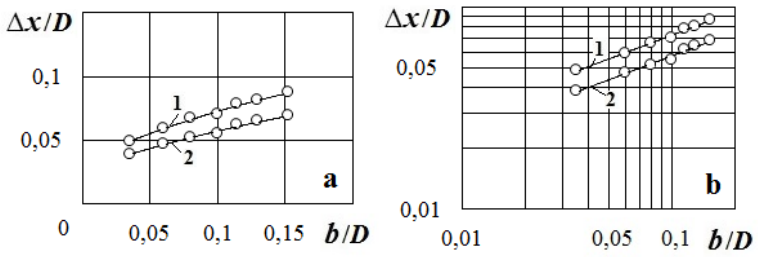

Fig.8. The same as in Fig.6, but for the MFF$_{Const}$ zone.

AN INFORMATION-THEORETICAL ANALYSIS OF THE SPIRIT OF THE AGE

J. J. Ramsden[1,*] A. A. Mamali[2], N.T. Athanassoulis[3]
[1]*Faculty of Medicine and Health Sciences, The University of Buckingham, England,*
[*]*jeremy.ramsden@buckingham.ac.uk*
[2] *Cass Business School Alumni, Athens, Greece*
[3] *Laboratory of Energy and Industrial Economics (LIEE), National Technical University of Athens, Greece*

Abstract

The expression "spirit of the age" first seems to have been used by Arndt in his book published in 1805. This was little more than a series of sketches of nations and personalities, a format more or less repeated in Hazlitt's work of the same title published in 1825. The concept acquired greater importance with the emergence of Tolstoy's theory of history, of which the main exposition is his work *War and Peace* (published in 1868), according to which events reflect the general "will of the people" rather than actions by prominent individuals. This "will of the people" would appear to correspond with the spirit of the age. It has also had a great bearing of the development of science. It has been aptly remarked by Lecky that the success of any opinion depends much less upon the force of its arguments, or upon the ability of its advocates, than upon the predisposition of society to receive it. The emergence of the theory of evolution provides a classic example of this phenomenon.

The matter clearly merits deeper investigation. Although Tolstoy makes eloquent arguments in favour of his theory, it contains no real mechanism for understanding how the spirit develops — as it evidently does — and hence it is of little use for making predictions. Of particular value would be a prediction of whether a certain new theory would be received by society. This contribution attempts to use the method of physical analogies to better understand the spirit of the age. Furthermore, the very recent development of large language models provide an unprecedented ability to efficiently capture the spirit of our age in different cultural spheres, thereby providing data more amenable to calculation than what was previously available.

The main idea developed in this contribution is that the "noise" of the almost infinitesimal array of actions of the individual denizens of Earth can, sometimes, be amplified up to macroscopic expression.

EFFECT OF NANOADDITIVES ON THE PROPERTIES OF PARTIALLY STABILIZED ZIRCONIA

A.G. Mamalis[1,a], E.S. Hevorkian[2,b], V.P. Nerubatskyi[3,c], M. Rucki[4,d] Z. Krzysiak[2], O.M. Morozova[3,e]

[1]Project Center for Nanotechnology and Advanced Engineering, Athens, Greece, [a]agmamalis@yahoo.com

[2]University of Life Sciences in Lublin, 13 Akademicka, Lublin 20-950, Poland, [b]cermet-u@mail.com

[3]Ukrainian State University of Railway Transport, Kharkiv, Ukraine, [c]nerubatskyi@kart.edu.ua, [e]oksanabakan2012@gmail.com

[4]Kazimierz Pulaski University of Technology and Humanities in Radom, Poland, [d]m.rucki@uthrad.pl

The structure determining factor for of nanocrystalline materials is the extremely small grain size, the resulting large area of the boundaries and correspondingly the length of their joints in the volume unit, the difficulty or suppression of dislocation mechanisms of plastic deformation at grain sizes below a certain limiting value and the nonequilibrium state of the grain boundaries [1]. The developed surface of isolated nanoparticles initiates dimensional effects of thermodynamic quantities. Due to the existence of a significant number of atoms near the surface of the nanomaterial, as well as the lattice dynamics, which undergoes substantial changes due to a number of features of the nanostate, such substance characteristics as values of heat capacity [2], thermal conductivity [3, 4], melting temperature, Debye temperature depend.

In the case of a non-electrically conductive pure zirconia sample, there is no joule heating during current flow through the powder mixture, i.e. the initial heating of the sample is done by current flow through the graphite mold , in contrast to the case of tungsten carbide samples, where joule heating starts immediately, i.e. the structure formation occurs mainly already during heating to the dwell temperature. The high heating rate minimizes the influence of diffusion processes on the particle surfaces, which do not contribute to densification, and the samples reach high temperatures faster while retaining the ability to sinter. That is, rapid heating accelerates densification due to earlier activation of dislocation creep mechanisms and due to reduction of the low-temperature stage sintering, when surface diffusion dominates.

Various nanoadditives to zirconium dioxide affect primarily the hardness and strength of the composite as a whole. They increase these values in different ways, depending on their content and sintering regimes. Hot pressing by electrosintering, significantly activates the compaction process, contributes to the formation of a fine microstructure. The mechanism of the sintering process occurs differently, depending on the ability to conduct electric current, strengthening additives. creation of a functional gradient material, the top layer of which will be ZrO_2-Al_2O_3, the middle ZrO_2-SiC, the bottom layer ZrO_2-WC. The material can have a polyfunctional application, one of the most promising applications would be the production of laminated plates for cutting tools. The question of choosing the optimal composition for each layer will be determined by the working conditions of this material.

Reference:

[1] Sirota V., Ivanisenko V., Pavlenko I., Hevorkyan E., Chishkala V., Kovaleva M..Synthesis and consolidation of (Zr0.94Y0.06)O1.88 nanopowders. Ceram International,2015;41:5263–9.

[2] Hevorkyan E., Lavrynenko S., Rucki M., Siemiątkowski Z., Kislitsa M. Preparation of nanostructured materials by electrical sintering 2017;11–15:663–6.

[3] Chena X., Liub L., Donga Y. Preparation of nano-sized Bi2Te3 thermoelectric material powders by cryogenic grinding. Progress in Natural Science. Materials International. 2012, 22, 3, 201–206.

[4] Vanleeuwen B.K., Darling K.A., Koch C.C., Scattergood R.O. Novel technique for the synthesis of ultra-fine porosity metal foam via the inclusion of condensed argon through cryogenic mechanical alloying. Materials science and Engineering: A. Structural Materials. 2011, 528, 4–5, 2192–2195.

THERMAL CONDUCTION AND MAGNETIC PROPERTIES OF MAGNETORHEOLOGICAL ELASTOMERS DISPERSING SENDUST PARTICLES

Y. Ido[1,a], Y. Hiroshima[1,b],Y. Iwamoto[1,c], Y. Hirota[2,d], S. Fujioka[2,e]

[1] *Department of Electrical and Mechanical Engineering, "Nagoya Institute of Technology", Japan,*
[a]*ido.yasushi@nitech.ac.jp*, [b]*y.hirosima.265@stn.nitech.ac.jp*, [c]*iwamoto.yuhiro@nitech.ac.jp*
[2] *"Ferrotec Materials Technologies", Japan,* [d]*hirota-yst@ft-mt.co.jp*, [e]*fujioka-stm@ft-mt.co.jp*

Abstract. A new magnetic functional material that is an elastomer dispersing micrometer-size sendust particles has been developed in this study. Sendust is a material which is the alloy composed of Fe, Si and Al, and has a high initial magnetic permeability and small hysteresis. Thermal conductivity of this new magnetic functional material was investigated by using the steady-state parallel-plate method while the magnetic properties of the materials were evaluated by using the BH analyzer.

1. Introduction

Magnetorheological elastomers are kind of magnetic functional materials that exhibit their functions in response to an applied magnetic field. The magnetorheological elastomers are basically composed of iron particles and carrier. The iron particles are embedded in the matrix [1]. When an external magnetic field is applied during the curing process to form chain-like clusters of iron particles in the material, magnetorheological elastomers with thermal conductivity anisotropy and magnetic anisotropy can be obtained [2,3].

In this study, we focused on sendust as dispersed particles in the magnetorheological elastomers, because sendust made of Fe, Si, and Al has a high initial magnetic permeability and low hysteresis. A new magnetorheological elastomer composed of sendust particles and silicone has been developed and its thermal and magnetic properties were investigated experimentally.

2. Experiments and sample preparation

Samples of magnetorheological elastomer made of sendust particles and silicone were prepared. The sendust particles were spherical particles whose average diameter was 16.8 μm (Sanyo Special Steel Co., Ltd., PST-S) and the base carrier was silicone elastomer (Dow, Sylgard184). We prepared two types of magnetorheological elastomer samples. The first one was a mixture of sendust particles without applying a magnetic field, basically the sendust particles are randomly and evenly distributed. The second one was produced with a uniform magnetic field, and the sendust particles formed chain-like clusters in the direction of the applied magnetic field inside the material. The volume fractions of the sendust particles in the samples were 5, 10, and 15 % and the size of the specimens was 40 mm square for the thermal conductivity experiments, while the volume fractions were 5, 7.5, and 10 % and the size of the specimens was 30 mm square for the experiments measuring magnetic properties.

To obtain the thermal conductivity of the samples, the steady-state parallel-plate method was used. Figure 1 shows the schematic of the core part of the experimental apparatus for steady-state parallel-plate method. The magnetization of the samples was measured by using the BH analyzer (Denshijiki Industry Co., Ltd., EMD-80M25M). The direction of the thermal conductivity and the

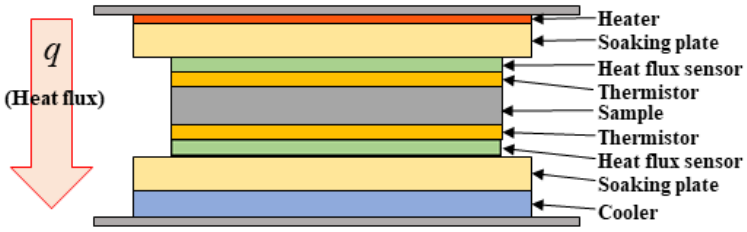

Fig. 1. Schematic of the experimental apparatus using the steady-state parallel-plate method.

applied magnetic field of magnetization measurements was set as the following three cases: perpendicular to the surface of the sample with randomly distributed particles (Random), parallel to the chain-like clusters in the samples (Parallel), and perpendicular to the chain-like clusters in the samples (Perpendicular).

3. Results and discussion

The larger the volume fraction of sendust particles dispersed in the sample, the higher the thermal conductivity. In addition, compared with the Random case, the Parallel case shows the higher thermal conductivity, while the Perpendicular case shows the lower thermal conductivity. Based on the Random case, when the particle volume fraction is 15%, the thermal conductivity increases by 43% in the Parallel case, and when the particle volume fraction is 10%, the thermal conductivity decreases by 10% in the Perpendicular case. These results are dependent upon the cluster structure formed inside the sample. When the volume fraction of the particles is relatively low, the chain-like clusters exist in isolation. However, when the volume fraction of the particles becomes high, the anisotropy of the thermal conductivity decreases because the contact between particles also increases in the direction perpendicular to the direction of the applied magnetic field due to the coalescence of chain-like clusters.

Figure 2 shows the magnetization of the samples when the volume fraction of the particles is 10%. From Fig.2, the initial permeability in case of Parallel takes larger value than those in the other case. The saturation magnetization does not depend on the microstructure inside the sample, and it only depends on the volume fraction of sendust particles.

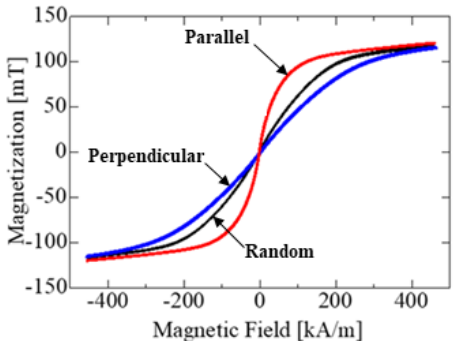

Fig.2. Magnetization-magnetic field curves of the samples when the volume fraction of the particles is 10 %.

Conclusions:

A new magnetorheological elastomer in which sendust particles are dispersed in a silicone material have been developed, and experimentally shown their thermal conductivity anisotropy and magnetic properties. The thermal conduction and magnetic properties of the magnetorheological elastomers with sendust particles depends on the microstructure like cluster formation inside the material except the saturation magnetization.

References:

[1] Zhou G.Y. Shear properties of a magnetorheological elastomer, Smart Materials and Structures, 2003, 12, 139-146

[2] Boczkowska A., Awietjam S.F., Wroblewski R. Microstructure-property relationships of urethane magnetorheological elastomers, Smart Materials and Structures, 2007, **16**, 1924-1930

[3] Schubert G., Harrison P. Magnetic induction measurements and identification of the permeability of magneto-rheological elastomers using finite element simulations, Journal of Magnetism and Magnetic Materials, 2016, **404**, 205-214

[4] Ido Y., Inagaki T., Yamaguchi T. Numerical analysis of microstructure formation of magnetic particles and nonmagnetic particles in MR fluids, Journal of Physics: Condensed Matter, 2009, **149**, 012057

THE CONCEPT OF OBTAINING SPINETRONIC NANOSTRUCTURES FOR QUANTUM DEVICES

Paata J. Kervalishvili

Georgian Technical University, Tbilisi, Georgia, paata.kervalishvili@gtu.ge

Abstract: The aim of the paper is elaboration of concept for obtaining spintronic nanostructures and quantum devices by Laser Plasma technology of 2D materials preparation.

Today when Moore law gradually loses its effect and conventional charge-based electronics will soon come to the end development of high speed and low energy consuming information systems is urgently needed. Up to now, many new methodologies have been proposed, such as molecular electronics, nanoelectronics, spintronics, magnetronics, optronics, etc. Modern Electronics (Micro Nano Spin Electronics) and its future mainly based on novel materials (metals and non metals), their preparation technologies and new properties. Perfection and ultra-purity are not the only parameters characterized materials usefulness for quantum devices. Modification of material properties by different structural nonperfections (structural defects: impurities, isotopes, etc.) is the smart instrument for regulation of their characteristics.

Based on difference from conventional electronics e electron's which uses the electron's charge degree of freedom for information processing, spintronics is devoted to incorporating the electron's spin degree of freedom. Despite its great potential advantages, spintronics now faces a number of challenges, such as generation of fully spin-polarized carriers (pure spins) and injection of spin into devices, long distance spin transport, and manipulation and detection of carriers' spin orientation. The solutions to these issues rely on the development of device fabrication and designing new spintronics materials with specific properties. Pure spin generation and injection mainly depends on the degree of spin polarization in the used semiconductors or metals. Thanks to the discovery of carbon-based nanomaterials such as graphene and carbon nanotubes, the challenge of long-distance spin transport is likely to be solved in the near future. Because of their very weak spin–orbit coupling (SOC), carbon-based nanomaterials can have a long spin coherence length up to a few micrometers, thus are very good spin transportation materials. As with spin manipulation and detection, there are some methods based on the coupling effects between spin and light, magnetic field, electric field, according to their electronic and magnetic properties, spintronics materials can be classified as magnetic metals, topological insulators, and magnetic semiconductors In a spintronic device, magnetic metals and topological insulators, serve as spin sources and drains, while magnetic semiconductors constitute the central region of the device.

At the same time usage of electron spins as quantum bits for quantum information processing in so called quantum computers is clear. Qubits in this state display a degree of correlations impossible in classical physics. This phenomenon is called entanglement and is crucial property of quantum computing. The main requirements of quantum computation are: Scalable physical systems with well characterized qubits (Zeeman Spliting); Long decoherence time: Existence of qubits at the ground state; Set of quantum gates; measurement capabilities, etc. Candidate for a qubit needs longer decoherence time than gate operation time. The transformation of digital computers from bulky machines to portable systems has been enabled by new materials and advanced processing technologies that allow ultrahigh integration of solid- state electronic switching devices. As this conventional scaling pathway has approached atomic- scale dimensions, the constituent nanomaterials increasingly possess properties that are dominated by quantum physics.

The convergence between quantum materials properties and prototype quantum devices is especially apparent in the field of 2D materials, which offer a broad range of materials properties, high flexibility in fabrication pathways and the ability to form artificial states of quantum matter. Along with the quantum properties and potential of 2D materials as solid- state platforms for quantum- dot qubits, single- photon emitters, superconducting qubits and topological quantum computing elements it is necessary to select the best method of their preparation.

Potential of laser plasma process for 2D materials preparation, particularly its usefulness for organization of nanostructures applicable in spintronic and quantum computing devices novadays is actively developing. Laser plasma formed under the ionizing effect of powerful laser radiation on the thing. For example, LP arises during optical breakdown in gaseous media, laser radiation on top solid body, in laser thermonuclear targets.

LP can exist in a wide range of temperatures - from 1 eV to 104 eV (104–108 K) and arising as a result of ionization of the electron impact with the subsequent image electronic avalanche, or as a result of many photons ionization. In LP. experimentally, self-focusing of the laser beam is observed. The impact of a light wave on LP leads to the formation of plasma waves (coil -ny electronic and ionic densities), which interact with the primary and scattered light then you wave. As a result, electric magnetic waves are formed with a frequency that is a multiple of the frequency of the incident light this wave (the so-called harmonics). The probability of generating high harmonics increases with an increase in intensity of laser radiation.

For preparation of 2D materials (semimetals, semiconductors) for novel quantum devices on the basis of our previous investigations we will develop and use the Laser-Plasma method which enables preparation of nanostructured layers with fine and perfect structures and high purity The properties of nanomaterials prepared by laser plasma technique are unique, and they are not reproducible by any other method including chemical ones. The usage of resonance light heat creates the opportunity to energize the selected atoms as well as their groups (assemble) and to produce plasma with the necessary properties relevant to structures which must be prepared. This technique was successfully used by the authors of the project to study the conditions for obtaining diamond-like films, as well as thin layers of boron carbide. See Fig.1.

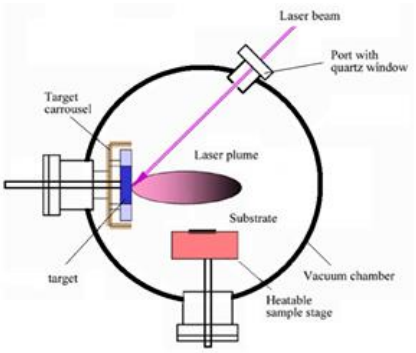

Fig.1. The scheme of experimental laser-plasma technology setup

In the last two decades, the Laser plasma method was used to form both homogeneously doped GaAs:Mn layers and two-dimensional structures, including a δ-doped GaAs:Mn layer and a InxGa1 – xAs quantum well separated by a GaAs spacer with a thickness of d = 3–6 nm. It is obvious that only Mn ions, which are part of the GaMnAs solid solution and are distributed almost uniformly in it, can noticeably exchange with quantum well carriers, leading to their spin polarization and, consequently, to the anomalous Hall effect.

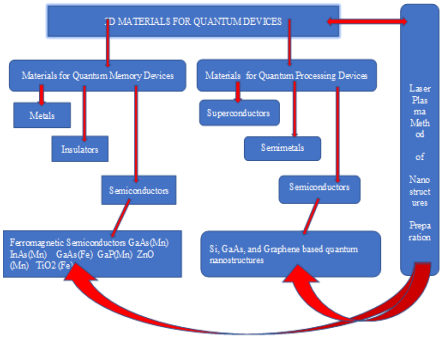

Fig.2 Roadmap of works related to obtaining spinelectronic nanostructures for quantum devices

We are looking for farther development of LP processes aim of preparation the next (higher) level of spintronic nanostructures based on above mentioned and some other diluted semiconductors.

Our works shown that the LP method and technology is very useful for preparation of semiconductor silicon and graphene nanosystem in one sandwich for creation of a new highly effective multiqubit element. (Fig.2). Graphene's multilayers are forming stack – cluster with sublattices, which is a most common arrangement of nearest neighbour layers observed in nature. Selection of laser sources and their parameters is giving the possibility to vary the energy of ionized atoms in plasma plum, activate them to the necessary level and deposit the hot atoms and their clusters on substrates of different origin (semiconductors: Silicon, GaAs, etc.; Metals: Fe, Ni, etc.; Insulators: Al2O3, etc). For organization of these processes it is also possible to use the resonance wavelength of the light sources in order to have the direct and strong interaction with electron's bonding energies.

References:

[1] Kervalishvili P.J. Novel nanostructured semiconductive materials for spinelectronics applications, Materials of ISTC Conference "SPINELECTRONICS 07" Tbilisi State University, October 22-24 2007. Tbilisi, Georgia.
[2] Fert, The origin, development, and future of spintronics, Nobel Lecture, December 8, 2007, Stockholm, Sweden.
[3] Novoselov K.S., Geim A.K., Morozov S.V. et al. Electric field effect in atomically thin carbon films. Science 2004; 306: 666–9.
[4] Xingxing L., Jinlong Y. First-principles design of spintronics materials, National Science Review 3: 365–381, 2016, doi: 10.1093/nsr/nww026.
[5] Kervalishvili P.J. Laser technologies of nanosystems preparation. Conference "Nanotechnology", Georgian Technical University, 4 – 7 October 2021, Tbilisi, Georgia, p. 62.

BULK MgB_2 AND MT-YBCO FOR SUPERCONDUCTING BEARINGS WORKING IN LIQUID HYDROGEN

Tetiana Prikhna[1, 4, 5, a], Michael Eisterer[2, b], Athanasios Mamalis[3, c], Viktor Moshchil[1, d], Bernd Büchner[4, e], Dirk Lindackers[4, f], Xavier Obradors[5, g], Teresa Puig[5, h], Frank N. Werfel[6, i], Uta Flögel – Delor [6, j], Volodymyr Sverdun[1, k], Alexey Vakaliuk[6, l], Semyon Ponomarov[7, m], Paul Sass[8, n]

[1]V. Bakul Institute for Superhard Materials of the National Academy of Sciences of Ukraine, 2, Avtozavodskaya Str., Kiev 07074, Ukraine

[2] Institute of Atomic and Subatomic Physics, TU Wien, Stadionallee 2, 1020 Vienna, Austria

[3] Project Centre for Nanotechnology and Advanced Engineering, NCSR "Demokritos", Athens, Greece

[4]Leibniz-Institut für Festkörper- und Werkstoffforschung Dresden e. V., Helmholtzstraße 20, 01069 Dresden, Germany

[5]Institute of Materials Science of Barcelona (ICMAB), CSIC, Universitat Autònoma de Barcelona, Campus de la, Carrer dels Til·lers, s/n, 08193 Bellaterra, Barcelona, Spain

[6]Adelwitz Technologiezentrum GmbH (ATZ), Naundorfer Str. 29, 04860 Torgau, Germany

[7]Institute of Semiconductor Physics of the National Academy of Sciences of Ukraine, 41, Nauky Ave., Kyiv 03028, Ukraine

[8] ScIDre – Scientific Instruments Dresden GmbH, Gutzkowstrasser 30, Dresden 01069, Germany

[a]prikhna@ukr.net, [b]michael.eisterer@tuwien.ac.at, [c]agmamalis@yahoo.com, [d]vik_ism@ukr.net, [e]b.buechner@ifw-dresden.de, [f]d.lindackers@ifw-dresden.de, [g]xavier.obradors@icmab.cat, [h]teresa@icmab.es, [i]werfel@t-online.de, [j]floegel-delor@t-online.de, [k]vsverdun@ukr.net, [l]vakaliuk@atz-gmbh.com, [m]s.s.ponomaryov@gmail.com, [n]p.sass@scidre.de

The development of hydrogen energy meet problems connected with liquid hydrogen transportation what, in particular, results in an increasing interest in the development of pumps working at liquid hydrogen temperature (20 K). High-performance submersible liquid hydrogen pumps requires superconducting bearings which can trap magnetic fields up to 1 T at 20 K. Operation of superconducting (SC) devices is independent from the superconductor type and the choice of material depends on the required operation temperature, superconducting characteristics, etc. The superconductors can operate as quasi-permanent magnets and can provide magnetic fields up to an order of magnitude higher than the best traditional permanent magnets. In the case of bulk superconductors it is not necessary direct, continuous connection to a power supply, as in the case of electromagnets. Bulk SC magnet may be safely and conveniently turned off by its heating.

MgB_2 and melt-textured YBCO (MT-YBCO) ceramics are promising candidates for this application. The present study aimed at investigation and comparison of superconducting properties and microstructure of differently prepared MgB_2 and differently oxygenated MT-YBCO. The ability of materials to trap magnetic fields was studied using hollow cylinders of the same geometry which were manufactured from hot pressed (under 30 MPa) blocks prepared from magnesium diboride with titanium, titanium oxide and titanium carbide additives as well as from melt-textured YBCO ceramics. The addition of titanium and titanium containing substances to MgB_2 was aimed not only for creating additional pinning centers in the material, but as well to avoid formation of cracks and voids in big blocks due to presence of admixture hydrogen in Mg:2B powdered mixture. Titanium is good getter of hydrogen when added to MgB_2 what has been shown by us earlier.

The results of magnetic induction measurement by Hall probe of the hot pressed MgB_2 rings with different additions show that despite the similar J_c and visual absence of cracks and same trapped field at 20 K, the materials with Ti-O addition (obtained by electroerosion dispersion method) when heated to higher temperatures demonstrated less flux jumps than that with Ti addition. And the worthiest behavior demonstrated material with TiC addition despite the higher J_c observed in the small sample cut from the same block studied by VSM. The structure of this material was the most inhomogeneous and it was very porous. The high porosity can be the obstacle of the material exploitation in submersible liquid hydrogen pump because of high surface area which will be in contact with liquid hydrogen and due to this the material can be less stable.

The high critical current densities and critical magnetic fields should ensure high trapped fields in all these materials. Indeed all materials demonstrated the required performance; however, flux jumps are a serious issue in MgB_2 even in crack free cylinders and impeded higher trapped fields. The superconducting properties

of all materials investigated in this study are sufficient for magnets in submersible liquid hydrogen pumps with a required trapped field of about 500-600 mT. Their stability in liquid hydrogen is under the study. An inhomogeneous and porous MgB_2 structure was found to be less stable against flux jumps. On the other hand, deviations of the material matrices from MgB_2 stoichiometry did not impede high J_c and trapped fields.

This work was supported by the project NATO SPS G5773 and National Academy of Sciences of Ukraine projects III-11-21 (0781) and grant of NAS of Ukraine III-11-21 (0781).

ORAL PRESENTATIONS

PREPARATION OF CORRUGATED TUBES FOR HIGH EFFICIENCY HEAT EXCHANGERS BY EXPLOSIVE TUBE FORMING

I. Zádor[1,a], A.G. Mamalis[2,b], A. Szalay[3,c],

[1] *KOGAT Ltd, Budapest, Hungary, [a]istvan.zador@kogat.hu*
[2] *Project Center for Nanotechnology and Advanced Engineering, NCSR "Demokritos", Greece, [b]agmamalis@yahoo.com*
[3] *Puraset Water and Metal Solution Ltd, Budapest, Hungary, [c]andras.szalay@puraset.hu*

1. Introduction

Large quantity of hot flue gases is generated from kilns, ovens and furnaces. If some of this waste heat could be recovered, a considerable amount of primary fuel could be saved. The energy lost in waste gases cannot be fully recovered. However, much of the heat could be recovered by heat exchangers (or recuperators) and the loss will be reduced.

A heat exchanger is an equipment built for efficient heat transfer from one medium to another. Generally, the two media are separated by a solid metallic wall, so that they never mix. These tubular heat exchangers are widely used in power plants, chemical plants, metal processing plants.

Main requirement for the heat exchanger tubes is that the heat transfer between the media inside the tube and outside the tube should be the maximum. That can be achieved in many ways. The most frequently used solution is the modification of the tube's construction as creation of enhanced surface or applying spiral strips for causing turbulences in the streaming media.

2. Experimental

An innovative solution is enhancing the efficiency of the heat exchanger tubes by creating spiral deformations on the tubes. The advantages of the properly designed deformation of the tube material are twofold: on one hand the heat transferring surface of the tubes will be enlarged and on the other hand the deformations will cause turbulences in the streaming media, enhancing the heat transfer.

The plastic deformation of the tubes are carried out by high pressure shock waves created by explosion of detonating cords positioned on the outer surface of the tubes.

Using the shock waves as tools acting on inner or outer surface of metallic tubes, shaped parts can be manufactured. The shock waves forming the metal tubes are created by chemical explosives. A chemical explosive is a compound or a mixture of compounds which, when subjected to heat, impact, friction, or shock, undergoes very rapid, self-propagating, heat- producing decomposition. This decomposition produces gases that exert tremendous pressures as they expand at the high temperature of the reaction. The work done by an explosive depends primarily on the amount of heat given off during the explosion. The high explosives can be utilized for many metalworking techniques.

The optimal form of the tubes has been designed by thermo-hydraulic computer simulation based on the ANSYS system.

Fig.1 Heat exchanger built with explosively formed tubes

Fig.2. Heat exchanger built with plain tubes

3. Results and conclusions

- Corrugation of the heat exchanger tubes creates extra turbulences resulting in enhancement of the heat transfer through the tube walls
- The heat transfer of the corrugated tubes are 8-15 % higher compared to the plain tubes
- The enhanced heat transfer gives the following advantages:
  - ✓ the heat transfer area (the geometry of the heat exhanger) can be reduced
  - ✓ a part of waste heat of the flue gases could be recovered so a considerable amount of primary fuel could be saved
- Corrugation can be carried out by shock waves acting on either the inner or outer surface of the tubes
- For industrial application more practical is the deformation of the tubes by shock waves acting on the outer suface of the tubes

4. References

[1] Mamalis A.G., Szalay A., Rath T., Preparation of metal/metal and metal/ceramic component parts by explosive compaction. Proc. 5th European Federation of Explosives Engineers (EFEE) World Conf., 26–28 April 2009, Budapest, pp. 279–284.

[2] Prümmer R, Explosive Welding, Forming and Compaction. Ed. T.Z. Blazynski, Applied Science, London 1983.

[3] Szalay A., G. Mamalis A. G., Zador I., Vortselas A.K., Lukacs L., Explosive metalworking: experimental and numerical modeling aspects International Symposium on Explosion, Shock wave and High-energy reaction Phenomena 2013 March 27 - 29, 2013 Nago, Okinawa, Japan

HIGH QUALITY SPLICES OF SUPERCONDUCTORS

A.Szalay[1a], A.G. Mamalis[2b], I. Zador[3c]

[1] *Puraset Water and Metall Solutions Ltd, Budapest, Hungary,* [a] *andras.szalay@puraset.hu*
[2] *Project Center for Nanotechnology and Advanced Engineering, NCSR "Demokritos", Greece,* [b] *agmamalis@yahoo.com*
[3] *KOGAT Ltd, Budapest, Hungary,* [c] *istvan.zador@kogat.hu*

1. Introduction

Important developments have been made in the technology over the last 50 years for the large-scale applications of superconductivity in terms of field strength, scale, field volume, and stored energy. The development of new conductors has increased their capabilities to withstand high current densities and large mechanical forces and stresses. The use of superconductors allows production of high field magnets. The magnets for NMR and MRI generally require superconducting splices.

Splice: a join consisting of two ropes, pieces of tape, etc. joined together at the ends.
(Definitions from Oxford Languages)

Reasons to prepare splices in NMR and MRI magnets:

- connection to power supply
- joining the preprepared superconducting units

Thus, the splicing technology is very important in developing applied products and expanding the practical applications.

To prepare splices is crucial from point of quality of the superconducting circuits: to ascertain superconducting quality of the splices is not an easy task.

Main requirements regarding the superconducting splices:

- Mechanically and electrically sound (low sub nΩ electrical resistance)
- Dismountable if necessary – multiple times
- Compact – space many times is an issue
- Use of tooling easy to multiply
- Possibly industrially based tooling

Based on our preliminary experiments, the explosive welding technique could satisfy all the criteria above for making high quality splice joints.

2. Experimental

Systematic R&D work was carried out for splicing together copper stabilized superconductor cables using the explosive welding technique. This technique represent new paradigm in the field of metalprocessings: joining of the materials can be carried out directly, by high speed, high energy shock waves. The shock waves can be created by high explosives.The high explosives are chemical systems, produced in different forms as powder, plastic or detonating cords. During the chemical reactions of these systems high pressure gases are created resulting high energy shock waves which prssed together the metals to be bonded. Advantages of the explosive cladding process over the conventional ones:

- Bond can be created between normally incompatible metals (e.g. titanium and copper)
- There is no practical limit to the ratio of thickness of the metals to be bonded
- The explosive cladding process requires minimum facilities and tooling

The general concept of the splicing technology is the following:

The superconducting cable will be embedded into a copper matrix (sleeve) by using the explosive welding technique. A shallow angle cut is introduced that splits the cable (where the sleeve is located) into two pieces.

NbTi foil is placed in between the two cable pieces at the location where the cut has been made. The NbTi foil will cover only the superconducting cable cross-section. The sleeve area will not be covered.

The two cable pieces will be cold welded together using the explosive welding technique. Series of experiments were performed according to the arrangement in Fig.1.

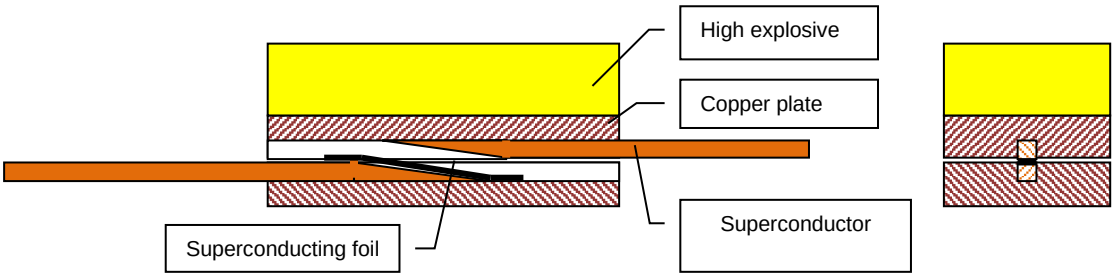

Fig.1. Arrangement of explosive splicing technology

Characteristic parameters of the components used for the experiments:

- Superconducting cable: NbTi 2,17mm*1,45mm
- Copper plate: CuE 50mm*35mm*4mm
- Superconducting foil NiTi 20mm*1,45mm*0,15mm
- High explosive: Permon 55 gramm

3. Results

The method applied for qualify the quality of the splices is based in making the splice in a loop of cable, inducing a current in it and measuring its decay time constant.

The electrical resistance of superconducting cable splices is in the 10^{-9} Ω range.

Conclusions:

- By applying the properly calculated and directed shock waves on a carefully designed experimental arrangement it is possible to weld superconducting wire ends creating splices
- Explosive material selection is of outmost importance, as critical diameter of the explosive will impose a minimal size constraint. By decreasing the critical diameter the splice size can be decreased. Performing of further systematic R&D work is needed to achieve practical application of this technique.
- NiTi foil can be welded on copper surface, material properties permit the use of foil insert. In splices the realization of foil insert needs further research

References:

[1] Kuchnir M., Electrical Resistance of Superconducting Cable Splices, Part of the Advances in Cryogenic Engineering book series (ACRE,volume 44)
[2] Decool P., Joints for superconducting magnets, MATEFU training school 05-09 April 2009 CEA
[3] Vincenzo D'Auria V., Bykovskiy N., Bruzzone P., Sedlak K., Diffusion-bonding between strands and modeling of splices of Nb3Sn Rutherford cables, EUCAS2021-269

ALGORITHMIC FOUNDATIONS OF OPTIMIZATION USING FINITE ELEMENT MODELING OF HIGH-SPEED GRINDING TECHNOLOGY IN APPLICATION TO 3D MICRO-LEVEL MODELS

A.G. Mamalis,[1,a] V.A. Fedorovich[2], D.V. Romashov[2,b*], Y.V. Ostroverkh[2]

[1] *Project Center for Nanotechnology and Advanced Engineering, NCSR "Demokritos", Athens, Greece,* [a]agmamalis@yahoo.com

[2] *Department of Integrated Engineering Techniques named after M.F. Semko, National Technical University "Kharkov Polytechnic Institute", Kharkov, Ukraine,* [b]romashov86@ukr.net

Abstract

Optimization consists in choosing the best of all possible options for implementing high-speed grinding technology. A complete enumeration of all options may turn out to be inefficient or practically impossible. Therefore, to solve such a problem, we should apply fundamental mathematical results and numerical methods of optimization theory, which allow choosing the best option without directly checking all possible solutions. Such a choice is realized by means of calculations carried out using special algorithms and is practically impossible without the use of computer technology.

Keywords: 3D modelling, methodology, diamond wheel, high-speed grinding, finite element method, simulations, micro-scale, optimization.

1. Introduction

The results of dynamic 3D modeling of high-speed diamond grinding processes allow to solve the following problems: at the design stage - calculation of the tool design for certain processing modes; at the manufacturing stage - determination of rational conditions for sintering the diamond-bearing layer of the wheel; at the stage of application - the theoretical determination of processing productivity, specific consumption of diamond grains. The solution of these problems allows to significantly increase the efficiency of processing during high-speed grinding.

2. Research methodology

As applied to ultrahigh-speed diamond grinding, the above scheme for solving optimization problems takes the following form.

The boundary of the object under study separates this object from other objects interacting with it and allows to separate the characteristics (object parameters into external and internal). [1] When considering the problems of optimization of high-speed grinding, the boundary of the object under study is chosen by the content of the problem under consideration. The boundary of the object under study can be determined by the spatial area of the cutting tool when solving problems of choosing the optimal characteristics of diamond wheels at the stage of their design and manufacture. [2] When solving problems of optimizing high-speed grinding processes using available cutting tools, taking into account the characteristics of the processed material, the boundary of the object under study can be determined by the area covering the processing diamond grain with the processed material around their contact interaction.

The obtained preliminary results for the values of the characteristic function of the problem of optimizing the processes of super hard material (SHM) high-speed grinding show that such a function can be quite accurately represented by approximation in the form of a quadratic function (1), which in the general case of n independent variables (factors) is written as follows:

$$Y = b_0 + \sum_{i=1}^{n} b_i X_i + \sum_{i=1}^{n-1} \sum_{j=i+1}^{n} b_{ij} X_i X_j + \sum_{i=1}^{n} b_{ii} X_i^2 \quad (1)$$

3. Maximizing the performance of high-speed SHM diamond grinding

In accordance with the initial data obtained from the results of 3D modeling [3], the matrix [A] (function (1) presented in matrix form) and the vector {B} (variables of function (1) presented in matrix form) are obtained as:

$$[A] = \begin{bmatrix} -7{,}66 & -0{,}001 & 0{,}01 & -0{,}001 \\ -0{,}001 & -6{,}5 & -0{,}02 & 0{,}06 \\ 0{,}01 & -0{,}02 & -24{,}1 & 0{,}32 \\ -0{,}001 & 0{,}06 & 0{,}32 & -19{,}04 \end{bmatrix}, \{B\} = \begin{Bmatrix} 0{,}02 \\ -0{,}07 \\ -6{,}79 \\ 0{,}51 \end{Bmatrix}, B_0 = 55{,}91 \quad (2)$$

As a result of solving the system, a stationary point X_{stat} was obtained:

$$X_{stat} = \begin{Bmatrix} \text{-2.24194024298796E-0003} \\ \text{9.70029544277527E-0003} \\ \text{2.81441311184647E-0001} \\ \text{-2.20249223085138E-0002} \end{Bmatrix}, Y_{stat} = \text{5.3025585390789573E+001} \quad (3)$$

where X_{stat} is the coordinate vector of the stationary point of the function; Y_{stat} is the value of the characteristic function at the stationary point

4. Accounting and risk assessment in the process of quantitative analysis and decision-making in expert systems

To do this, we use the basic scheme of statistical tests, which we use according to the scheme of the well-known sampling method. In accordance with this method, we consider the object under study (in this case, the results of optimizing the processes of high-speed grinding and sintering of diamond wheels) in the form of a general population, which is a set of possible results corresponding to various initial data. Thus, the errors in the result of optimizing the processes of high-speed grinding and sintering of diamond wheels will be presented as a result of the error in the initial data.

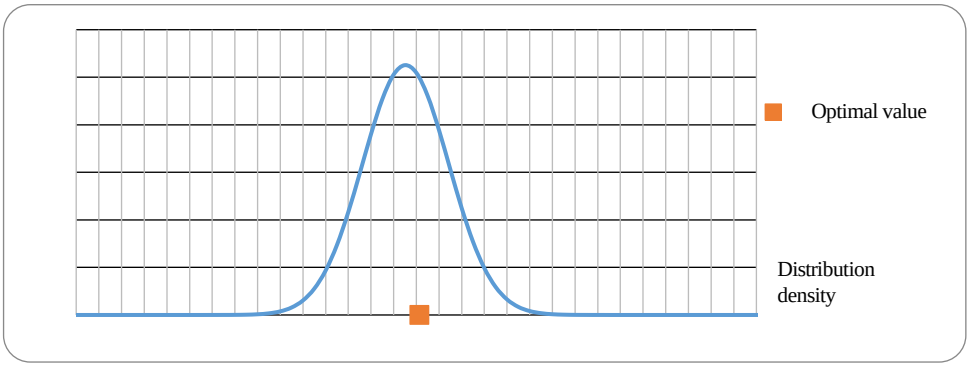

Fig. 1. The distribution density of the obtained optimization results and the optimal value for an example of optimizing the performance of high-speed diamond grinding

Conclusion

Fundamental mathematical approaches to optimization issues applicable to the study of the process of high-speed diamond processing of SHM are considered.

It is shown that in order to estimate the error of the results, it seems to apply the methods of mathematical statistics and consider the results obtained as one of the many possible implementations, i.e. estimate the probability that the result obtained has a predetermined error.

Special software has been developed that combines all the simulation results into an expert system that allows, with a certain probability and error, to predict the main indicators of the grinding process, depending on the various properties of the tool and processing modes.

References:

[1] Botta A., De Donato W., Persico V., Pescapé A. Integration of Cloud computing and internet of things: a survey. Future Generation Computer Systems, 56 (2016), pp. 684-700.

[2] Palsson F., Sveinsson J.R., Ulfarsson M.O. Multispectral and Hyperspectral Image Fusion Using a 3-D-Convolutional Neural Network. IEEE Geoscience and Remote Sensing Letters, 14 (5) (2017), pp. 639-643.

[3] Mamalis A.G., Grabchenko A.I., Romashov D.V., Fedorovich V.A., Kundrak J. Determination of the diamond wheel structure in high-speed grinding using nanoindentation techniques: Experimental and numerical simulation, Nanotechnology Perceptions, 2013, 9(3), pp. 187–197

COMPUTER SIMULATIONS OF STATIC STRESS-STRAIN STATES FOR LONG-LENGTH PRESSURISED PIPES WITH EXTERNAL PROTECTIVE THIN NANOENGINEERED COATING UNDER NONUNIFORM TEMPERATURE FIELDS

I.Sh. Nevliudov[1,a], A.G. Mamalis[2,b], Yu.V. Romashov[1,3,c]

[1]Kharkiv National University of Radio Electronics, Ukraine, Kharkiv, [a]igor.nevliudov@nure.ua
[2]Project Center for Nanotechnology and Advanced Engineering, NCSR "Demokritos", Greece, Athens, [b]agmamalis@yahoo.com
[3]V.N. Karazin Kharkiv National University, Ukraine, Kharkiv, [c]yurii.romashov@nure.ua

Abstract

Influence of nonhomogeneous temperature fields on the stress-strain state of the pressurized pipes is due to temperature dependencies of the structural material properties like Young's module, Poisson's ratio and linear expansion coefficient, so that the nonuniform temperature fields leads to the inhomogeneous of the material properties. It is proposed to use the differential equations formulated through the displacement and the stresses to consider the stress-strain state for axisymmetric long-length pipes with external protective thin nanoengineered coating taking into account the nonuniform temperature fields. The finite differences are used to make the computer simulations of the pipes with the external protective thin nanoengineered coating, and the cladding of nuclear fuel rods made from the Zr-based alloy with the thin protective coating made from the stainless steel is considered as the example. It is shown that consideration of structural material properties temperature dependencies can have the noticeable influence on the stress-strain-state estimations for the pressurized pipes with external protective thin nanoengineered coating under nonuniform temperature fields.

1. Introduction

The thin protective coatings are widely used for operability enhancing of different pressurised pipes including for the oil industry pipelines [1], for natural gas transportation pipelines [2], for steam boilers high-temperature pipes [3], for nuclear fuel claddings [4], as well as for other purposes. Effects of thin coating application is significant, so this idea has the further development, including through application of multilayers thin coatings [5], so that the researches about the pipes with thin protective coatings are in current interests at present, and a lot of existed scientific publications in this field confirm it.

The principal purpose of thin coating application for pressurized pipes is in corrosion protection of the main metal of the pipes from aggressive external mediums [6]. Different kinds of corrosion processes require developing of different protective coatings, so we have a lot of researches about the pipelines then coating to protect the particular kind of corrosion. The research [3] deals with the vanadium oxides induced high-temperature corrosion inherent for the steam boilers. The pipelines protective coatings to prevent the hydrogen embrittlement are considered in [7]. The specific corrosion processes of coated pipelines in soils taking into account of bacterial influencing are explored min [8]. At the same time, the protective coatings can be used to protect pipes not only from the corrosion, but also from other external influencing, including from the higher temperatures, like it is discussed in [9].

The implementation possibilities of thin coatings to protect the pipes are restricted by manufacturing capabilities and by the operability of such coatings under the pipes' exploitation conditions. In the research [10], the fabrication and behaviour investigation of new composite coating kinds for oils and gas pipelines are studied. The research [11] deals with studying about the manufacturing possibilities for making the internal coatings on the pipes. Possibilities of some manufacturing technology for making the nanocomposite coating with enhanced mechanical and corrosion protection are explored in [12]. Although, it is important to research influences of the manufacturing processes on the properties of pipes with thin protective coatings, but the principal difficulties are in anticipating these properties under the actual exploitation conditions of the pipes as the structural elements of complicated systems under influencing of different external factors. So, in the research [3], the corrosion processes from the vanadium oxide are considered taking into account a lot of different factors like the high temperature and the cyclic conditions. The crack safety of the cladding with the protective coating is considered in [13] with taking into account of the structural materials plastic behaviour. Protective thin coatings operability estimation is especially complicated for the claddings of nuclear fuel rods due to the specifics of the exploitation conditions in the cores of nuclear reactors, but this is principally required for design substantiation of the accident tolerant nuclear fuels [4]. The qualities of the coatings required to have the enhanced accident tolerant fuel claddings are researched in [14], and the performance of the nuclear reactor core loaded with such accident tolerance fuel is analysed in [15].

2. Computer simulations and discussing of the results

As the example, we will consider the pressurised pipe representing the nuclear fuel rod cladding made from the Zr-based alloy with the design similar to the well-known VVER-1000 nuclear reactor, but with the thin protective coating made from the stainless steel. The input data for the computer simulations will be following [16]:

$a = 3{,}9$ mm, $b = 4{,}55$ mm, $E_c = 177$ GPa, $\alpha_c = 17{,}5 \cdot 10^{-6} K^{-1}$, $h_c = 10\ \mu m$, (1)

$p_a = 10$ MPa, $p_b = 16$ MPa, $T_a = 340\ ^\circ C$, $T_b = 300$ °C, $T_0 = 20\ ^\circ C$. (2)

We can see (fig.1), that the temperature dependency of the linear expansion coefficient for the Zr-based alloy has the complicated form, and to take it into account we will use the cubic splines to interpolate the known values.

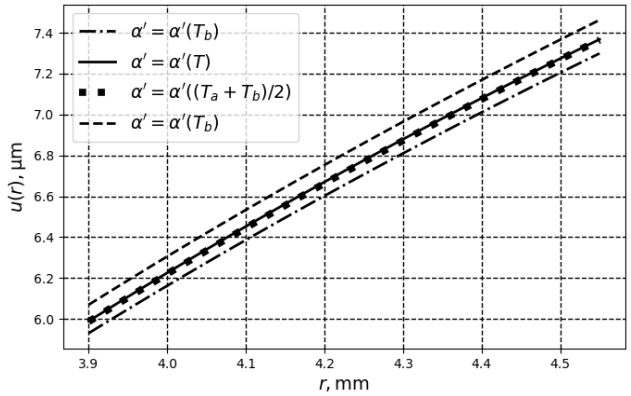

Fig.1. The radial displacements estimations

Conclusions

Due to the accomplished researches presenting in this article, the following conclusion can be formulated.

It is suitable to use the differential equations formulated through the displacement and the stresses to make the computer simulations of the static stress-strain states of the axisymmetric long-length pipes with external protective thin nanoengineered coating taking into account the nonuniform temperature fields. These differential equations can be numerically solved by using the finite differences, and it can be realised through the Python programming language to have the primary results.

The inhomogeneous of the material properties induced by the nonuniform temperature fields have noticeable influence on circumferential stresses leading, but it has no effects on the radial stresses and radial displacements of the pipes with the external thin protective coating. These regularities are shown for the particular example, and it is impossible to distribute them to all the cases, so that to have the reliable estimation for the stress-strain states in the pipes with the thin coatings, it is necessary to make the computer simulations for each particular case.

To have the reliable estimations of the stress-strain states in the pressurized pipes with thin protective nanoengineered coatings under exploitational conditions leading to nonuniform temperature fields, it is necessary to take into account the actual temperature dependencies of the structural materials properties, but not the different constant values estimating these properties on the average or others different senses.

References:

[1] Al Jabri H., Devi M.G., Al-Shukaili M.A. Development of polyaniline – TiO2 nano composite films and its application in corrosion inhibition of oil pipelines. *Journal of the Indian Chemical Society* **100(1)** (2023) 100826.

[2] Zhu L., Tang Y., Cao S., Jiang J., Wu C., Zhao K. Enhanced anti-microbial corrosion of nano-CuO-loaded Ni coatings on pipeline steels in simulation environment of natural gas transportation pipeline *Ceramics International* **49(3)** (2023) 5543-5549.

[3] Singh G., Bala N., Chawla V., Singla Y.K. Hot corrosion behavior of HVOF-sprayed carbide based composite coatings for boiler steel in Na2SO4–60 % V2O5 environment at 900 °C under cyclic conditions. *Corrosion Science* **190** (2021) 109666.

[4] Yang J., Steinbrück M., Tang C., Große M., Liu J., Zhang J., Yun D., Wang S. Review on chromium coated zirconium alloy accident tolerant fuel cladding. *Journal of Alloys and Compounds* **895(1)** (2022) 162450.

[5] He H., Liu C., He L., Wang G., Zhang W., Zhao S., Xiang Y., Yi J. Microstructure, mechanical properties and high temperature corrosion of [AlTiCrNiTa/(AlTiCrNiTa)N]20 high entropy alloy multilayer coatings for nuclear fuel cladding. *Vacuum* **212** (2023) 112057.

[6] Hussein Farh H.M., Ben Seghier M.E.A., Zayed T. A comprehensive review of corrosion protection and control techniques for metallic pipelines. *Engineering Failure Analysis* **143(A)** (2023) 106885.
[7] Lei Y., Hosseini E., Liu L., Scholes C.A., Kentish S.E. Internal polymeric coating materials for preventing pipeline hydrogen embrittlement and a theoretical model of hydrogen diffusion through coated steel. *International Journal of Hydrogen Energy* **47(73)** (2022) 31409-31419.
[8] Wei B., Xu J., Cheng Y.F., Sun C., Yu C., Wang Z. Effect of uniaxial elastic stress on corrosion of X80 pipeline steel in an acidic soil solution containing sulfate-reducing bacteria trapped under disbonded coating. *Corrosion Science* **193** (2021) 109893.
[9] Abu-warda N., López A.J., López M.D., Utrilla M.V. Ni20Cr coating on T24 steel pipes by HVOF thermal spray for high temperature protection. *Surface and Coatings Technology* **381** (2020) 125133.
[10] MacLean M., Farhat Z., Jarjoura G., Fayyad E., Abdullah A., Hassan M. Fabrication and investigation of the scratch and indentation behaviour of new generation Ni-P-nano-NiTi composite coating for oil and gas pipelines. *Wear* **426–427(A)** (2019) 265-276.
[11] Sousa F.A., da Costa J.A.P., de Sousa R.R.M., Barbosa J.C.P., de Araújo F.O. Internal coating of pipes using the cathodic cage plasma nitriding technique. *Surfaces and Interfaces* **21** (2020) 100691
[12] Sliem M.H., Shahzad K., Sivaprasad V.N., Shakoor R.A., Abdullah A.M., Fayyaz O., Kahraman R., Umer M.A. Enhanced mechanical and corrosion protection properties of pulse electrodeposited NiP-ZrO2 nanocomposite coatings. *Surface and Coatings Technology* **403** (2020) 126340.
[13] Wei J., Xu Z., Li J., Liu Y., Wang B. Crack safety analysis of coating with plastic behavior in surface-coated Zircaloy cladding. *Engineering Fracture Mechanics* **280** (2023) 109134.
[14] Ridley M., Bell S., Garrison B., Graening T., Capps N., Su Y.-F., Mouche P., Johnston B., Kane K. Effects of Cr/Zircaloy-4 coating qualities for enhanced accident tolerant fuel cladding. *Annals of Nuclear Energy* **188** (2023) 109799.
[15] Jeong E., Jo Y., Shin C.H., Yang Y.-S., Kim J.-Y., Lee D. Performance analysis of nuclear reactor core loaded with Accident-Tolerant Fuel: Mo/Cr metallic microcell UO2 pellets and CrAl coating. *Annals of Nuclear Energy* **175** (2022) 109217.
[16] Mamalis A.G., Romashov Yu.V. Enhanced operability of nuclear fuel rod cylindrical cladding made with thin protective nanoengineered coatings. *Nanotechnology Perceptions* **17(1)** (2021) 74–81.

MAGNETIC SHIELDING MATERIALS FOR ELECTRIC VEHICLES

T. Damatopoulou[1,a], S. Angelopoulos[1,b], A. Ktena[2], P. Svec[3,c], A. Mamalis[4,d], E. Hristoforou[1,e]

[1] Laboratory of Electronic Sensors, National TU of Athens, Zografou Campus, Athens 15780, Greece,
[a]damatat5@central.ntua.gr, [b]spyrosag@central.ntua.gr , [c]hristoforou@ece.ntua.gr
[2]National Kapodistrian University of Athens, Greece
[3]Slovak Academy of Sciences, Bratislava, Slovakia, [c]peter.svec@savba.sk
[4]Project Center for Nanotechnology and Advanced Engineering (PC-NAE), NCSR Demokritos, Athens, 15310, Greece, [d]agmamalis@yahoo.com

Abstract. In this paper, the classic low carbon steel used as structural part of the bottom part of the car is tested to additionally become operational part of the electric vehicles as the magnetic shielding material after magnetothermal annealing. The low carbon steels (LCS) were studied in their as-received form and after thermal annealing in 350oC for 1 hour in inert atmosphere with a consequent slow cooling for 24 hours, followed by magnetic annealing in 350oC for 1 hour in inert atmosphere under 0.1T field, followed by slow cooling for 24 hours under the presence of the applied field. A typical change in the differential magnetic permeability of LCS after the annealing process increased up to 200,000. In the meantime, hardness tests illustrated a negligible change (decrease) of mechanical stiffness. Apart from that, the magnetic anisotropy of welded samples has been determined by monitoring the permeability in different in-plane axes, since these steel sheets are to undergo a welding process during manufacturing. The study of the samples with TEM (JEOL operating at 220 kV) was done to monitor the disorder structures created in LCS before and after magneto-thermal treatment. Indeed, a remarkable decrease in dislocation density was observed, thus correlating the increase of permeability with the microstructure enhancement.

Keywords: **Soft magnetic materials, magnetic field shielding, electric vehicles (EV)**

OPTIMIZING QE OF CCD BY MODIFYING BLACKCOMET DETECTOR

J.J. Shainidze[1, a], N.K. Gomidze[1, b]

[1] *Batumi Shota Rustaveli State University, Batumi, Georgia*
[a] *jaba.shainidze@bsu.edu.ge*, [b] *gomidze@bsu.edu.ge*

Abstract. Charge-Coupled Device (CCD) is a type of image sensor technology used in digital cameras, video cameras, and various scientific and industrial applications to capture and convert light into electronic signals. Such sensors offer several advantages, including high sensitivity to light, low noise levels, and good image quality with high dynamic range. They are commonly used in applications that require precise and high-quality imaging, such as astronomy, microscopy, and spectroscopy. However, there are many ways to improve and optimize the role of CCD sensors in spectroscopy, and this could have a significant impact on the sensitivity, safety, and accuracy of measurements.

1. Introduction

One of the ways of optimization of a CCD (Charge-Coupled Device) sensor involves improving its performance in various aspects such as sensitivity, noise reduction, dynamic range, resolution, and overall image quality. One of the common techniques used for optimizing CCD sensors is enhancing the sensor's quantum efficiency (QE) to improve its sensitivity to light. The way we process the data can also affect the QE of CCD detector. It is essential to make sure that we have used appropriate data processing techniques, such as using background subtraction or noise reduction techniques, which will ultimately give us one opportunity to improve the signal-to-noise ratio.

One of the ways of optimizing a CCD (Charge-Coupled Device) sensor involves improving its performance in various aspects such as sensitivity, noise reduction, dynamic range, resolution, and overall image quality. Khajishvili et al. [1] investigated the estimation of signal-to-noise ratio (SNR) of a CCD camera for OD medium, highlighting the importance of optimizing CCD performance. Gomidze et al. [4] discussed the problems related to fluorescence excitation spectra, emphasizing the significance of addressing these issues in CCD sensor design. Gomidze et al. [3] conducted 3D fluorescence spectroscopy to study the distribution of bioparticles, highlighting the need for improved CCD performance to enhance data quality.

Furthermore, research by Khajisvili et al. [2] focused on 3D fluorescence spectroscopy of liquid media via the internal reference method, highlighting the importance of optimizing CCD sensitivity for accurate measurements. Groom et al. [5] developed a quantum efficiency model for a thick back-illuminated astronomical CCD, contributing to the understanding of CCD performance optimization. Prasad and Sinha [6] provided a comprehensive review of signal-to-noise ratio in CCD imaging systems, highlighting the significance of noise reduction techniques for improved performance. Kumar et al. [7] discussed optimizing the signal-to-noise ratio of CCD cameras for quantitative optical microscopy, emphasizing the role of data processing techniques.

Considering the impact of data processing techniques, it is crucial to utilize appropriate approaches such as background subtraction and noise reduction techniques to enhance the signal-to-noise ratio [6]. These techniques, combined with advancements in CCD design and optimization, contribute to improving the overall image quality and quantum efficiency of CCD sensors.

One of the impotent problem is the "Noise Reduction". By addressing this problem, we can improve the signal-to-noise ratio (SNR) of the BlackComet detector.

To decrease the SNR of the BlackComet detector, applying specific code that allows changing the quantum efficiency (QE) of the CCD sensor can be beneficial. By optimizing the QE, which affects the sensitivity of the detector to light, we can enhance the overall performance and reduce the noise in the captured images.

In addition to data processing, implementing efficient image processing algorithms is another crucial aspect. Techniques such as background subtraction, flat-field correction, or deconvolution can effectively reduce noise and enhance the signal-to-noise ratio of the detector. By optimizing these algorithms and incorporating them into the data processing pipeline of the BlackComet detector, we can achieve improved image quality and more accurate measurements.

2. Experiment and program overview

The experimental part of our research is performed on the detector BlackComet produced by StellarNet, which includes a CCD sensor. Black Comet spectrometers are equipped with high-performance CCD sensors with excellent sensitivity and low noise over a wide wavelength range. These detectors feature a thermoelectric cooling system to reduce noise levels and increase stability. This is why these detectors are ideal for

applications such as absorption/transmission spectroscopy, fluorescence spectroscopy, and Raman spectroscopy.

One of the techniques to optimize the characteristics of the CCD sensor of the BlackCommet detector is to manage the hardware capabilities in software. However, it is important to note that optimizing the CCD sensor code of the BlackCommet detector is a complex task that requires deep knowledge of both the detector and the programming language used. Below is one of the codes specially developed for our detector (BlackCommet) and whose purpose is to clean and process the detrended spectra by comparing them with the reference spectra. The code is presented in the Mathematics language of the wolfram software package:

```
(* Load the CCD image *)
ccdImage = Import["path/to/image.fits"];
(* Perform background subtraction *)
background = MedianFilter[ccdImage, 5];
backgroundSubtracted = ImageSubtract[ccdImage, background];
(* Perform flat-field correction *)
flatField = Import["path/to/flatfield.fits"];
flatFieldCorrected = ImageMultiply[backgroundSubtracted, 1/flatField];
(* Perform deconvolution *)
psf = Import["path/to/psf.fits"];
deconvolved = ImageDeconvolve[flatFieldCorrected, psf];
(* Display the results *)
ImageCollage[{ccdImage, backgroundSubtracted, flatFieldCorrected, deconvolved}]
```

In this code, we first loaded the spectral image formed by the CCD sensor using the import function. We then performed background subtraction by calculating the median of the image using the MedianFilter function and subtracting it from the original image using the ImageSubtract function.

Next, we performed flatfield correction by loading a flatfield image using the Import function and multiplying it by the background-subtracted image using the ImageMultiply function.

Finally, we performed deconvolution by loading the point spread function (PSF) using the import function and deconvolving the flat field corrected image using the ImageDeconvolve function.

The results were then displayed using the ImageCollage function, which created a composite image showing the original image formed by the CCD sensor, the background subtracted image, the flat-field corrected image, and the deconvolved image.

3. Results

Obtained images allowed us to obtain the graph of SNR dependence on path length and detector integration time.

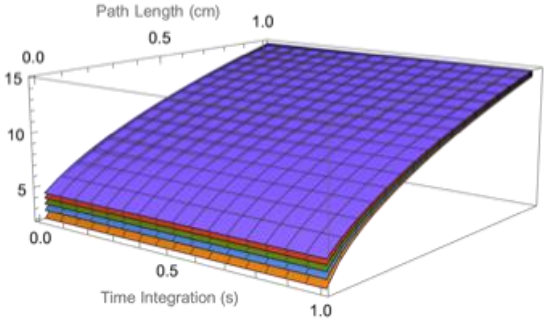

Fig. 1. SNR three-dimensional dependence on beam path length and detector integration time, when the concentration is c=0.01 mol/L, and molar absorption coefficient ε=20000 L/(mol*cm)

Conclusions

- Decreasing of SNR of BlackComet detector is possible by applying specific code, which allows change of the QE of the CCD of the detector.
- The way we process the data can also affect the QE of our detector. It is essential to make sure that we have used appropriate data processing techniques, such as using background subtraction or noise reduction techniques, which will ultimately give us one opportunity to improve the signal-to-noise ratio.

- Implementing efficient image processing algorithms can help reduce noise and improve the detector's signal-to-noise ratio. This may include techniques such as background subtraction, flat-field correction, or deconvolution.

References

[1] Khajishvili M., Gomidze N., Shainidze J. Estimation SNR of CCD camera for OD medium. The Eurasia Proceedings of Science, Technology, Engineering & Mathematics (EPSTEM). ISBN:978-605-73797-9-5 ISSN: 2602-3199, Publication date: 2022, Pages: 130-138.

[2] Khajisvili M.R., Gomidze N.Kh, ShainidzeJ.J. 3D FluorescenceSpectroscopyof Liquid mediavia internal reference method. INTER-ACADEMIA 2021: Research and Education: Traditions andInnovations, Partof the Lecture Notes in Networks and Systems book series (LNNS,volume 422,pp.59-71). DOI: 10.1007/978-981-19-0379-3_7.

[3] Gomidze N.Kh., Shainidze J.J., Khajishvili M.R., Jabnidze I.N., Makharadze K.A., Kalandadze L.G., Nakashidze O.M., Surmanidze Z,J., Mskhaladze E.N., Gomidze L.N. 3D fluorescence spectroscopy to study the distribution of bioparticles. International Scientific Conference Modern Research Methods of Bio-Nano-Agents, 24-26 November, pp.21-27, BSU, Batumi. ISBN: 978-9941-488-46-7.

[4] Gomidze N., Shainidze J., Shengelia G., Turmanidze R. *To the problems of fluorescence excitation spectrums.* International scientific journal "machines. Technologies. Materials." web ISSN 1314-507X; print ISSN: 1313-0226, pp.279-282, 2018.

[5] Groom D.E., Haque S., Holland S.E., Kolbe W.F., Quantum efficiency modeling for a thick back-illuminated astronomical CCD, Journal of Applied Physics, 122, 2017

[6] Prasad S., Sinha S.K., Signal-to-Noise Ration in CCD Imaging Systems: A Revies, 2021.

[7] Kumar D. et al, Optimizing the Signal-to-Noise Ratio of CCD Cameras for Quantitative Optical Microscopy, 2020

INFLUENCE OF SURFACE ROUGHNESS ON THE AMPLITUDE OF GIANT MAGNETORESISTANCE EFFECT IN MULTILAYERED THIN FILMS

A. Melikadze[1,a], L. Kalandadze[1,b], N. Gomidze[1,c]

[1] *Department of Physics, Batumi Shota Rustaveli State University, Georgia*

[a] aleksander.melikadze@gmail.com, [b] lali.kalandadze@bsu.edu.ge , [c] gomidze@bsu.edu.ge

Since the discovery of one of the most engrossing advances in solid state physics occurred, the discovery of the giant magnetoresistance effect (GMR) by Grünberg and Fert in 1988 the theoretical treatment of this effect became the subject of much attention [1-6]. It is considered that the effect of giant magnetoresistance is due to the spin-dependent scattering of charge carriers in the volume of magnetic layers and at their boundaries, and its amplitude depends on the degree of roughness of the outer and interlayer boundaries. Nevertheless, when it comes to detail, discrepancies between experimental observations and theoretical models can arise: a realistic theoretical description of electron scattering at lattice discontinuities, disorder or defects is still a crucial factor [6,7]. Despite a large number of both experimental and theoretical works, in which the influence of the state of outer boundaries and interfaces on the magnitude of the giant magnetoresistance was studied, conclusions do not coincide [1-6]. The need to resolve these contradictions should be carried out within the framework of an extended theoretical study of the giant magnetoresistance effect using more complex models for describing the interaction of charge carriers with the structure and interlayer boundaries. This was the subject of our study. As an example, we considered a three-layer film (fig.1) consisting of ferromagnetic metal layers of different thicknesses separated by a nonmagnetic ultrafine metal layer (sandwich).

Fig.1 Model of the three-layer sandwich

The giant magnetoresistance effect is the change of the electrical resistance in a system of layers when an external magnetic field changes the magnetization of the ferromagnetic layers relative to each other. A parallel orientation is characterized by an electrical state of low resistance, while an antiparallel orientation is a state of high resistance. The effect size is defined as:

$$\delta = \frac{R_H - R_0}{R_0} = \frac{(R_\uparrow - R_\downarrow)^2}{4R_\uparrow R_\downarrow} = \frac{(J_\uparrow - j_\downarrow)^2}{4J_\uparrow J_\downarrow} \quad (1)$$

where, $J_{\uparrow\downarrow} = eq_{\uparrow\downarrow}\langle V_{\uparrow\downarrow}\rangle$ is the current density; $q_{\uparrow\downarrow}$, is the density of electrons with spin projections on the z axis equal to +1/2 and -1/2, $q = n_\uparrow + n_\downarrow$ is the total electron density, $\langle V_{\uparrow\downarrow}\rangle$ is the average velocity of electrons with corresponding spin projections.

The longitudinal conductivity σ of a magnetic sandwich is calculated using the semi-classical Boltzmann kinetic equation for the boundary conditions to describe the transport of electrons in metals, according to which [1]:

$$\sigma_{\uparrow\downarrow} = \sum_{s=\pm} \sum_{j\neq n=1}^{2} \sigma_j^{(n-j)s} = \frac{1}{d} \sum_{s=\pm} \sum_{j\neq n=1}^{2} d_j \, \sigma_{0j}^{(n-j)s} \Phi_J^{(n-j)s} \quad (2)$$

$\Phi_J^{(n-j)s}$ Dimensional functions that determine the effect of layer sizes for the samples with constant roughness amplitude [1,6]. For $\delta_{\uparrow\uparrow}$, when magnetization of adjacent ferromagnetic layers is in a parallel:

$$\sigma_{\uparrow\uparrow} = \sum_{s=\pm} \sum_{j=1}^{2} \sigma_{\uparrow\uparrow\, j}^{s} = \frac{1}{d} \sum_{s=\pm} \sum_{j=1}^{2} d_j \, \sigma_{0\, j}^{s} \Phi_{\uparrow\uparrow j}^{s} \quad (3)$$

For numerical calculations, it was assumed that the magnetic anisotropy is relatively small and can be neglected. It is convenient to write delta in the following form:

$$\delta_{\uparrow\downarrow} = \frac{\sum_{j\neq n=1}^{2} (d_{j,n}\, \sigma_{0j,n}^{-})^{j-1} (\Phi_{\uparrow\uparrow,j}^{-} + \alpha_{b.j} \Phi_{\uparrow\uparrow,j}^{+})}{\sum_{j\neq n=1}^{2} (d_{j,n}\, \sigma_{0j,n}^{+})^{j-1} (\Phi_{\uparrow\downarrow,j}^{-} + \alpha_{b.j} \Phi_{\uparrow\downarrow,j}^{+})} - 1 \quad (4)$$

$\alpha_{b,j}$ determines the spin asymmetry $\alpha_{b,j} = \frac{\sigma^{+}_{0,j}}{\sigma^{-}_{0,j}}$.

We performed calculations for a classical Fe/Gr/Fe sandwich, for which the velocities of charge-carrying particles are known, $v_j^{+} = 7{,}1 \times 10^5$ m/s ϙϑ $v_j^{-} = 8{,}51 \times 10^5$ m/s;

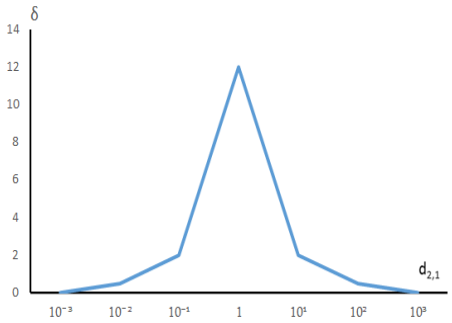

Fig.2. Dependence of the change in electrical Conductivity δ on the ratio of the layer thicknesses $d_{2,1} = d_2/d_1$

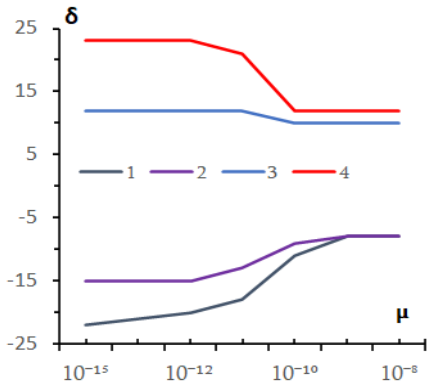

Fig.3. Dependences of the change in conductivity δ on the magnitude of the roughness μ of the interlayer and outer boundaries for Fe/Gr/Fe

Fig.2 presents that if the thickness of the ferromagnetic conducting layers is of the same order $d_{2.1} = d_2/d_1 \sim 1$, then the graph will show the maximum conductivity value, which is due to the spin scattering of bulk and interface electrons of the sample. From the Fig.3 we can conclude that the specular scattering of charge carriers by the interlayer and outer boundaries increases the amplitude of the giant magnetoresistance effect due to the fact that they do not lose their spin information when reflected from the surface. However, it should be noted that in the case when scattering centers are concentrated at the interlayer boundary, this leads to screening of charge carriers and, accordingly, to a decrease in the effect.

References

[1] Shkurdoda Yu.O., Dekhtyaruk L.V., Basov A.G., Chornous A.M., et al. The giant magnetoresistance effect in Co/Cu/Co three-layer films, Journal V.477, Pages 88-91, 2019. https://www.sciencedirect.com/science/article/abs/pii/S0304885318329597

[2] Cyrille M.C., Kim S., Gomez M.E. et al., Enhancement of perpendicular and parallel giant magnetoresistance with the number of bilayers in Fe/Cr superlattices / // Rev. B:– 2000.– V.62, №5. pp. 3361 – 3367. (2000) DOI: https://doi.org/10.1103/PhysRevB.62.3361

[3] Olligs D., Burgler D.E, Wang Y.G., et al. Roughness - induced enhancement of giant magnetoresistance in epitaxial Fe/Cr/Fe (001) layers, Europhysics Lett. V.59, №3, pp.458 – 464. (2002) 10.1209/epl/i2002-00217-9

[4] Bae Seongtae, J. Jack H., P.J. Chen/ Dependence of physical properties and giant magnetoresistance ratio on substrate position during rf sputtering of NiO and Fe_2O_3 for bottom spin valves J. Appl. Phys. Lett. V.81, №12. P. 2208 – 2210. (2002)

[5] Bae, S., Chen, P., Egelhoff Jr., W. and Judy, J. Effects of Sputtering Angle on Surface Roughness, Chemical Composition and Giant Magnetoresistance Properties of NiO and α-Fe_2O_3 Bottom Spin-Valves, IEEE Transactions on Magnetics (Accessed February 1, 2023) https://www.nist.gov/publications/effects-sputtering-angle-surface-roughness-chemical-composition-and-giant

[6] Shabelnyk Y. M et al. Dimensional Effect in Magnetoresistance in the Three-Layer Magnetic Films, *IEEE 11th International Conference Nanomaterials: Applications & Properties (NAP)*, Odessa, Ukraine, 2021, pp. 1-3, doi: 10.1109/NAP51885.2021.9568401

[7] Melikadze A. Kalandadze A. Gomidze N. Effects of Surface Roughness on the Giant Magnetoresistance Performance in Magnetic Sandwiches. Abstract book of 66th International Open Readings Conference for students of Physics and Natural Sciences, April 18th-21st, (2023), p.393 https://www.openreadings.eu/wpcontent/uploads/2023/05/OpenReadings23_abstract_book.pdf

FEATURES OF MAGNETIZATION OF FERROMAGNETIC COMPOSITES: ROLE OF GRAIN CHAINS ON AN EXAMPLE OF GRANULATED MEDIA

D.A. Sandulyak[1], A.A. Sandulyak[1], M. N. Polismakova[1], A.V. Sandulyak[1], I.A. Solovev[1], A.P. Dwivedi*[2] , C.C. Doumanidis[2]

[1]MIREA — Russian Technological University, Moscow, Russia
[2]Guangdong Technion-Israel Institute of Technology, Shantou, China, [*]anand.dwivedi@gtiit.edu.cn

Abstract: The purpose of the article is to develop a model of chain-by-chain magnetization of granular media, in which chains of granules are basic elements. When a granular medium is magnetized, such as when consisting of ferromagnetic spheres, the chains of contacting granules (spheres) serve as self-sufficient conductors of the magnetic flux Φ. Each of these chains is characterized by a pronounced redistribution Φ in its cross section. If in the chain of spheres with radius R the conditional core with radius r is selected and for measurements Φ to surround its loop placed between the contacting spheres, then an increase in r decreases the thread density (magnetic induction B). According to Φ, detailed information on B in the cores and their magnetic permeability μ with the magnetization of the chains in the solenoid is obtained.

Keywords: Magnetic Permeability, Magnetic Flux, Granulated Medium, Grain Chains.

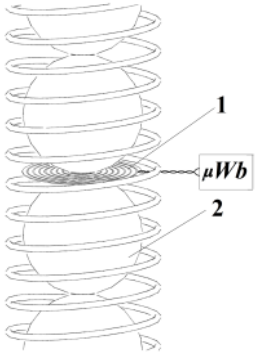

Fig.1. A chain of spheres *2* (located in solenoid) with a circular loop-sensor *1* connected to the microwebermeter

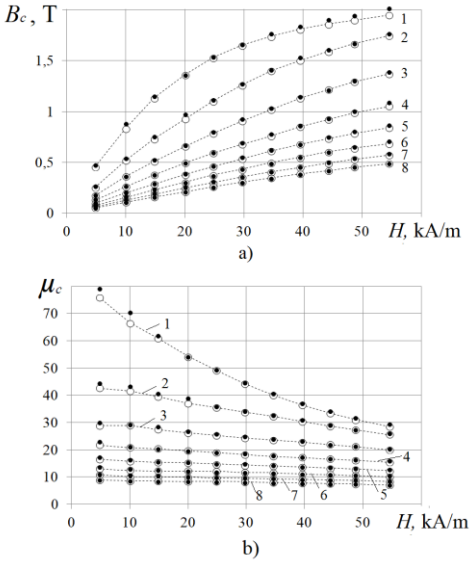

Fig.2. Magnetic induction B_c data (a) and magnetic permeability μ_c (b) for different (r_c/R) cores of chain of spheres in the dependence from intensity of the magnetizing field H: *1* – r_c/R=0.2; *2* – 0.3; *3* – 0.4; *4* – 0.5; *5* – 0.6; *6* – 0.7; *7* – 0.8; *8* – 0.9. Shaded (•) and not shaded (○) points belong to chain of spheres with a radius R = 15 mm and R = 20 mm accordingly

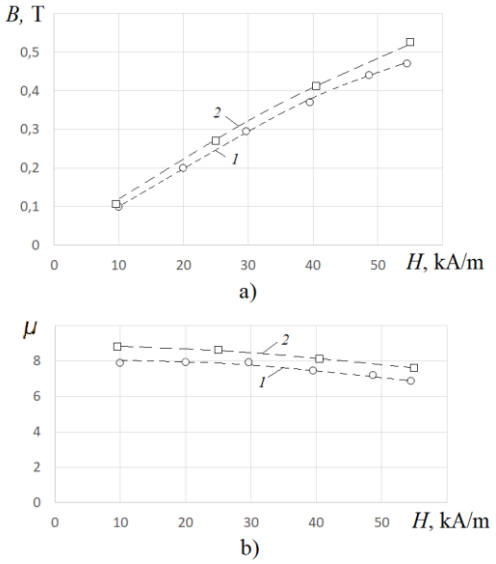

Fig.3. Field dependencies of magnetic induction *B* (a) and magnetic permeability *μ* (b): *1* – for chain of spheres (at r_c/R =0.9-1); *2* – for polyball media

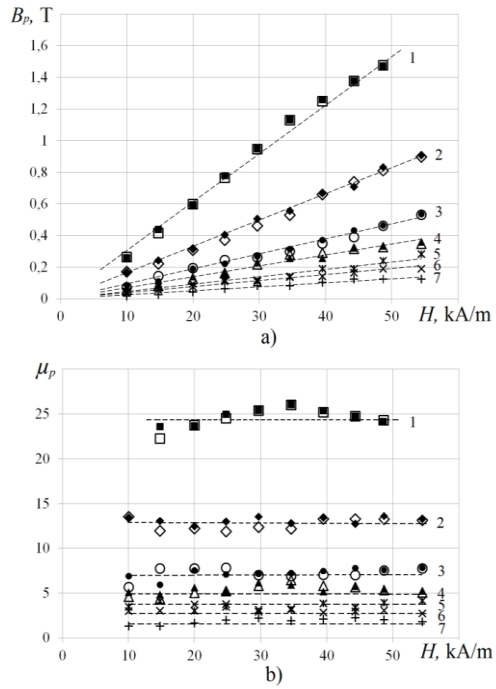

Fig.4. Magnetic induction B_p data (a) and magnetic permeability μ_p (b) for different relative radius of pipe "layer" of chain in the dependence from intensity of the magnetizing field *H*: *1* – r_p/R = 0,25; 2 – 0,35; 3 – 0,45; 4 – 0,55; 5 – 0,65; 6 – 0,75; 7 – 0,85. Shaded (■, ♦, ●,▲) and not shaded (□, ◊, ○, Δ) points of dependences 1-4 belong to chain of spheres with a radius *R* = 15 mm and *R* = 20 mm accordingly; points (✳, ×, +) of dependences 5-7 are common for *R* = 15 mm and *R* = 20 mm

EXCITONS AND BIEXCITONS IN CYLINDRICAL NANOWIRES OF GROUP II-IV MATERIALS

Z.S. Machavariani[1,3,a], R.Ya. Kezerashvili [2,c] and T. Tchelidze[1,b,c]

[1] *Department of Exact and Natural Sciences, Tbilisi State University, 0179, Tbilisi, Georgia*
[2] *Physics Department, New York City College of technology, The City University of New York, Brooklyn, New York 11201, USA*
[3]*Doctoral School, Kutaisi International University, Youth Avenue, 5th Lane, 4600 Kutaisi, Georgia*
[a] zaal.machavariani@tsu.ge , [b] rkezerashvili@citytech.cuny.edu, [c] tchelidze@tsu.ge

Abstract. A study of the trion and biexciton in a nanowire (NW) in the framework of the effective-mass model is presented. We consider the formation of trions and biexcitons under the action of both the lateral confinement and the localization potential. The analytical expressions for the binding energy and eigenfunctions of the trion and biexciton are obtained and expressed by means of matrix elements of the effective one-dimensional cusp-type Coulomb potentials whose parameters are determined self-consistently by employing eigenfunctions of the confined electron and hole states. Our calculations for the ZnO/ZnMgO, CdSe/ZnS and CdSe/CdS core/shell cylindrical shaped NWs show that the trion and biexciton binding energy in NWs are size-dependent and for the same input parameters the biexciton binding energyin NWs is always larger than the binding energy of the trion. The associative ionization of biexciton antibonding states into trion bonding states that leads to the formation of trions is studied. Based on the results for size dependence of biexciton binding energy and probability associative ionization an optimal radius for optoelectronic application NW is suggested.

1. Introduction

Recent studies of one-dimensional (1D) nanostructures nanowires [1] and nanotubes [2] show trion and biexciton binding energy depend on the electron ratio and the geometric characteristics of a nanostructure. exciton complexes like trions in solid state physics are very the few-body bound systems in atomic and nuclear physics major difference related to band effects, which make masses of the electrons and holes smaller than the bare electron and screening effects, resulting from the host lattice, which Coulomb force much weaker than in atomic systems. we present a theoretical approach to study a trion and a biexciton in a NW in the framework of the effective-mass model. We consider the formation of trions and biexciton under the action of both the lateral confinement and the localization potential. Our approach allows us to obtain analytical expressions for the binding energy and eigenfunctions of the trion and biexciton.

2. Theoretical formalism

To solve the problem of a positive trion (two holes and one electron) and biexciton (two holes and two electrons) laterally confined in a quantum NW we adopt the Born-Oppenheimer approximation, very well known in physics of molecules. The Born-Oppenheimer approximation accounts for a difference in masses of light and heavy particles and assumes that the light particles can respond almost instantly to heavy particles' displacement. The best example for a such system is a hydrogen molecular ion H_2^+ and a hydrogen molecule H_2 , which as a positively charged trion and biexciton consist from two heavy and one light and two heavy and two light particles, respectively. Therefore, instead of solving the three-body Schrödinger equation for all particle simultaneously one can treat heavy particles as motionless and solve the Schrödinger equation for a definite position of heavy particles, taking the interparticle separation as a parameter R [3]. After that calculations are carried out for different R. The application of the Born-Oppenheimer approximation naturally separates the calculation into the following steps: due to the strong lateral confinement perpendicular to the NW one first calculates the two dimensional (2D) energies and wave functions of the electron and hole, while neglecting the Coulomb interaction between them. Therefore, the fast transverse motions of charge carriers remain independent of each other. Next, using these wave functions of transverse electron and hole motion, one can average the three-dimensional (3D)Coulomb potential to a 1D Coulomb interaction between the charge carriers along the NW. Finally, after an appropriate modeling of these potentials by functions which depend on the distance between the charge carriers, one should find energies and wavefunctions for a trion or a biexciton for each fixed position of the holes by solving the corresponding reduced 1D Schrödinger equations.

3. Results

We calculate the trion and biexciton binding energies in ZnO/ ZnMgO, CdSe/ZnS and CdSe/CdS core/shell quantum structures of a cylindrical shape and study the dependence of their binding energies on the radius of the NW. Biexciton binding energy in such NWs is size-dependent. In Fig.1 we present the calculated

biexcitons's bounding energy dependence on NW's core radius (a) and shell thickness (b) for ZnO/ZnMgO and CdSe/ZnS core/shell cylindrical shaped NWs, which are prime examples for group II –IV materials. It was revealed that a radius reduction down to 1.5 nm enhances binding energy of the exciton, trion and biexciton in ZnO/ZnMgO NW, while for the biexciton in CdSe/CdS quantum NW the maximum binding energy is obtained for the thinner NW with 1 nm radius. The excitonic complexes remain stable in CdSe/ ZnS NW with the increase of the dielectric shell, while in ZnO/ZnMgO NW the trion and biexciton become unstable when the surrounding dielectric shell exceeds 2-2.5 nm.

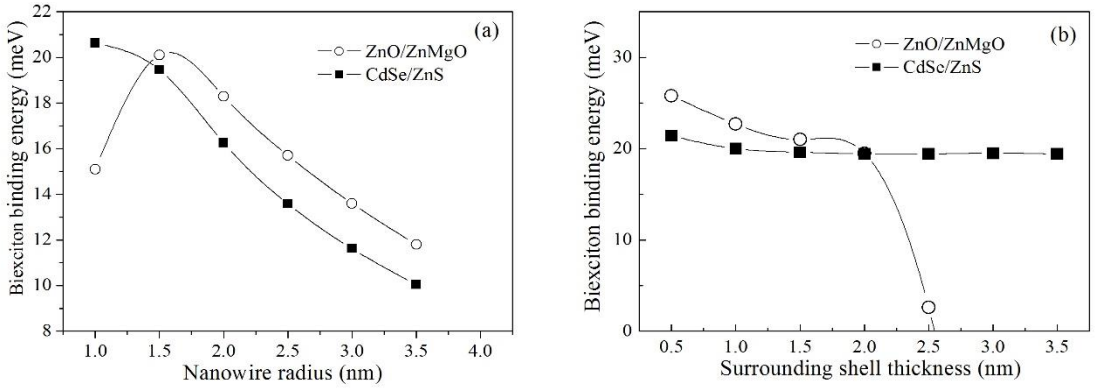

Fig.1. Dependence of the biexciton binding energy (a) on NW's core radius when shell thickness is 2 nm and (b) on the thickness of the surrounding dielectric shell when core radius is 1.5 nm.

Conclusions:

Based on the results for size-dependence of biexciton binding energy and probability associative ionization optimal radii of NWs for optoelectronic application are suggested. We suggest the mechanism of formation of the trion via associative ionization of a biexciton. As for probability of the associative ionization of biexciton into vulnerable to Auger decay trion states, it continually decreases with increasing the radius of NW. This leads us to the conclusion that 1–2 nm radius of NW should be optimal for optoelectronic application at high excitation intensity.

References:

[1] Kezerashvili R.Ya., Machavariani Z.S., Beradze B., Tchelidze T. Physica E: Low-dimensional Systems and Nanostructures 109 pg 228-241 (2019)
[2] Santos S.M., Yuma B., Berciaud S., Shaver J., Gallart M., Gilliot P., et al., Phys. Rev. Lett. 107 (2011) 187401. I.V. Bondarev, Phys. Rev. B 83 (2011) 153409.
[3] Atkins P., Friedman R. Molecular Quantum Mechanics, fifth ed., Oxford University Press, New York, 2011.

CAN THE FORMATION OF COMPENSATING DONORS BE SUPPRESSED IN MODULATED P-DOPPED GALLIUM OXIDE QUANTUM WELLS?

T. Tchelidze[1,a], Z. Machavariani[1,2,b], E. Chikoidze [3]

[1] *Department of Exact and Natural Sciences, Tbilisi State University, 0179, Tbilisi, Georgia,* [a]*tchelidze@tsu.ge*

[2]*Doctoral School, Kutaisi International University, Youth Avenue, 5th Lane, 4600 Kutaisi, Georgia,* [b]*zaal.machavariani@tsu.ge*

[3] *University Paris Saclay, Grp Etud Matiere Condensee GEMaC, UVSQ CNRS, 45 Ave des Etats Unis, F-78035 Versailles, France*

Abstract. The actual problem of obtaining hole conductivity in ultra-wide bandgap semiconductor Ga_2O_3 is considered. It is proposed to use Aa_2O_3/Ga_2O_3 quantum structures for increasing hole concentration, and their mobility. The dependence of theses parameters on system geometry and composition is studied.

1. Introduction

One of the main goals of semiconductor material science is controlling the electrical and optical properties of materials, which is fulfilled by means of controlling charge carrier concentration. Most of the materials valuable for electronic application supper from monopolar doping problems; oxide semiconductors are easily n-doped, however, p-doping is a big challenge still. The difficulties of p-doping are connected to the creation of compensating donors, low mobility of holes, low lying valence band, high ionization energies of acceptors. Modulated doping, in which the impurities are separated from the layer where current flows, gives one possibility to decrease scattering with ionized impurities and increase carrier mobility. In this case, the barrier layers are doped, while carriers reside in quantum well layers and do not experience scattering with ions. However, it is counted that modulation doping cannot reduce the compensation processes. The essence of compensation is that the free energy of the pair [negatively charge acceptor-hole] is more than the free energy of the pair [negatively charge acceptor – positively charged donor]; that is why for crystal it is energetically more favorable to create a positively charged donor defect (hole killer) rather than to maintain a hole in a valence band. Therefore, the efficiency of compensation depends on the band-gap, the ionization energy of compensating donors, their creation enthalpy, and controlling of all these parameters is crucial to achieve the above mention goal.

Gallium oxide is ultra-wide band gap (~ 4.85 eV) material with great perspectives of application in optical and power electronics [1]. It also suffers from monopolar n-conductivity. High ohmic p-conductivity has been obtained [1,2], however, it low-ohmic samples suitable for practical application is still challenging.

2. Theoretical framework

It is expected that in nanostructures many desired properties that are impossible to realize in bulk materials can be obtained. This is connected to the appearance of now controlling parameters, such as size, shape, geometry. In the condition of space confinement all the characteristics, which are important to achieve high hole conductivity, change and become size dependent.

In this work, we study the possibilities of suppressing the formation of compensating intrinsic defects in modulated p-doped $AlGaO_3/Ga_2O_3$ quantum well heterostructures in order to obtain p-type gallium oxide layers.

The basic idea is that because of very high conduction band offset aluminum and gallium oxides [3], it is possible to construct two-step quantum wells with double barriers with different aluminum concentrations – $Al_{(1-x)}Ga_{(x)}O_3/Al_{(1-y)}Ga_{(y)}O_3/Ga_2O_3$ with y less than x. If the modulated doped barrier $Al_{(1-y)}Ga_{(y)}O_3$ that immediately borders Ga_2O_3 quantum well, is of a few nanometer sizes, the ionization energy of compensating donors will increase because of space confinement. The ionization energy of acceptors is expected to be much less affected by space confinement. This is mainly conditioned by a very low barrier for holes in the heterostructure, and also a big effective mass of holes, comparing with electron effective mass.

3. Results

We calculated the band structure and ionization energies of donors, acceptors for different thicknesses for quantum well and barrier of the $Al_{(1-x)}Ga_{(x)}O_3/Al_{(1-y)}Ga_{(y)}O_3/Ga_2O_3$ heterostructure in the frame of single-band effective mass approximation and perturbation theory. The obtained results then were used for the Kroger method of quasi-chemical reactions to define the equilibrium concentrations of careers, acceptor and donor

defects vs system geometrical parameters. Calculations revealed that the electronic structure of the system strongly depends on system geometry on the one hand, and impurity location on the other hand. For the quantum wells with total thickness bellow 5 nm increase of hole conductivity is predicted by thermodynamic analyses.

Acknowledgment:
The work is supported by Shota Rustaveli National Science Foundation of Georgia, Grant Number STEM-22-188.

References:

[1] Chikoidze E., et al. Materials Today Physics, 2017, 3, 118-126
[2] Chikoidze E., T. Tchelidze T., et al. Materials Today Physics, 2017, 15, 100263
[3] Shun Zhou et al. Journal of Vacuum Science & Technology, 2021, A 39, 030403.

MATERIALS AND DEVICES FOR SPIN-QUBIT QUANTUM COMPUTERS

P. Kervalishvili[1,a], R. Vardapetian[2,b]

[1]Georgian Technical University, Tbilisi, Georgia, [a]paata.kervalishvili@gtu.ge
[2]European Centre for Knowledge and Technology Transfer Brussels, Belgium, [b]rv.eurotex@gmail.com

Abstract: The aim of the paper is elaboration of the concept for obtaining spintronic and spinqubit nanostructures applicable in quantum computing and quantum information technologies.

The convergence between the properties of quantum materials and prototype quantum devices is especially apparent in the field of 2D materials, which offer a broad range of properties, high flexibility in fabrication pathways and the ability to form artificial states of quantum matter. Along with the quantum properties and the potential of 2D materials as solid-state platforms for quantum-dot qubits, single-photon emitters, superconducting qubits and topological quantum computing elements, it is necessary to select the best methods of their preparation. 2D thin films, promising for spintronic applications, are mainly prepared by annealing of the stacks with layers of separate materials (metals, semimetals, semiconductors) received by traditional and reactive magnetron sputtering and novel laser plasma deposition techniques.

Today, usage of electron spins as quantum bits for quantum information processing in the so called quantum computers, where a qubit exists in more than one state simultaneously (until its state is measured}, is clear. Qubits in this state display a degree of correlations impossible in classical physics. This phenomenon is called entanglement and is a crucial property of quantum computing. It is also possible to create qubits from the "up" or "down" spin-states of electrons in quantum dots. But they lack the ability to control the state of a single electron well enough to perform calculations using them.

The main requirements of quantum computation are: Scalable physical systems with well characterized qubits (Zeeman Splitting); Long decoherence time; Existence of qubits at the ground state; Set of quantum gates; measurement capabilities, etc. A candidate for a qubit needs longer decoherence time than gate operation time [1]. The relevant candidates to be a qubit in quantum computing are leptons – elementary particles with spin-1⁄2, playing an important role in the Standard Model. The spin-statistics theorem implies that they are fermions and thus they are subject to the Pauli Exclusion Principle: No two leptons of the same species can be in the same state at the same time. Furthermore, it means that a lepton can have only two possible spin states namely up or down. The charged lepton is the electron; the next lepton to be observed was the muon, which was classified as a meson at the time. After investigation, it was realized that the muon did not have the expected properties of a meson, but rather behaved like an electron, only with higher mass. Another lepton - the first neutrino, the electron neutrino, was proposed in order to explain certain characteristics of beta decay.

The muon and the tau neutrinos were discovered later, up to the end of the 20th century.

According to the known properties of neutrinos, each neutrino flavor state is a linear combination of the three discrete mass eigenstates, the flavor eigenstates (creation and annihilation combinations) are not the same as the neutrino mass eigenstates and they are in associated specific quantum superposition of all three mass eigenstates it is possible to consider this family also as a good candidate to be the a qubit for quantum information systems [2].

The challenge here is to develop novel quantum circuits and qubits with better performance compared with the state-of-the-art competitors. Such components are key units for implementation of reliable practical quantum computers and quantum simulators. Success in this direction will result in a qualitatively new level of processing the quantum information using novel electronic circuits. Ultimately, our research addresses new paradigms of quantum computation for the benefit of digital economy and modern society.

Spintronics is a rapidly developing field that allows insight into fundamental spin-dependent physical properties and the development of practical applications, such as the read head sensors for hard drives in computers [3]. Recently, the so-called superconducting spintronics, which involves structures formed by ferromagnetic (FM) and superconducting (SC) layers, has emerged, promising advances in the fundamental understanding of the competition between superconducting and magnetic ordering, as well as new device functionalities. The most conventional spintronic element consists of two ferromagnetic layers coupled by a spacing layer. Its electrical resistance depends on the relative alignment of the magnetization directions of the

two ferromagnets. This can be modified either by applying external magnetic fields or by injecting spin-polarized electrons.

For the progress in the field of high–performance computing and artificial intelligence, it is necessary to improve the energy efficiency and density of integration of existing circuits, which can be realized only with the superconducting (SC) electronics, mainly based on new elements - superconducting neurons and synapses. The proposed study is relevant due to the possibility of developing new energy-efficient computers with non-von Neumann architecture based on elements of superconducting spintronics. Indeed, the best modern systems on specialized semiconductor microprocessors simulate the work of about 1 million neurons and a quarter of a billion synapses. However, the largest and the most ambitious projects declare the goal of 1010 neurons and 1014 synapses. The key problem on the way to such goals is the reduction of energy release in all active elements of neuromorphic computing systems. For this reason, the use of superconducting materials seems to be the most promising direction for meeting these tasks [4].

Energy efficient memory has been the main detractor for multiple superconducting digital properties. Recently, fundamental research in superconductor-ferromagnet thin-film tunnel structures created a new opportunity
to solve this long-standing problem. Superconductivity and ferromagnetism, two deeply antagonistic electronic properties, can co-exist in the form of Magnetic Josephson Junctions (MJJs) [5].

The interplay between superconductivity and ferromagnetism in artificial multi-layer hybrid systems is very promising for the application in superconducting electronics, spintronics and magnonics. In the last decade various areas of the so-called alternative or post-silicon electronics have been actively developed. The search for alternatives to silicon electronics is associated with the impossibility of a further fundamental increase in the integration of semiconductor elements due to the manifestation of quantum phenomena that disrupt the normal functioning of integrated circuits, as well as the impossibility of efficient heat dissipation in the circuit elements.

References:

[1] Kervalishvili P.J. Quantum information technology: Theory and applications. Published in: 2015 IEEE Seventh International Conference on Intelligent Computing and Information Systems (ICICIS), IEEE Xplore: 04 February 2016, DOI: 10.1109/IntelCIS.2015.7397187, Publisher: IEEE. 15p.

[2] Kervalishvili P.J. Movement of information and its carriers, WCPF-2023, World Congress of Physics Frontier 2023, (May 17-19, 2023), Osaka, Japan.

[3] Kervalishvili P. Quantum processes in semiconducting materials and spinelectronics. Rev.Adv. Mater. Sci. (RAMS), No 1. Vol 14, 2007.

[4] Golubov A., Kupriyanov M. Controlling magnetism. Nature Mater 16, 156–157 (2017). https://doi.org/10.1038/nmat4847.

[5] Morari R., Zdravkov V., Antropov E., Sidorenko A. Nanolayers with Advanced Properties for Superconducting Spintronics. J. of Nanoelectronics and Optoelectronics 7 (2012) 678–680. https://doi.org/10.1166/jno.2012. 1417.

HEALTH HAZARDS AND POLLUTION RISK FROM LARGE BATTERY ENERGY STORAGE SYSTEMS

Jeremy J. Ramsden

Faculty of Medicine and Health Sciences, The University of Buckingham, England
jeremy.ramsden@buckingham.ac.uk

Abstract

Energy storage systems are deployed to decrease the costs and improve the dependability of a power supply, especially electricity generation. Conventional generating stations (hydroelectric or powered by fossil fuels) tend to work continuously at the same rate, whereas demand fluctuates. On the other hand novel "renewable" sources such as wind turbines fluctuate more than demand. In both cases it is useful to store electricity when there is a surplus, and release it when there is a shortage. In the case of hydroelectricity, the same infrastructure can be used for this purpose — surplus power is used to pump water back up into the reservoir. Most other sources require special infrastructure. For example, surplus power can be used to split water into hydrogen and oxygen by electrolysis; the hydrogen is stored and can later be used as fuel to power a generating station. The drawback is not only the expense of the infrastructure but also the significant exergy losses during the process. Hence the attraction of "battery" storage, by which is meant electrochemical cells such as those based on nickel–manganese–cobalt, vanadium, sodium or lithium. The enormous worldwide increase in the number of electric automobiles has provided a strong impetus for developing such "batteries", especially the lithium ion type, and large batteries of such batteries can be used to store energy on a scale commensurate with the requirements of a countrywide electricity grid. Since intermittency of supply is of particular problem with the so-called "green" or renewable sources, governments have provided subsidies for energy storage, typically by selling surplus electricity very cheaply. This has encouraged the construction of battery energy storage systems (BESS), for which a business case can be made because of the price differential of electricity between times of surplus and scarcity, regardless of whether the surplus electricity actually comes from a renewable source. Nevertheless, these installations are not hazard-free. Those based on lithium ions, in particular, are susceptible to overheating ("thermal runaway"). In a dense array typical of BESS, fire can percolate from one battery to another and a major conflagration, possibly accompanied by explosions, can result. This in turn implies release of toxic contaminants to the air and to groundwater. This contribution assesses the hazards and risks of such incidents.

ANALYSIS OF POSSIBILITIES THE CURRENT SITUATION FOR USING AND ACCUMULATING GREEN ENERGIES IN GEORGIA

R. Turmanidze[1,a], N. Gomidze[2,b], G. Popkhadze[1,c], L. Gomidze[3,d], K. Tchanidze[4,e]

[1] *Georgian Technical University, Tbilisi, Georgia,* [a] *inform@gtu.ge,* [c] *popxadzegiorgi@gmail.com*

[2] *Batumi Shota Rustaveli State University, Batumi, Georgia,* [b] *gomidze@bsu.edu.ge*

[3] *Department of Exact and Natural Sciences, Tbilisi State University, 0179, Tbilisi, Georgia,* [d] *lukagomidze@gmail.com*

[4] *Batumi State Maritime Academy, Batumi, Georgia, ketevan.tchanidze@bsu.eduge*

Abstract

The present paper is dedicated to addressing the challenge of efficiently accumulating energy generated by solar modules and wind farms—a significant international issue that currently requires substantial financial investment. The paper emphasizes the feasibility of implementing this concept in countries equipped with operational hydroelectric power plants with dams. Such a strategy presents a cost-effective and efficient means of energy storage for these renewable sources. Furthermore, the paper delves into the potential for enhancing the energy efficiency of wind farms and solar panels through a comprehensive analysis of their structural design and component characteristics.

Keywords: Renewable Energy (RE), Green Energy (GE), PV Panel, Pumped – Storage Plant, Fill factor (FF)

I. Introduction. Global renewable energy (RE) trends

Renewable energy RE encompasses energy derived from continually replenished natural sources and environmental processes, such as wind, solar, and biofuels, in stark contrast to non-renewable sources like coal and fossil fuels, which require extensive time for replenishment. As detailed in reports from the International Energy Agency (IEA) [9], global trends in renewable energy adoption, including the expansion of solar photovoltaic (PV) capacity [5,8,16-17] (fig.1), exemplify the world's evolving energy landscape.

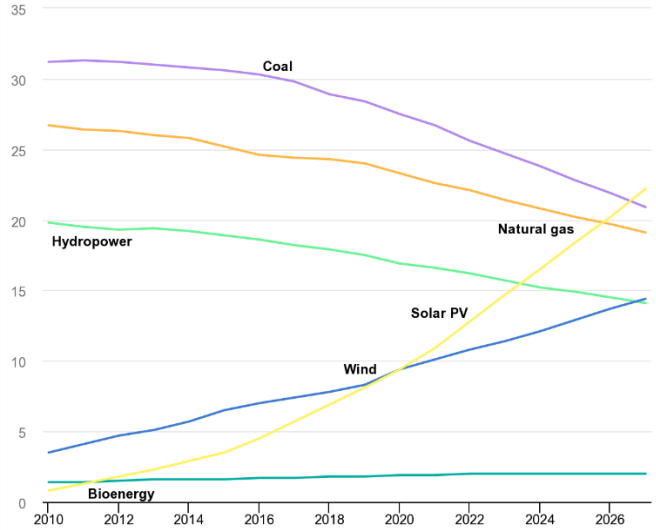

Fig.1. Global RE trends, including solar PV capacity additions [9]

Several studies have examined the economic aspects of wind energy, including cost competitiveness with conventional energy sources. The literature explores factors such as levelized cost of electricity (LCOE), subsidies, and financial incentives [1,22]. Wind energy is often lauded for its environmental benefits, but it also faces scrutiny regarding potential ecological and visual impacts. In [2,11] reviews delve into topics like bird and bat collisions, noise pollution, and visual aesthetics. As wind energy capacity increases, integrating it into existing electrical grids becomes a significant challenge. In [10,21] examine grid stability, energy storage solutions, and the role of smart grids in accommodating variable wind power. In [7,26] discusses the future of wind energy, including offshore wind farms, advancements in wind turbine technology, and policy frameworks that could support further growth. References [14,27] represent a starting point for a literature review on wind energy.

II. Creation of a multi-profile industrial-scientific-educational complex

All the aforementioned innovations and advantages are safeguarded by the patent held by Raul Turmanidze and his group, known as the "Wind and Solar Energy Accumulating Energy System U 2016 1906." It is noteworthy that the groundbreaking concepts outlined in this patent have already found practical application in a hydroelectric station constructed in the city of Haibei (2021) by China's largest corporation, the "CHINA ENERGY ENGINEERING CORPORATION LIMITED." Furthermore, there are ambitious plans for the serial construction of similar accumulative power plants, with a combined capacity of 120 GW.

Fig.2 presents a schematic representation of the energy system designed to accumulate hydro, wind, and solar energy. This integrated system comprises a hydroelectric power station (2) that interfaces with Energoline (1), which encompasses an upper basin (3) and hydrounits (5 and 6, comprising turbines and generators) situated within a hydrotechnical facility (4). These hydrounits are supplied with water through aqueducts (7). Additionally, the system is equipped with wind and solar energy conversion devices (8 and 9), a reversible pipeline (10), a pumping unit (11) integrated into said pipeline or connected to it, and a control unit (12). The wind and solar energy conversion devices are electrically connected to the control unit through the inventor (14) and the hydroelectric units of the hydroelectric plant. The control unit is designed to manage and direct the energy generated by these devices and/or hydro-units to either the energy storage cell and/or the pumping equipment. The schematic representation of the substation is indicated on (13).

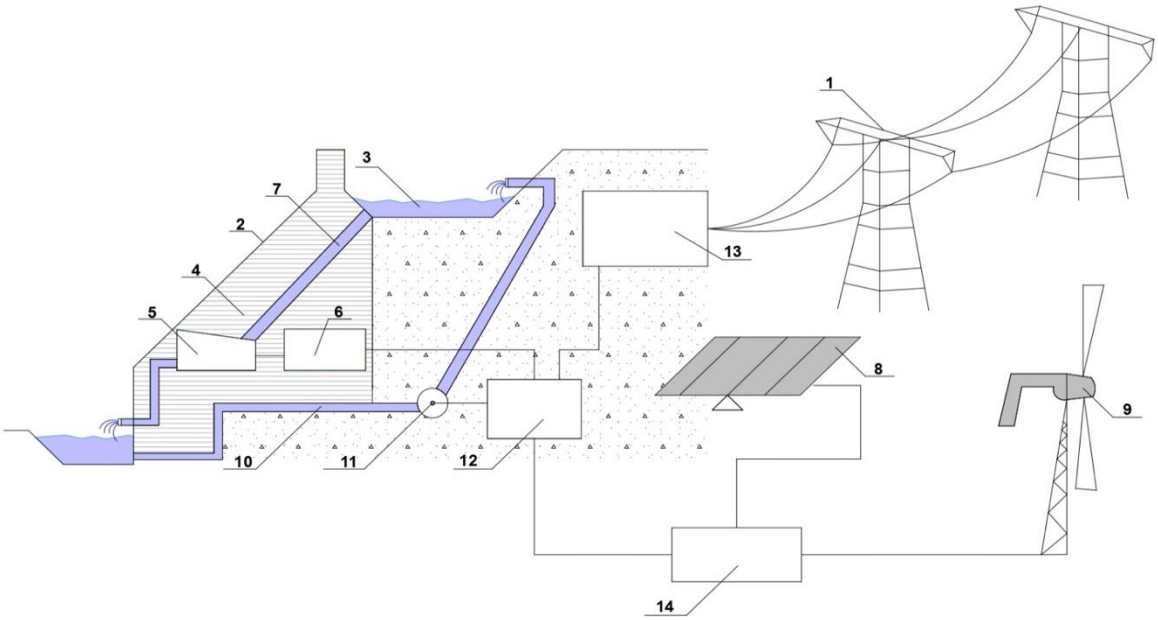

Fig.2. 1- Energoline, 2 - hydroelectric power station, 3 - upper basin, 4 – hydrotechnical facility, 5 turbine, 6 – generator, 7 - aqueducts, 8 – wind generator, 9 – solar panels, 10 - reversible pipeline, 11 - pumping unit, 12 - control unit, 13 – substation, 14 - control unit

III. Prospects for increasing Solar Panels manufacturing research and study its characteristics

On another front, the research group at Batumi University is actively engaged in studying the characteristics of solar panels [6,20].

Efficiency comparisons were conducted among solar panels from different manufacturers, specifically between the NURZAMAS solar cell and the STC solar module. The NURZAMAS solar cell boasts dimensions of 90x60x2 mm and a surface area of 54 cm². It achieves a maximum voltage of 6V and a maximum power output of 0.6W. In contrast, a typical solar module adhering to STC specifications encompasses an area of 1 square meter and operates under standard test conditions (STC) of 1000 W/m² and 25°C (Fig.3). The module's maximum power output varies according to the specific model and manufacturer.

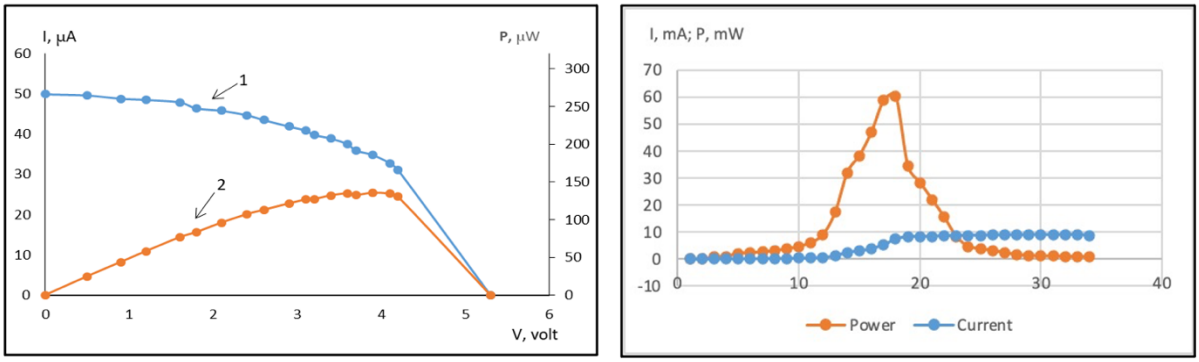

Fig.3. a) characteristics of solar cell manufactured with NURZAMAS: I-V (1) and P-V (2) I_{SC} = 49.9 μA, u_{OC} = 5.1 V, I_{mpp}=34,8 μA, u_{mpp}=3,9 V; b) characteristics of solar module with the specification of the PV module at STC (1000 W/m 2 and 250C): P_{max} = 50 W, u_{mpp}= 18.2 V, I_{mpp} = 2.7 A, u_{OC} = 22.7 V, I_{SC} = 3.1 A

Conclusion

The focal point of this research has been the effective accumulation of energy harnessed from wind aggregates and solar modules, achieved at relatively modest costs. This endeavor addresses a critical international challenge, one that necessitates the allocation of hundreds of millions of US dollars annually for its resolution.

Within the context of constructing a multifaceted production complex encompassing the aforementioned autonomous enterprises, it is substantiated that wind stations and solar modules produced in Georgia, utilizing local and cost-effective raw materials along with novel designs and technologies pioneered by Georgian scientists, will yield significant cost reductions in the resulting products.

In closing, it's noteworthy that the performance of a solar cell can be substantially enhanced through the application of various techniques. These include the use of anti-reflection coatings, surface texturing, and material doping. These methodologies serve to augment light absorption, mitigate reflection losses, and enhance the collection of charge carriers, thereby contributing to the overall efficiency and effectiveness of solar energy conversion.

Reference:

[1] Archer, C. L., & Jacobson, M. Z. (2007). Evaluation of global wind power. Journal of Geophysical Research: Atmospheres, 112(D12).
[2] Bolinger, M., & Wiser, R. (2021). 2020 Wind Technologies Market Report. Lawrence Berkeley National Laboratory.
[3] Electricity – installed generating capacity. The World Factbook. Archived from the original on 26 September 2021. Retrieved 26 September 2021.
[4] ETEnergyworld. https://energy.economictimes.indiatimes.com
[5] Filippov, S.; Mikova, N. & Sokolova, A.: Green energy prospects: Trends and challenges. International Journal of Social Ecology and Sustainable Development, Vol. 6, Issue 3 (July 2015), pp. 1–20. ISSN 1947-8402. doi: 10.4018/IJSESD.2015070101.
[6] Gomidze, N., Kalandadze, L, Nakashidze, O., Jabnidze, I., Khajishvili M., Shainidze J. About DC parameters of PV panels. 11. Eur. Conf. Ren. Energy Sys. 18-20 May 2023, Riga, Latvia.
[7] Hatziargyriou, N., Asano, H., Iravani, R., & Marnay, C. (2007). Microgrids: An overview of ongoing research, development, and demonstration projects. IEEE Power and Energy Magazine, 5(4), 78-94.
[8] Hoogwijk, M.M.: On the global and regional potential of renewable energy sources. Ph.D. Thesis. Utrecht (Nederlands): Utrecht University, Faculty of Chemistry, 2004. – 256 pp. ISBN 978-90-393-3640-3.
[9] International Energy Agency. https://www.iea.org/
[10] Jobert, A., & Laborgne, P. (2012). Local acceptance of wind energy: Factors of success identified in French and German case studies. Energy Policy, 41, 476-485.
[11] Lazard. (2020). Lazard's Levelized Cost of Energy Analysis—Version 14.0.
[12] Marrou, H. et al. 2013. Agricultural and Forest Meteorology doi:10.1016/j.agrformet.2013.04.012.
[13] Marrou, H., L. Dufour and J. Wery. 2013. European Journal of Agronomy doi:10.1016/j.eja.2013.05.004.
[14] Musial, W., & Ram, B. (2010). Large-scale offshore wind power in the United States: Assessment of opportunities and barriers. NREL Technical Report NREL/TP-500-40745.
[15] NEA Backtracks from Pumped Storage Hydropower Projects. https://www.newbusinessage.com/Articles/view/15318.
[16] Nguyen, Q.H.; Hoai Ta, Q.T. & Tran, N.: Review on the transformation of biomechanical energy to green energy using triboelectric and piezoelectric based smart materials. Journal of Cleaner Production, Vol. 371 (October 2022), Article no. 133702. ISSN 0959-6526. doi: 10.1016/j.jclepro.2022.133702.

[17] Panwar, N.; Kaushik, S. & Kothari, S.: Role of renewable energy sources in environmental protection: A review. Renewable and Sustainable Energy Reviews, Vol. 15, Issue 3 (April 2011), pp. 1513–1524. ISSN 1364-0321. doi: 10.1016/j.rser.2010.11.037.
[18] PV MAGAZINE, FEBRUARY 11, 2021. https://www.pv-magazine.com/issue/02-2021/page/2/.
[19] ROBERTSON B. Solar power guide. https://solarpower.guide.
[20] Shainidze J., Kalandadze L., Nakashidze O., Gomidze N. Estimation of Parameters for a Model of Polycrystalline Solar Cells. Journal Nanotechnology Perceptions, 16 (2020), 52-55 doi: 10.4024/N17SH19A.ntp.16.01. http://www.colbas.org/ntp/abstracts/N17SH19A-abs.pdf.
[21] Smallwood, K. S. (2013). Comparing bird and bat fatality-rate estimates among North American wind-energy projects. Wildlife Society Bulletin, 37(1), 19-33.
[22] Sperling, D., & Simpson, T. W. (2017). Wind energy: renewable energy and the environment (2nd ed.). CRC Press.
[23] Tchanidze K., Tkhilaishvili G. Prospects of use of the renewable energy resources in Georgia. Proceedings of materials of international scientific conference dedicated to the 80th birth anniversary of doctor of economic sciences, professor Alfred Kuratashvili. Economic, Social, Ecological and Technological Challenges in XXI-st century. 3-4 July, Tbilisi, 2021.
[24] Turmanidze, R. & Popkhadze, G.: Classification of green energies and possibilities of their effective
[25] Turmanidze, R.; Kervalishvili, P. & Popkhadze, G. New designs of rotors with variable geometry parameters in dynamics and their effective use in aviation and wind energy. 2018 sustainable industrial processing summit and exhibition. 4-7 November 2018, Rio De Janeiro, Brazil.
[26] Zakeri, B., & Syri, S. (2015). Energy storage systems in islanded power systems with high penetration of wind power. IEEE Transactions on Sustainable Energy, 6(2), 492-501.
[27] Zong, Y., Yang, J., Zeng, X., & Zhang, J. (2021). Wind energy technology trends and enabling technologies: A review. Renewable and Sustainable Energy Reviews, 140, 110762.

DISCOVERING THE CAUSE OF AEROTOXIC SYNDROME: A CAUSAL CALCULUS APPROACH

Jeremy J. Ramsden

Faculty of Medicine and Health Sciences, The University of Buckingham, England
jeremy.ramsden@buckingham.ac.uk

Abstract: Aerotoxic syndrome (AS) is a collection of symptoms of ill health experienced by pilots, cabin crew and passengers, especially frequent flyers, after a journey in a jet airliner. The syndrome is especially, but not exclusively, associated with the occurrence of "fume events", in which cockpit and cabin are filled with smoke. The problem started to arise when large aircraft interiors began to be heated and pressurized using air bled off from the main engines. Some of the symptoms are consistent with inhalation neurotoxicity due to compounds either present in fresh lubricating oil or as decomposition products resulting from the harsh environment of the engine oil. The seals separating the oil from the air invariably leak to a greater or lesser extent, depending on design and maintenance history, and the idea that AS is due to contamination of cockpit and cabin air by traces of engine oil has emerged. The matter is currently much debated and there are increasing attempts to better understand the origin of AS. The classic Bradford Hill criteria of medical causation have been applied, but rather inconclusively. Very recently, however, significant advances in developing the calculus of causality have been made. This contribution makes use of these advances to gain deeper understanding of the origins of AS.

AN OVERVIEW OF LIFE CYCLE ASSESSMENT CRITERIA FOR TRANSPORTATION DECISION-MAKING

Nikolaos T. Athanassoulis[1, a], Anggelos Tsakanikas[1, b]

[1]*Laboratory of Industrial & Energy Economics, National Technical University of Athens*

[1]nathanas@*ce* [2]atsaka@central.ntua.gr

As the demand for passenger and goods transport continues to grow across all modes, so does the consumption of carbon-intensive fuels. According to the EIA's World Energy Outlook 2022, the transport sector consumes approx. a quarter of total final energy consumption today and accounts for almost 40% of emissions from end-use sectors i.e. 7,7 Gt CO_2 (2021). As the transport sector is one of the main contributors to Climate Change, it is at the center of attention for global decarbonization efforts to limit global warming well below 2ºC.

In this paper, a review of the available and promising alternative fuels and decarbonization technologies of the transport sector is carried out, exploring various parameters such as (TRL, Capex, Opex, fuel availability, supporting infrastructure, etc.) considering both direct and the indirect emissions in a "Cradle-to-Grave" level. Furthermore, various literature-based emission factors and associated methodologies are presented in a non-exhaustive table, to support the transportation decision-making for the sectors of urban mobility, international trade, international passenger transport. This paper also discusses, relevant concerns regarding issues of safety, just transition and other environmental impacts beyond climate change

EFFECT OF CRB_2 REINFORCEMENT ON THE MECHANICAL PROPERTIES OF CERAMIC MATRIX COMPOSITES (CMCS) AND METAL MATRIX COMPOSITES (MMCS)

M. Rucki [1,a], E. Hevorkyan[2,b], V. Mechnik[3,c], B. Ratov[4,d], S. Muratova[5,e]

[1] *Kazimierz Pulaski University of Technology and Humanities in Radom, Radom, Poland,* [a] *m.rucki@uthrad.pl*

[*2] *University of Life Sciences in Lublin, Lublin, Poland,* [b] *edsgev@gmail.com*

[3] *Bakul Institute for Superhard Materials, National Academy of Sciences of Ukraine, Kyiv, Ukraine,* [c] *vlad.me4nik@ukr.net*

[4] *Satpayev University, Almaty, Kazakhstan,* [d] *b.ratov@satbayev.university*

[5] *Caspian University, Almaty, Kazakhstan,* [e] *samal.muratova@cu.edu.kz*

Both ceramic matrix composites (CMCs) and metal matrix composites (MMCs) are widely used in the tool applications [1-2]. Among others, reinforced with diamond grit, they constitute superhard material suitable for well drilling through the rock formations [3]. The tools working in such a harsh conditions should exhibit, apart from high hardness and Young modulus, also elastic deformation resistance that can be expressed by ratio H/E, and resistance to plastic deformation H^3/E^2 [4].

In the frames of the research program aimed to obtaining enhanced tool materials, several composites with various reinforcements were tested. In particular, CrB_2 was used as the particulate reinforcing material both for CMCs [5] and MMCs designed for drill bit cutting inserts [6]. Interestingly, the effect of the addition was quite different. Figure 1 (left) illustrates the impact of CrB_2 percentage on the hardness of the composite. For the MMCs, the trend is almost proportional, and with increased CrB_2 concentration, the hardness increased, too. Noteworthy, hardness of the specimens with 8 wt.% of CrB_2 was more than two times larger than that of Fe-Cu-Ni-Sn matrix with no reinforcement. In turn, CMC matrix composite exhibited opposite trend with decrease of hardness for larger percentage of CrB_2 reinforcement, so that with 8 wt.%. of CrB_2 the hardness dropped down by ca. 15%.

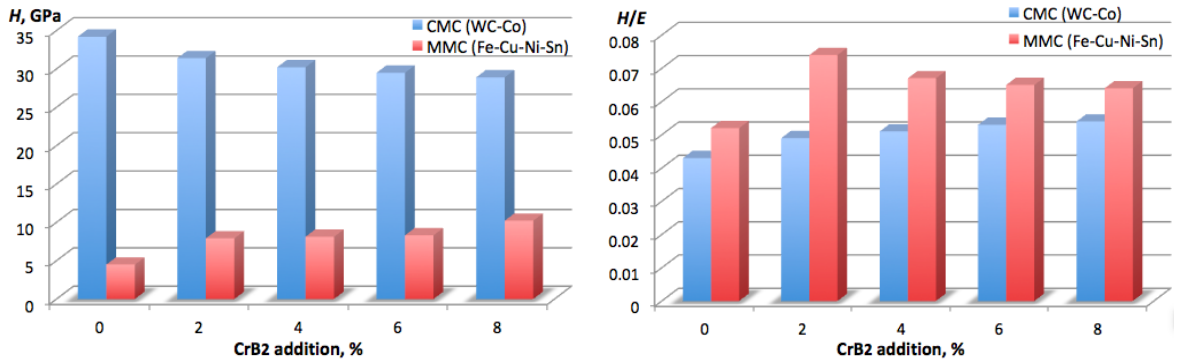

Fig. 1. Effect of the CrB_2 percentage in the Fe-Cu-Ni-Sn-based MMC and in the WC-Co-based CMC on the microhardness *H* (left) and elastic deformation resistance ratio *H/E* (right)

Noteworthy, even though both hardness and elastic modulus of tested MMC were smaller than that of CMC, the ratio H/E was higher for the MMC. However, the elastic deformation resistance index H/E exhibited more complex dependence on the reinforcement amount. As it can be seen in Fig. 1 (right), CMC exhibited improvement of H/E index with the increase of CrB_2. However, for the MMS, it was not the case. All the samples with CrB_2 reinforcement had elastic deformation resistance higher, than that of the pure Fe-Cu-Ni-Sn matrix, but the highest index $H/E = 0.074$ exhibited the composite with 2 wt.% of CrB_2. Further increase of the reinforcement percentage resulted with elastic deformation resistance decrease. Compared to the pure matrix, addition of CrB_2 provided 25% improvement of the elastic deformation resistance index H/E in the case of WC-Co-based CMC, while in the case of Fe-Cu-Ni-Sn-based MMC the improvement by 42% took place. The difference between CrB_2 effect on CMC and MMC appears even more spectacular when analyzing

resistance to plastic deformation index H^3/E^2. After addition of 2 wt.% CrB_2 to the CMC, H^3/E^2 increased by 25%, while in the case of MMC the index increased 3.4 times.

The observed relations can be explained by the dependence of the modulus E on the CrB_2 reinforcement percentage. Presumably, CrB_2 powder served a grain growth inhibitor in WC-Co system during sintering process. As a result, reduction of the grain side took place with the increase of interfaces area in the WC-Co-CrB_2 composite. For Fe-Cu-Ni-Sn MMC, the dimensions of grains the main components appeared to be the smallest in presence of 2 wt.% of CrB_2 powder. Here, even a nanoscale inclusions were found between the matrix grains. However, at higher percentage of CrB_2, excessive chromium diboride due to its brittleness [7] might have formed structures that contributed to decrease of the composite resistance to elastic deformation. It can be concluded, that further improvement of the tested composites may be reached through application of the initial nanopowders that would ensure smaller grains, and through other sintering methods with shorter holding times, preventing from grain growth.

References:

[1] Parikh V.K., Patel V., Pandya D.P., Andersson J. Current status on manufacturing routes to produce metal matrix composites: State-of-the-art. Heliyon, 2023;9(2):e13558.
[2] Lu Y., Sun P., Yang X., Guo X., Li X., Ming W. Review of Research Progress in Nontraditional Machining of Ultrahigh-Temperature Ceramic Matrix Composites. Coatings. 2023;13(1):187.
[3] Sun Y., Li X.S., Harbers C., Williams D., Boland J.N. Wear and cutting temperature of thermally stable diamond composite tipped pick in hard rock cutting. Wear, 2023;523:204848.
[4] Beake B.D. The influence of the H/E ratio on wear resistance of coating systems – Insights from small-scale testing. Surface and Coatings Technology, 2022;442:128272.
[5] Ratov B.T., Mechnik V.A., Bondarenko M.O., Kolodnitskyi V.M. Physical and Mechanical Properties of WC–Co–CrB_2 Matrices of Composite Diamond-Containing Materials Sintered by Vacuum Hot Pressing for Drilling Tool Applications. Journal of Superhard Materials, 2022; 44(4),240–251.
[6] Mechnik V.A., Bondarenko N.A., Kolodnitskyi V.M., Zakiev V.I., Zakiev I.M., Ignatovich S.R., Yutskevych S.S. Mechanical and Tribological Properties of Fe−Cu−Ni−Sn Materials with Different Amounts of CrB_2 Used as Matrices for Diamond-Containing Composites. Journal of Superhard Materials, 2020;42(4):251–263.
[7] Paul B., Okamoto N.L., Kusakari M., Chen Z., Kishida K., Inui H., Otani S. Plastic deformation of single crystals of CrB2, TiB2 and ZrB2 with the hexagonal AlB2 structure. Acta Materialia, 2021;211:116857.

PECULIARITIES OF OBTAINING NANOSTRUCTURED MATERIALS COMPACTED BY THE METHOD OF HOT PRESSING DUE TO THE PASSAGE OF DIRECT ELECTRIC CURRENT

A.Mamalis[1,a], E.Hevorkian[2,b], V. Nerubatskyi[3,c], Z. Krzysiak[2], O. Morozova[3,d], L. Chalko[4]

[1]Project Center for Nanotechnology and Advanced Engineering, Athens, Greece,
[a]agmamalis@yahoo.com
[2]University of Life Sciences in Lublin, 13 Akademicka, Lublin 20-950, Poland, [b]cermet-u@mail.com,
[3]Ukrainian State University of Railway Transport, Kharkiv, Ukraine, [c]nerubatskyi@kart.edu.ua,
[d]oksanabakan2012@gmail.com
[4]Kazimierz Pulaski University of Technology and Humanities in Radom, Poland

Abstract. The aim of this work was to study the regularities of structure formation in composites based on zirconium dioxide nanopowders in the process of hot pressing with direct alternating current. . It was found that the microstructure of the samples in which zirconium dioxide was obtained in different ways strongly depends on tetragonal-monoclinic transitions. Optimal composition of initial mixtures and sintering modes using alumina nano additives was established in order to improve the physical and mechanical properties of the material. To improve the mechanical properties of the samples, sintering temperature and holding time can be raised because alumina grain growth is less rapid at a 30 % content than at lower contents.

1. Introduction

Materials based on partially stabilized zirconium dioxide with various additives nanopowders are promising in designing of hydro abrasive nozzles with enhanced mechanical properties as well as a material for endoprostheses in medicine [1,2]. Formation of microstructure in composites based on chemically synthesized zirconium nanopowders obtained by the method of decomposition from fluoride salts has been considered in this work.

2. Experimental procedure

Samples were proceed via hot vacuum pressing installation. Morphology and structural analysis were performed by scanning microscopy (Nova NanoSEM scanning ion-electron microscope, Quanta 200 3D scanning electron microscope); AFM scanning was performed by the semi-contact method in the air in two modes: at a constant amplitude (topography) and in the mode of phase contrast. Shots of 1×1 μm, 2.5×2.5 μm and 5×5 μm.

3. Results and discussions

It was shown, increasing of the additive of nanopowders of alumina in the content, results in an increase in strength and crack resistance of the samples due to simultaneous inhibition of abnormal grain growth and formation of a finer structure with a high content of tetragonal phase.The microstructure of the samples strongly depends on tetragonal-monoclinic transitions. The nature of the structure and pores formed in the samples of ZrO_2– 10 wt. % Al_2O_3 composition with grains of spherical shape inhibit the formation of Palmquist cracks at the loadof 10 N [3].

The increase in the content of nano Al_2O_3 additives from 10 wt. % to 30 wt. % has improved strength and crack resistance of the samples. At the same time, there was a restraint of abnormal grain growth and formation of a finer structure at high content of tetragonal phase.

Composition marking	ZrO_2 powder type
P–1	Spray drying, spherical shape, d_{av}=70 nm (NANOE Company, France)
P–2	Deposition from fluoride salts, disc- shaped, d_{av}=80 nm (Institute of Monocrystals, Kharkiv, Ukraine)
P–3	Chemical deposition, spherical shape, d_{av}=10 nm (I.M. Frantsevich Institute for Problems of Materials Science, Kyiv

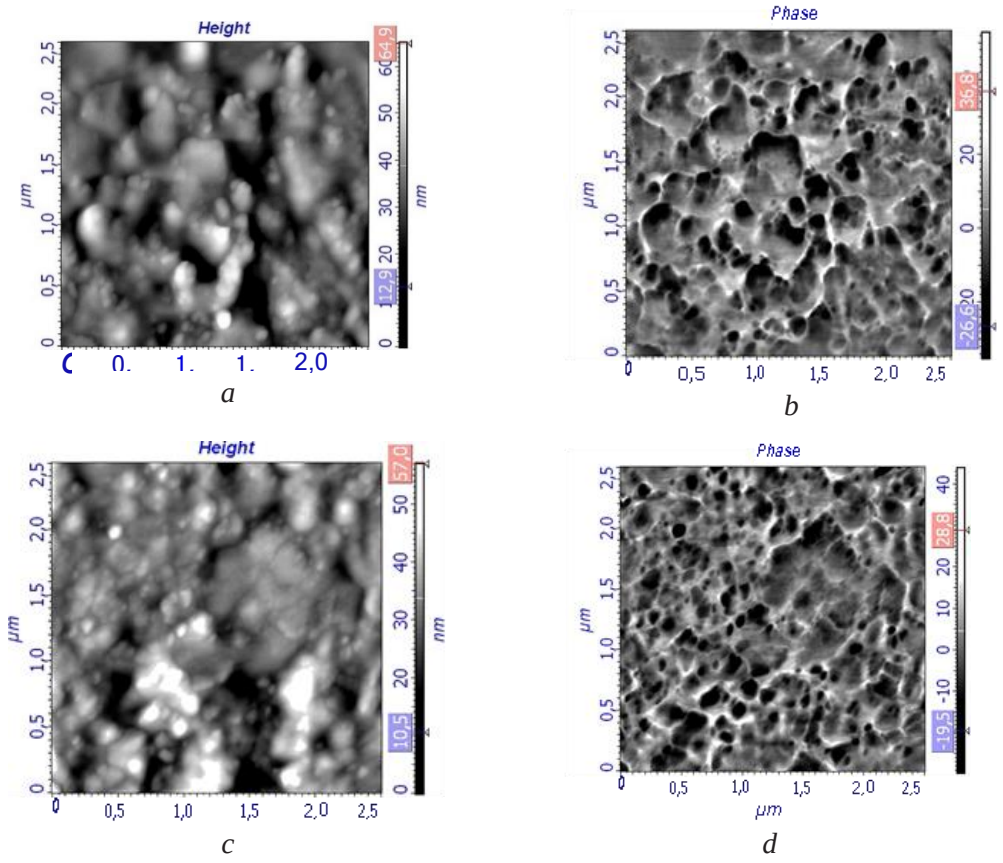

Fig.1. AFM image of chips from samples with ZrO_2–30 wt. % Al_2O_3 composition sintered at 1,200 °C: *a* – fracture height in samples prepared from P–2 powder; *b* – structure of fracture in samples prepared from P–2 powder; *c* – fracture height in samples prepared from P–3 powder; *d* – structure of fracture in samples prepared from P–3 powder

Conclusions

To conclude, study the microstructure of composite materials based on chemically synthesized nanopowders of zirconium dioxide obtained by the method of electric sintering (electroconsolidation) with additives of Al_2O_3 has been investigated in this work. Zirconium oxide, obtained by chemical decomposition from fluoride salts, has crack resistance of 7.8 MPa·$m^{1/2}$ at a strength of 820 MPa. Total density level for the ceramic increases with increasing of electroconsolidation temperature. The combination of different nano additives along with alumina, could increase the physical and mechanical properties of the resulting composites.

References

[1] Hevorkyan E. S., Vovk R. V., Sofronov D. S., Nerubatskyi V. P., Morozova O. M. (2021). The composite material based on syn- thesized zirconium oxide nanopowder for structural appliance. 17th Edition of Advanced Nano Materials. Aveiro, p.267.

[2] Morozova O.M., Timofeeva L. A., Chyshkala V. A., Hevorkyan E. S., Nerubatskyi V. P., Rutskyi M. (2021). Improvement of metrological support of a new material composition based on zirconium dioxide. Abstracts of the 2nd International Scientific and Technical Conference «Intelligent Transport Technologies». Kharkiv: USURT, pp.154–155.

[3] Hevorkyan E., Nerubatskyi V., Chyshkala V., Morozova O. (2021). Revealing specific features of structure forma- tion in composites based on nanopowders of synthesized zirconium dioxide. Eastern-European Journal of Enterprise Technologies,5 (12 (113)),pp. 6–19. doi: https://doi.org/10.15587/1729-4061.2021.242503.

2D LAYERS OF MOS_2 GROWN BY THE METHOD OF PULSED LASER DEPOSITION ON GLASS AND POLYIMIDE SUBSTRATES

S.G. Petrosyan[a], A.M. Khachatryan[b]

Institute of Radiophysics and Electronics, NAS of Armenia, Ashtarak, Armenia
[a]*stepan.petrosyan@rau.am*, [b]*ashot.khacahtryan@mail.ru*

Abstract. We presents the results of the synthesis and studies of the properties of MoS_2 monolayer and multilayer films deposited by pulsed laser deposition on glass and flexible polyimide substrates. Atomic force microscopy (AFM), X-ray diffractometry, Raman scattering spectroscopy, optical absorption, photoluminescence and Hall measurements used to characterize the structural, morphological, optical and electrical properties of the films confirm the correlation between the strain effects and properties of the films appearing due to the large mismatch between thermal expansion coefficients (TEC) of the substrate and ultrathin MoS_2 layers.

1. Introduction

Currently, two-dimensional (2D) materials are attracting great interest for applications in post-silicon electron devices, particularly in next-generation flexible electron devices [1].The physical properties of MoS_2 can be significantly affected by its interaction with substrate [2]. One of the prominent substrate effects is the strain created in the MoS_2 layer due to the large lattice mismatch between the TEC of the substrate and MoS_2 [3]. A large TEC mismatch between the substrate and MoS_2will introduce internal biaxial tensile or compressive strain to the MoS_2 layer and therefore TEC mismatch may become a prominent temperature factor that modulates all the films properties.In this study large-area MoS_2 films of a few atomic layer thicknesses were successfully prepared by the pulsed laser deposition (PLD) technique on a polyimide and glass substrates under the same deposition conditions. The observed experimental features indicate the evolution of all properties of such a two-dimensional material with an increase in the number of atomic layers and the role of strain effects due to a large mismatch between the substrate and MoS_2.

2. Experimental procedure and sample preparation

To deposit thin films up to seven of atomic mono-layers, a Q-switched neodymium laser with the following parameters was used: wavelength 1.064 μm, pulse duration 30 nsec, pulse energy 0.35J, pulse repetition rate 0.1 Hz, beam diameter 20 mm. Polyimide film of 40 μm thickness were chosen as a flexible substrate on the bases of its ability to maintain excellent physical, electrical and mechanical properties over a wide temperature range (up to 400^0 C). Polyimide films and glass substrates are characterized by TEC about $20 \cdot 10^{-6}K^{-1}$and $9.10^{-6}K^{-1}$, correspondingly, which are much larger than nor few-layer thick ($0.5 \cdot 10^{-6}$ 1/C) MoS_2 [4]. The substrate was heated up to 350°C.

3. Discussions of the results

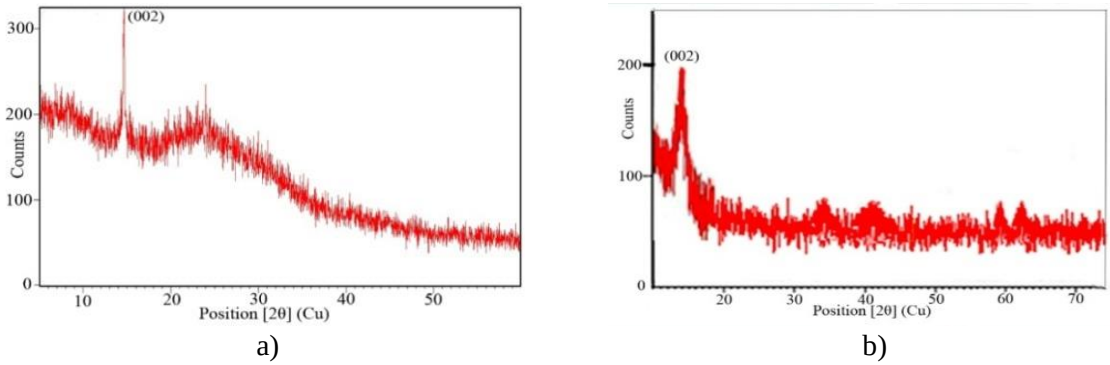

a) b)

Fig.1 XRD pattern of 2L MoS_2 films of thickness 4.7 nm (7L) grown on polyimide (a) and glass (b) substrates

The results of measurements of the X-ray diffraction spectra of the films deposited on polyimide and glass substrates are illustrated in Fig. 1 (a) and (b), respectively. The film thickness in both cases was 4.7 nm (i.e. about 7 atomic layers). A clearly pronounced diffraction peaks are seen at $2\vartheta = 14{,}2^0$, which is characteristic of the crystallographic plane (002) of both a bulk MoS_2 material and thin films consisting of several of its atomic layers .

Raman spectroscopy was used in order to define the number of layers and strain effects in the film.We found the thickness dependent Raman spectra for MoS_2 films deposited on both glass and polyimide substrates.

It is seen from Fig.2 (a) that there are small shifts in the peak position among samples, deposited on glass and polyimide substrates due to different residual strain arising from different TEC mismatch. As it is expected the frequency of in-plane E^1_{2g} Raman mode is less sensitive to strain, which red-shifts with respect to the bulk sample by 1-1.5cm^{-1} as the strain increases in the films grown on glass and polyimide. Meantime the frequency of out-of-plane A_{1g} Raman mode is changed more significantly (about 2.4 cm^{-1}) under strains introduced by polyimide substrate [5,6].

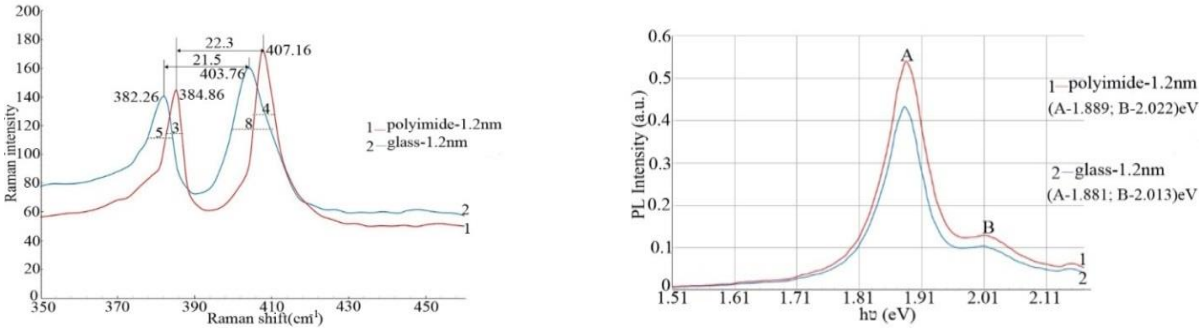

a) b)

Fig. 2 Raman scattering (a) and photoluminescence spectra of 2L MoS_2 films deposited on glass and polyimide substrates

The strain-caused band-gap shift was validated in PL spectra as it is shown in Fig.2 (b), where PL spectra are plotted for 2LMoS_2, deposited on glass and polyimide substrates under the same technological conditions. From the PL spectra two peaks at 659 nm (1.887eV) and 616 nm (2.013eV) were clearly observed, corresponding to a direct transition between the top valence band K point and the bottom conduction K points in the Brillouin zone [4]. In comparison with the MoS_2films grown on polyimide, a blue shift (about 12 meV) of the direct band transition was observed in MoS2 films grown on glass.Also the PL intensity sharply increases with decreasing film thickness and the transition to a direct-gap semiconductor in the limit of a monolayer film.The PL intensity of the films grown on polyimide is substantially larger than that of deposited on glass, probably due to better crystalline quality of the film.

We have measured also the optical absorbance of the MoS_2 films deposited on polyimide and glass substrates. These absorbance spectra also show the formation of excitons of types A and B [4]. The difference between the exciton binding energies for the samples of MOS2 grown on different substrates can be caused by strain shift of the band gap, arising due to TEC mismatch between the film and substrate.

Conclusions:

In conclusion, we demonstrated the possibility of growing by PLD technique high quality few-layer MoS_2 on glass and flexible polyimide substrates. The studies of XRD, Raman scattering, PL and optical absorption spectra revel the correlation between the strain effects and properties of the films.

References:

[1] Singh E., Singh P., Kim K. S., et al. Flexible Molybdenum Disulfide (MoS_2) Atomic Layers for Wearable Electronics and Optoelectronics, ACS Appl. Mater. Interfaces, 2019, 11, pp.11061-1110
[2] Sun Y., Wang R., Liu K. Substrate induced changes in atomically thin 2-dimensional semiconductors: Fundamentals, engineering, and applications, Appl. Phys. Rev., 2017, 4, pp. 011301-1-19
[3] Yang L., Cui X., Zhang J., et al. Lattice strain effects on the optical properties of MoS2 nanosheets, Scientific Reports, 2014, 4, p. 5649
[4] Buscema M., Steele G.A., Van der Zant H.S.J., et al: The effect of the substrate on the Raman and photoluminescence emission of single-layer MoS2, Nano Res. 2014, 7, pp. 561–571.

RHEOLOGICAL PROPERTIES OF THIN-FILM PERMANENT MAGNET ELASTOMERS IN STRETCH DEFORMATION

Y. Iwamoto[1,a], T. Minakawa[1], Y. Ido[1,b], M. Kamezaki[2]

[1] *Department of Electrical and Mechanical Engineering, Nagoya Institute of Technology, Japan,*

[a] *iwamoto.yuhiro@nitech.ac.jp*

[2] *Department of Electrical Engineering and Information Systems, Graduate School of Engineering, The University of Tokyo, Japan*

Abstract. Permanent magnet elastomers are three-dimensional deformable permanent magnets, which are novel functional materials in which the magnetic field around the elastomer changes during deformation. The detection of the magnetic field variation enables the realization of tactile sensors. Considering the application of tactile sensors, it is important to understand their viscoelastic properties. In the present study, the rheological properties of permanent magnet elastomers in stretch deformation were investigated. The results show that the viscoelasticity changes due to magnetization. Additionally, this variation due to magnetization was discussed by fitting it into a four-element mechanical model.

1. Introduction

Recently, flexible tactile sensors have gained attention in applications such as artificial skin and soft actuators for robots. One such sensor is the magnetic-type tactile sensor that utilizes a film-shaped magnetic elastomer [1]. Magnetic elastomer is a functional material that exhibits the combined properties of viscoelasticity and magnetism. The elastomer is prepared by stably dispersing magnetic particles like iron powder in a viscoelastic material such as silicone gel. By applying an external magnetic field, the deformation and viscoelasticity can be controlled [2].

A recent development is the permanent magnet elastomer, which displays residual magnetization. The elastomer is prepared by dispersing magnetically-hard magnetic particles such as NdFeB in a viscoelastic material and then magnetizing it [3]. This magnet is highly deformable and has high coercivity and residual magnetization. When deformed, the PME shows a dramatic change in the surrounding magnetic field. This has potential applications in tactile sensors.

In the present study, film-shaped PMEs are prepared, and dynamic viscoelastic measurements in stretch deformation are performed considering the application of the tactile sensors. The rheological changes before and after magnetization were evaluated and discussed by fitting the mechanical models.

2. Experimental Procedure

The permanent magnet elastomers were prepared by dispersing neodymium particles (MQFP14-12-20000-089, Magnequench) in silicone polymer matrices (Sylgard18, The Dow Chemical Company) and then magnetized. The average diameter of the neodymium particles is 5 μm. The silicone gel and neodymium particles were mixed, vacuum-degassed, and then heated at 343 K and cured to shape a film of 2x5x20 mm. The volume fraction of neodymium particles is 20 vol.%. The mixing ratio of Sylgard184 main agent to curing agent was 40:1. The cured sample was magnetized by a pulse-uniform magnetic field of 6T. The magnetization direction was set to the thickness direction of the samples. Their rheological properties in stretch deformation were measured using a viscoelastic measurement device (DMS6100, Hitachi High-Tech Science Corporation).

3. Results and Discussion

The results of the experiment at an initial strain of 10% are shown in Fig.1. It was confirmed that both the storage modulus and the loss modulus increase with an increase in the excitation frequency. The enhancement of the loss modulus is larger than that of the storage modulus with increasing in the excitation frequency. The storage and loss moduli of the permanent magnet elastomer are larger than those of the magnetic elastomer. Here, we call the magnetized elastomer a permanent magnet elastomer and the non-magnetized elastomer a magnetic elastomer.

The influence of magnetization in the storage and loss modulus was discussed by fitting the experimental results into a four-element mechanical model (Fig. 2). The identified values of each mechanical element are shown in Table 1. All four parameters increased after magnetization compared to before magnetization. When the magnetic elastomer was magnetized, it is thought that the dispersed magnetic particles within it were

oriented in the direction of magnetization. Thus, the alignment of magnetic particles inside the elastomer may have formed a three-dimensional structure, leading to increases in both the elastic modulus and viscous modulus.

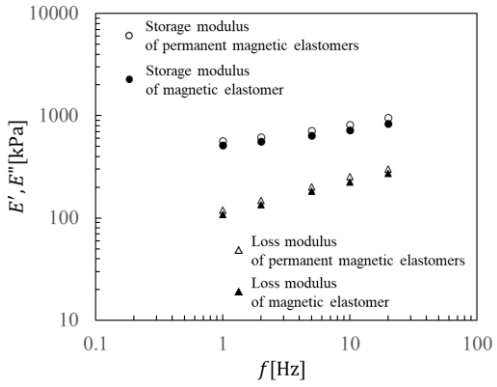

Fig. 1 Storage and loss modulus before magnetized (magnetic elastomer) and after magnetized samples (permanet magnet elastomer) at initial strain of 10%

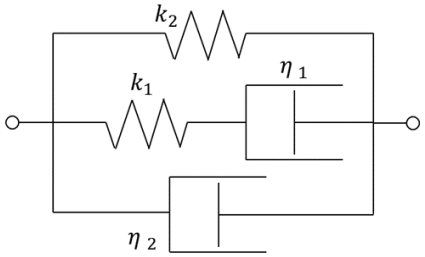

Fig. 2 Four-element mechanical model

Table 1. Value of each mechanical element in the four-element mechanical model

	Magnetic elastomer	Permanent magnet elastomer
k_1 [Pa]	272283	300520
k_2 [Pa]	480913	536196
η_1 [Pa-s]	14848	16368
η_2 [Pa-s]	2009	2225

Conclusions:

The dynamic viscoelastic measurements in stretch deformation were performed to investigate the rheological properties of the thin-film permanent magnet elastomers. As a result, it was confirmed that both storage modulus and loss modulus increase by magnetization. This change is thought to be influenced by the orientation of internal particles due to magnetization and the formation of a three-dimensional structure.

Acknowledgement:

This work was financially supported by the Naito Research Grant.

References:

[1] Wang Y., et al. Proceedings of AIM 2022, Sapporo, Japan: 2022, 302 p.
[2] Filipcsei G., Csetneki I., Szilágyi A., Zrínyi M. Magnetic field-responsive smart polymer composites, Advances in Polymer Science, 2007, 137-189.
[3] Yamaguchi H., et al. Japan Patent P2016-152337A, (2016).

ALTERNATIVE DESIGN OF A HIGH TORQUE DENSITY TWO-PHASE BRUSHLESS DIRECT CURRENT MOTOR

Saeed Abareshi[a], Jawad Faiz[b], Mehrage Ghods[c]

School of Electrical and Computer Engineering, College of Engineering, University of Tehran, Tehran, Iran
[a]saeed.abareshi@ut.ac.ir, [b]jfaiz@ut.ac.ir, [c]ghods.mehrage@ut.ac.ir

Abstract: This paper proposes a design of a high torque density dual-stator brushless direct current (BLDC) motor. BLDC motors are known for their high torque capacity and power density characteristics, and therefore, they have many applications. The proposed BLDC motor is a two-phase motor with two stators, and each stator excited by one phase. The duty cycle of inverter switches is complete and coils are continuously excited. So, due to the full and uninterrupted use of all coils and core, the motor has a higher torque density compared to other BLDCs. The mathematical model of the motor provides a better understanding of motor performance. The performance of the designed motor is analyzed using finite element analysis.

1. Introduction

The BLDC motor has been used and rapidly developed in various applications such as home appliances, electric vehicles, medical equipment, spacecraft, and submarines. These motors have many advantages compared with conventional DC motors, induction motors, and PMs motors [1]. The BLDC motors have no mechanical brush and commutation is done electronically by switching. The duty cycle of switches is determined based on the structure and number of phases. However, in most structures, the switching duty cycle is not complete, which causes the coils and motor core not to be used optimally. In the structures of three-phase and multi-phase BLDC motors, the optimal duty cycle of the switches is less than 2/3 or 120º [2] .

2. Operation

A BLDC motor rotates as a result of the interaction between its permanent magnet (PM) field at the rotor and a magnetic field generated by a DC voltage applied to its stator coils. In the conventional three-phase BLDC motor, the back EMF has an appropriate value about two-third of the period due to the structure of the rotor teeth and poles as shows in Fig 1a. To achieve the maximum energy and optimal use of the core and coils, the back EMF should have value in the entire interval. This is done only when the stator tooth width is equal to the rotor pole pitch. Fig 1b shows a single-phase motor with its back EMF in which all stator coils and cores are utilized simultaneously and the power has its maximum value.

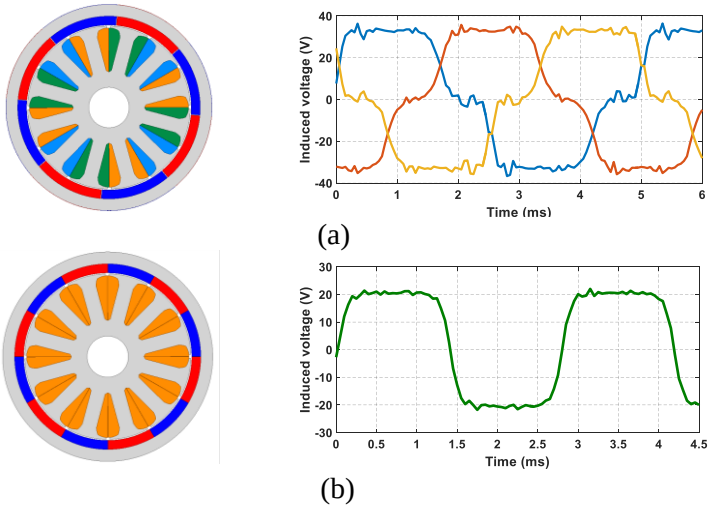

Fig. 1. Motor structure and back EMF of (a) three-phase BLDC motor and (b) single-phase BLDC motor

3. Design of proposed two-phase bldc

In this section, design procedure for two-phase dual stator BLDC motor is described. Two separate single-phase motors are designed. The first design is an internal rotor and the second design is an external rotor motor. It is noted that both motors have the same characteristics. After designing two motors, they are combined to form a dual stator motor.

4. Simulation and results

The proposed two-phase BLDC and a conventional 3-phase dual stator BLDC are simulated using Ansys Maxwell while their control circuit including inverter, supply, etc., are simulated using twin builder Simplorer transient coupling. Fig. 2 shows the structures of the motors. The windings of the two stator phases of the proposed motor must be independent, so, an inverter with 8 switches should be used, which has two more switches compared to that of the conventional three-phase type. With the optimal choice of 25º advance angel, the phase difference between the current and the induced voltage, which caused the increase of torque fluctuations and also the decrease of the average torque, was solved.

As shown in Fig. 2 the RMS current and voltage of the proposed motor is 33 A and 105 V, respectively, and they are 21 A and 81 V for the conventional motor. Fig. 3 shows the average torque and torque ripple of the proposed motor which is 46 Nm and 65% respectively; the corresponding values for the conventional three-phase motor is 32 Nm and 50%. The output powers of the proposed and conventional motors at the speed of 1000 rpm is 4.82 kW, 3.35 kW respectively. Therefore, the simulation also confirms the idea proposed in this paper that in the same volume and dimensions, the torque and output power of the proposed motor is 1.43 times that of the conventional motor. The loss of the proposed machine is slightly higher than that of the conventional machine; however, considering the higher power of the proposed machine, such higher loss is acceptable.

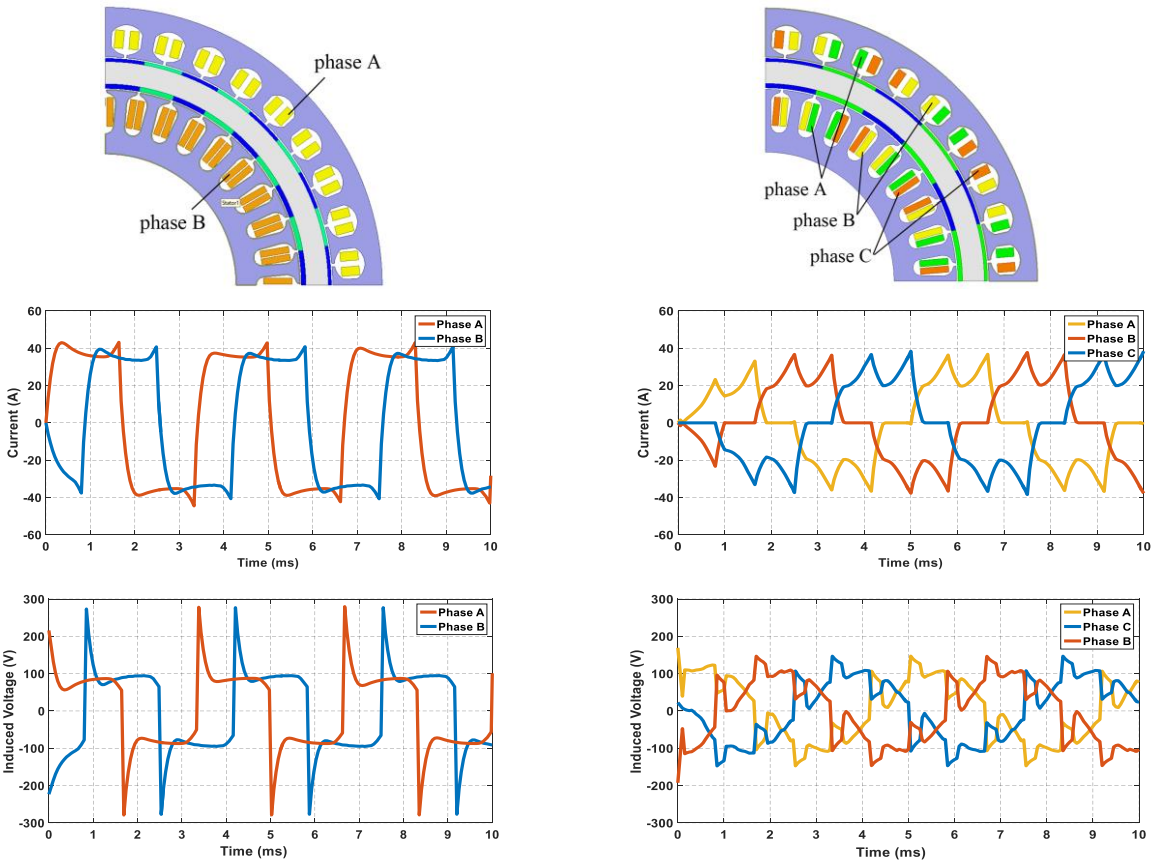

(a) **(b)**

Fig.2. Motor structure, induced voltage and current: (a) Proposed two-phase BLDC, (b) Conventional three-phase BLDC

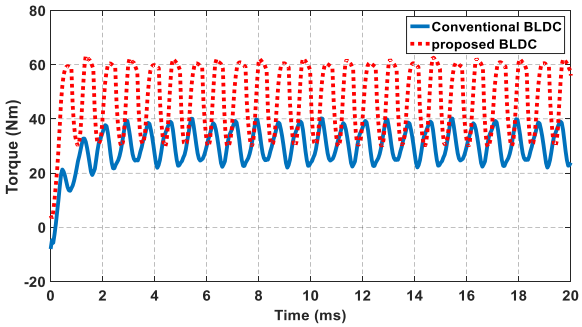

Fig.3. Developed electromagnetic torque

Conclusions:

This paper proposed a new structure for a two-phase BLDC motor. The advantage of this motor is its ability to receive a high energy or power, increasing the torque density compared to other motors with the same size.

Higher developed torque of this motor is due to the duty cycle of the inverter switches, because unlike the conventional motors these switches operate with a full duty cycle. Therefore, the windings and core are always passing the current and magnetic flux, causing optimal and complete utilization of the motor. In this paper, firstly, development of a higher torque was proved by a mathematical model of the motor, then, the desirable motor is designed. The proposed motor is simulated by finite element analysis and its optimal advance angle was selected to have a reasonable torque. To show the higher torque density of this motor, a conventional three-phase dual-stator motor with the same dimensions and specifications were simulated. Finally, the comparisons shown that the torque of the proposed motor is 1.43 times of the three-phase motor.

References:

[1] Tibor B., Fedak V., Ďurovský F. Modeling and simulation of the BLDC motor in MATLAB GUI, Proc. - ISIE 2011 2011 IEEE Int. Symp. Ind. Electron., pp. 1403–1407, 2011, doi: 10.1109/ISIE.2011.5984365.

[2] Gholase V., Fernandes B. G. Design of efficient BLDC motor for DC operated mixer-grinder, Proc. IEEE Int. Conf. Ind. Technol., vol. 2015-June, no. June, pp. 696–701, 2015, doi: 10.1109/ICIT.2015.7125179.

FUNDAMENTAL STUDY OF HAPTIC SENSOR UTILIZING MAGNETIC COMPOUND FLUID RUBBER SENSOR FOR INVESTIGATION OF NUCLEAR FACILITIES

R. Ikeda[1,a], K. Shimada[2,b], H. Kikura[3,c]

[1] *Nuclear Engineering Course, Tokyo Institute of Technology, Japan,* [a]*ikeda.r.ah@m.titech.ac.jp*
[2] *Faculty of Symbiotic Systems Sciences, Fukushima University, Japan,* [b]*shimadakun@sss.fukushima-u.ac.jp*
[3] *Laboratory for Zero-Carbon Energy, Tokyo Institute of Technology, Japan,* [c]*kikura.h.aa@m.titech.ac.jp*

Abstract. Humanoid robots are expectable in a nuclear facility for their manipulation and operation in a nuclear power plant. Therefore, it is necessary to develop a haptic sensor can be adapted to radiation environment. Recently, we have been developed haptic sensor utilizing functional fluids involving MCF (Magnetic Compound Fluid) for artificial skin. Magnetic Compound Fluid (MCF) rubber is a new smart sensor obtained by mixing rubber with MCF. In this study, we clarify the adapatability of tactile function of MCF rubber for investigation of nuclear facilities.

1. Introduction

The robots are expectable in the nuclear facilities for their manipulation and operation in a nuclear power plant involving inspection, prevention [1], decommissioning [2], etc. An important element in developing of a robot for internal investigation in the nuclear power plant is sensing technique. Requirements for sensor loaded on a robot are as follows: (1) it has flexibility and elasticity like a human skin; (2) it does not deteriorate by radiation environment; (3) it can be used in water.

The optimal material fulfilled the overall above-mentioned prerequisites, elasticity and softness of haptic rubber having sensor with sensibility to overall electromagnetic waves, is magnetic compound fluid (MCF), which is one of magnetically responsive fluid consisted of nm-ordered magnetite (Fe3O4) and μm-ordered metal particles such as Ni, Fe etc. When a magnetic field is applied on the rubber compounded with the MCF which is vulcanized by drying or electrolytic polymerization under the production, the Fe_3O_4 and metal particles aggregate needle- or network-like clusters aligned along the applied magnetic field lines like needles in the MCF rubber. Therefore, the MCF rubber exhibits electrically and mechanically anisotropy enough to be haptic for typically sensing force such as piezoelectricity and piezoresistivity along the aligned particles. Futhermore, MCF rubber is not easily degraded by γ-ray irradiation [4]. In this study, we focus on a tactile function of MCF rubber, and clarify the adapatability of tactile function of MCF rubber sensor at nuclear facilities.

2. Foot-type MCF rubber sensor

To confirm the developed foot-type MCF rubber sensor, I experimented at the Cobalt Irradiation Experimental Facility. We measured the electrical signals of a humanoid robot with tactile MCF rubber sensors attached to its legs while it performed a walking motion in an irradiation chamber (Fig.1).

Fig.2 shows the results of the voltage change of tactile MCF rubber during 90 Gy/h of γ-ray irradiation. Since MCF rubber measures tactile sensation as a voltage, the vertical axis is the change of voltage. The graph area is divided into three sections, each displaying the voltage values in the standing, walking, and standing. First, the voltage values in standing were constant, as shown "standing". Then when the robot performs a walking motion, the voltage value fluctuates as shown "walking". Finally, when the robot was once again in an standing position, the voltage values were measured to be the same as the steady-state values measured at the beginning.

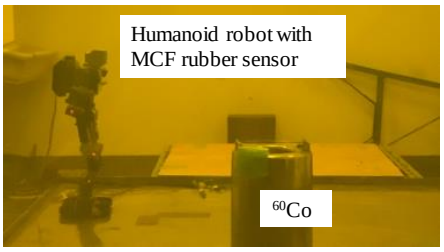

Fig.1. Image of irradiaiton chamber through lead grass for irradiation experiment

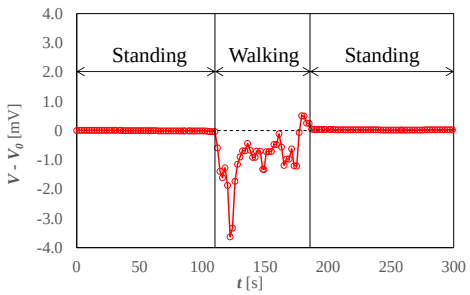

Fig.2. A voltage of tactile MCF rubber sensor during walking in radiation environment

3. Finger-type MCF rubber sensor

The artificial finger mimicking a human body can be simulated the finger embedded with mechanoreceptors or thermoreceptors, μm-scaled cell-like fabric, for example, nerve endings of the receptor, Meissner corpuscles, Pacinian corpuscles, Merkel cells, Ruffini endings, etc. Where by the kind of these receptors, the sensitivity to normal force, shear stress and temperature is different.

In procedure of finger-type MCF rubber sensor, first, we fabricated a sensor simply imitating human somatosensory receptors using Electrolytic polymerization, then to form the shape of human fingers, MCF rubber were coated with urethane rubber, silicone rubber,then finaly made a finger-type tactile sensor as shown in Fig.3.

Experiments were conducted on the fabricated finger-type tactile rubber sensor as shown Fig.4. The finger sensor was lowered vertically into the bottom of a container using a compression tester, and the change in voltage was measured with a digital meter. The results of experiment are shown in Fig.5. A Change in voltage occurs at the moment of contact with the surface. These phenomena depend on the piezoelectricity and piezoresistivity of the electrolytically polymerized MCF rubber resulting from dielectric polarization. Then, when a finger touches the bottom, i.e., when the pressure changes, a change in voltage occurs, indicating that it works as a tactile sensor.

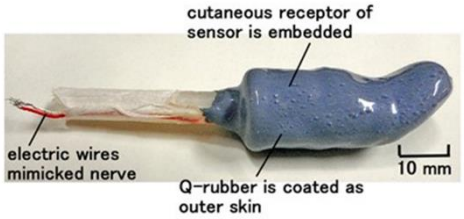

Fig.3. Image of finger-type MCF rubber sensor

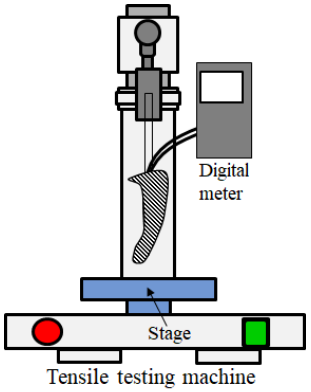

Fig.4. Experimental applatus

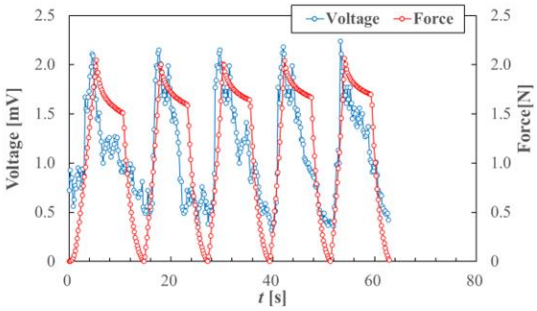

Fig.5. A change of voltage when a finger touches on the surface

Conclusions

Through the development of energy harvesting and haptic enhancement application to sensors that mimic the human body, it will be developed sensing technique for nuclear facilities by haptic sensor utilizing magnetic functional fluid.

References

[1] Zhang Z. L., Fu B., Li L.Q., Yang E. C. Design and function realization of nuclear power inspection robot system, Robotica 2021, 39, 165-180.

[2] Zhao Y., Zhang Y., Xie Z. Allocation of radiation shielding boards to protect the urban search and rescue robots from malfunctioning in the radioactive environments arising from decommissioning of the nuclear facility, Symmetry 2020, 12, 1297.

[3] Shimada K., Kikura H., Takahashi H., Ikeda R. Development of a Magnetic Compound Fluid Rubber Stability Sensor and a Novel Production Technique via Combination of Natural, Chloroprene and Silicone Rubbers, Sensors, 19 (2019), 689.

[4] [4] Ikeda R., Shimada K., Takahashi H., Kikura H. Fundamental Study of Sensing Technique Utilizing Magnetic Compound Fluid Rubber Sensor Under Radiation Environment, Advanced Experimental Mechanics, Vol. 5, pp.185-190.

EXPERIMENTAL STUDY ON SEALING PERFORMANCE AND FLOW CHARACTERISTICS OF MAGNETIC FLUID IN EXTREMELY TINY CLEARANCE UNDER MAGNETIC FIELD

Y. Kato[1], M. Motozawa[2,a], W. Rakpakdee[2], M. Fukuta[2]

[1] *Graduate School of Integrated Science and Technology, Shizuoka University, Shizuoka, Japan*
[2] *Faculty of Engineering, Shizuoka University, Shizuoka, Japan, [a]motozawa.masaaki@shizuoka.ac.jp*

Abstract. Sealing performance and flow characteristics of magnetic fluid in extremely tiny clearance less than 30 μm under magnetic field are investigated experimentally. The extremely tiny clearance in the test section is set to 5, 10, 15, 20 and 30 μm, and magnetic field is applied to magnetic fluid flow at this clearance. The results show that maximum of 1.2 MPa of pressure resistance was obtained at 5 μm of tiny clearance from the sealing test and the relationship among frictional coefficient, magnetic field and *Re* is quite different between 5 and 30 μm of tiny clearance from the flow characteristic test.

1. Introduction

A magnetic fluid is a colloidal dispersion of ferromagnetic nanoparticles in carrier liquids such as water, kerosene and so on. It is well known that it has possibility to control actively flow characteristics by magnetic body force by application of the magnetic field because the magnetic fluid behaves liquid as if it has strong magnetism under the magnetic field. As popular application, the magnetic fluid is applied to sealing technologies. Generally, the clearance of magnetic fluid seal is hundreds of microns and the pressure resistance of single seal is not so large (tens kPa order) [1].

The sealing technologies are very important in many fields. For instance, regarding the sliding part in a compressor, as leakage of compressed gas directly affects the compressor performance, several sealing technologies are proposed [2]. Generally, the clearance of the sliding part of compressor is around few microns, and high-pressure resistance (e.g. MPa-order in some cases) is required. If the sealing technique of the magnetic fluid can be applied to the extremely tiny clearance (around few μm) and high-pressure condition (around 1 MPa), the application of magnetic fluid seal becomes expanding more. In addition, the flow characteristics of magnetic fluid may change in such extremely tiny clearance. However, there are few studies on the sealing performance and flow characteristics in tiny clearance.

In this study, we investigated the sealing performance (Exp. 1) and flow characteristics (Exp. 2) of magnetic fluid in extremely tiny clearance less than 30 μm experimentally. Experiment was carried out by a micro-channel flow path which has 5, 10, 15, 20 and 30 μm of clearance (i.e. channel height), and magnetic field is applied at this clearance.

2. Experimental apparatus and test magnetic fluid

Figure 1 shows the overview of experimental apparatus. Experimental apparatus consists of nitrogen cylinder, regulator, flow meter, and the test section. In case of the Exp. 2, the test fluid tank and electronic balance are installed at upstream and downstream of the test section, respectively. The detailed structure of the test section is shown in Fig. 2. The test section consists of bottom plate, middle part, sight glass, and glass holder. Flow path which has extremely tiny clearance is formed by sandwiching a thickness gauge as a spacer between the middle part and sight glass. The tiny clearances h (i.e. channel height) are set to 5, 10, 15, 20, 30 by changing thickness gauge, and channel width and length are 10 mm and 20 mm, respectively. Magnetic field can be applied at the center of the tiny clearance by embedding the magnet in a magnet groove under the tiny clearance.

For Exp. 1, magnetic fluid is provided at the tiny clearance, and pressure is applied to the clearance of the test section from the nitrogen cylinder. The maximum pressure, at which the seal breaks and leakage starts to occur, is measured. The magnetic field intensity is 0 and 300 mT. On the other hand, for Exp. 2, the test magnetic fluid is filled in the tank which is located at the upstream of the test section, and the test magnetic fluid flows through the channel in the test section by pressure applied by the nitrogen cylinder. The magnetic field intensities are 0, 54.4, 102.6, 136.3 and 330 mT.

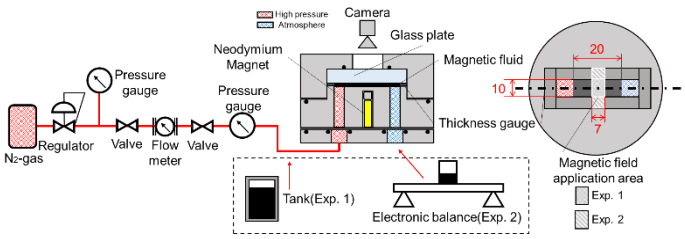

Fig.1. Experimental apparatus

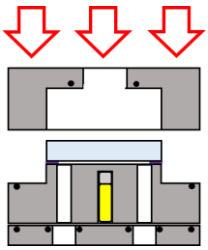

Fig.2. Detail structure of test section

Table 1. Physical properties of test magnetic fluids

Sample	Base	Viscosity Pa·s	Density kg/m^3	Saturation magnetization mT	Experiment
A	Poly-□-Olefin	0.06	1267	48.5	Exp. 1
B	Alkyl benzene	0.65	1357	49.5	Exp. 1
C	Alkyl benzene	0.85	1339	50.2	Exp. 1
D	Kerosene	0.0055	1332	58.6	Exp. 2

Table 2 Pressure resistance (Exp. 1)

Condition	Sealing performance MPa	
	h=5 μm	h=10 μm
A-Mag	0.05	<0.05
A-Nomag	0.05	<0.05
B-Mag	0.4	0.1
B-Nomag	0.2	<0.05
C-Mag	1.2	0.2
C-Nomag	0.65	0.1

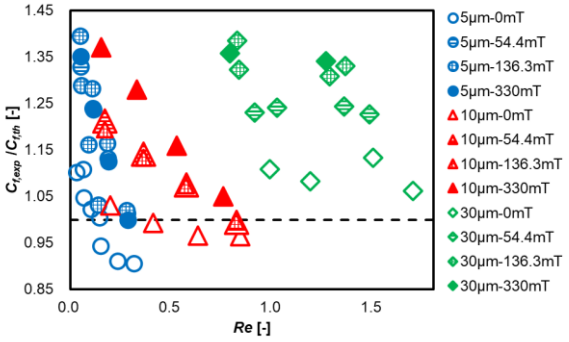

Fig. 3. Relationship between $C_{f.exp}/C_{f.th}$ and Re (Exp. 2)

Four test magnetic fluid samples A, B, C, and D, which have different base fluids and viscosities, are used. These test magnetic fluids were prepared by Ferrotec Material Technologies, inc., and their physical properties are listed in Table 1.

3. Results and discussion

Table 2 lists the pressure resistance obtained from Exp. 1. In this experiment, extremely tiny clearance is set to 5 and 10 μm. This table clearly indicated that the pressure resistance drastically increases in narrower tiny clearance, with increasing viscosity of test magnetic fluid, and by applying magnetic field. The maximum sealing performance of about 1.2 MPa at 5 μm of tiny clearance is obtained. Therefore, it was found that the sealing performance of the magnetic fluid is significantly improved in case of extremely tiny clearance such as 5 μm.

Figure 3 shows the relationship between the increasing ratio of experimental and theoretical pipe friction coefficient $C_{f.exp}/C_{f.th}$ and Re number obtained from Exp. 2. The theoretical pipe friction can be given by $C_{f,th}$=96/Re and the tiny clearance is set to 5, 10 and 30 μm in this figure. The increasing ratio is close to 1 under no magnetic field. The tendency of the change in the increasing ratio is quite different between 5 and 30 μm of tiny clearance, but the maximum increasing rate is similar for each clearance. The increasing ratio at 30 μm of tiny clearance is gradually increases with decreasing Re number and increasing magnetic field intensity. On the other hand, this ratio in case of 5 μm sharply increases with decreasing Re number, and although this ratio increases by applying magnetic field, the increasing level does not change even if magnetic field intensity increases.

References:

[1] Mizutani et al., *Procedia CIRP*, 33, 2015, pp. 581-586.
[2] JSRAE, *Compressors for Air Conditioning and Refrigeration*, JSRAE Technical Books Series, 2018, p. 91

BARIUM TITANATE BASED ACOUSTIC SENSING ELEMENTS

N. Motsi[1,a], N. Siafakas[1], A.Mamalis[2,b], E.Hristoforou[1,c]

[1]School of Electrical and Computer Engineering, National Technical University of Athens, Iroon Polytechniou 9, 15780 Zografou, Greece, [a]nefelimotsi@mail.ntua.gr, [c]hristoforou@ece.ntua.gr
[2]Project Center for Nanotechnology and Advanced Engineering (PC-NAE), NCSR Demokritos, Athens, 15310, Greece,[b]agmamalis@yahoo.com

Abstract. Materials with the ability to generate voltage when subjected to mechanical stress, such as PZT and $BaTiO_3$ are used in various applications such as supercapacitors, dielectrics ceramics and catalysts. Barium titanate ($BaTiO_3$) possesses various advantageous properties in terms of its structure, piezoelectricity and ferroelectricity. Yet, to further enhance these properties, barium was substituted with strontium using both sintering and sol-gel methods. Barium strontium titanate (BST) ferroelectric materials have attracted significant interest due to their chemical stability, high permittivity, excellent tunability and minimal dielectric losses. This study demonstrates the synthesis of perovskite $Ba_xSr_{(1-x)}TiO_3$ materials, with varying strontium content ranging from 0% to 50%, using the sintering and the sol-gel processes. In addition, the samples were examined using scanning electron microscopy (SEM), X-ray diffraction (XRD), differential thermal analysis (DTA) and thermogravimetry analysis (TGA).

1. Introduction

Barium titanate ($BaTiO_3$), a commonly used piezoelectric ceramic material, possesses a high dielectric constant and low dielectric loss, which render it an exceptional choice for electronic applications and piezoelectric sensors [1-2]. By replacing barium with strontium in $BaTiO_3$ through sintering and sol-gel techniques, the development of Barium Strontium Titanate (BST) material aimed to improve its sensitivity and response. The properties of BST ceramics, such as ferroelectricity and dielectricity, are affected by factors including sintering conditions, grain size, porosity, doping amount, and structural defects [3]. The enhancement of dielectric properties can be achieved by optimizing the doping and sintering conditions. BST is a solid solution that combines barium titanate ($BaTiO_3$) and strontium titanate ($SrTiO_3$), and its Curie temperature varies depended on the Ba/Sr ratio. To determine the most effective approach, this study synthesized $Ba_xSr_{(1-x)}TiO_3$ with different Sr contents and analyzed their structure and properties.

2. Experimental procedure and sample preparation

To synthesize $Ba_xSr_{(1-x)}TiO_3$ materials via sintering, a powder mixture consisting of barium carbonate ($BaCO_3$), strontium carbonate ($SrCO_3$), and titanium dioxide (TiO_2) was used. The mixture was ball milled in distilled water, and then the samples underwent Differential Thermal Analysis (DTA) to identify the temperatures at which the reactions resulting in the formation of $BaCO_3$ and $SrCO_3$ occur. Subsequently, the calcined powders were subjected to cold isostatic pressing at a pressure of 200 MPa, forming discs with a weight of 3g, a diameter of 3cm, and a width of 1.5mm. These discs were then sintered in an air atmosphere at 1500°C for 4 hours.

For the production of $Ba_xSr_{(1-x)}TiO_3$ using the sol-gel method, the raw materials consisted of barium acetate ($Ba(CH_3COO)_2$), strontium acetate ($Sr(CH_3COO)_2$), and titanium isopropoxide ($Ti(OC_3H_7)_4$). Solvents such as acetic acid (CH_3COOH), acetylacetone ($CH_3COCH_2COCH_3$), and propylene glycol ($C_3H_8O_2$) were used, along with distilled water as an additional agent. Initially, the solutions were subjected to calcination at 120°C to form xerogels. Subsequently, the xerogels were analyzed using Thermogravimetric Analysis (TGA) and Differential Thermal Analysis (DTA). The xerogels were then sintered in an air atmosphere at 750°C for 90 minutes, with a heating rate of 5°C/min. Following this, the calcined xerogels were cold isostatically pressed at a pressure of 200 MPa, resulting in the formation of discs weighing 3g, with a diameter of 3cm and a width of 1.5mm. Finally, the disks were sintered at 1500°C for 2 hours.

All the samples produced via sintering and sol-gel method, were examined by X-ray diffraction (XRD) and scanning electron microscopy (SEM).

3. Results of characterization techniques

Based on the XRD graphs presented in Figure 1(a), it can be observed that all the samples produced through the sintering and the sol-gel methods exhibit a perovskite structure. The predominant crystalline orientation is directed towards the [111] crystallographic axis across various Sr concentrations. It is evident that the formation of barium-strontium titanate has been successfully achieved. Yet, when examining the

samples with 30% Sr and 50% Sr in $Ba_xSr_{(1-x)}TiO_3$ prepared via the sintering process, the presence of a $SrTiO_3$ peak indicates an unsuccessful blending of $BaCO_3$ and $SrCO_3$ powders prior to the calcination step.

Figure 1(b) illustrates SEM micrographs of piezoelectric materials produced by both the sintering and the sol-gel methods. One the one hand, the sintering process results in materials that possess uniform microstructures and the formation of necks between particles. On the other hand, samples produced via the sol-gel method exhibit nonuniform microstructures with the presence of aggregations. However, as the amount of Sr increases in the barium-strontium titanate (BST) material, the microstructure appears to improve and become more uniform.

Figure 1(c) displays that at temperatures above approximately 160°C, water and other liquids undergo vaporization. At temperatures below 300°C, the deposits of organic solutions onto xerogel powders vaporize. The peaks observed in the DTA curve correspond to the deconstruction of carboxyls and alkoxides. Within the temperature range of 300°C to 400°C, the formation of carbides and oxides (such as $BaCO_3$ or TiO_2) occurs, followed by the eventual production of the desired perovskite structure of BST through the sol-gel method. Between 450°C and 550°C, the plateau in the plot signifies a loss of mass, which correlates with the peaks observed in the DTA curve.

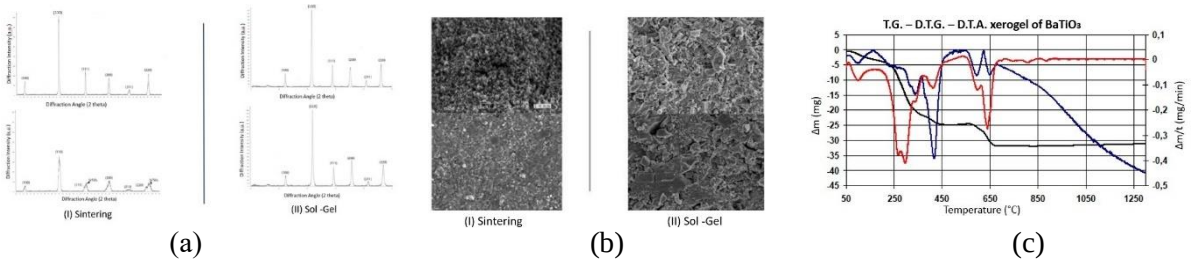

Fig. 1 Characterization techniques: (a) XRD diagrams, (b) SEM micrographs and (c) T.G. - D.T.G. - D.T.A of $Ba_xSr_{(1-x)}TiO_3$ piezoelectric materials.

Conclusions:

- The formation of barium-strontium titanate has been successfully accomplished.
- The Differential Thermal Analysis (DTA) indicates that the process for creating $BaTiO_3$ occurs at a temperature of 950°C. Additionally, the formation of $SrTiO_3$ takes place at a higher temperature of 1050°C.
- Sintered BST materials exhibit a more consistent microstructure and the formation of necks between particles, whereas samples produced by the sol-gel method display a nonuniform microstructure with the presence of aggregations.
- Based on the XRD analysis, samples synthesized using the sol-gel method demonstrate superior crystallographic properties compared to those obtained through sintering.

References:

[1] Duong N.X., Bae J.S., Jeon J., Lim S.Y., Oh S. H., Ullah A., ... & Kim T.H. Polymorphic phase transition in $BaTiO_3$ by Ni doping, Ceramics International, (2019), **45(13)**, 16305-16310.

[2] Mi L., Zhang Q., Wang H., Wu Z., Guo Y., Li Y., ... & Qi X. Synthesis of $BaTiO_3$ nanoparticles by sol-gel assisted solid phase method and its formation mechanism and photocatalytic activity, Ceramics International, (2020), **46(8)**, 10619-10633.

[3] Reddy S. B., Rao K. P., & Rao M. R. Effect of La substitution on the structural and dielectric properties of $BaZr_{0.1}Ti_{0.9}O_3$ ceramics. Journal of alloys and compounds, (2009), **481(1-2)**, 692-696.

STUDY OF SILICON-GRAPHENE PROPERTIES

A. Bakhtiari[1,a], T. Berberashvili[1], P. Kervalishvili[1], A. Bilbilashvili[2], Z. Kushitashvili[2]

[1] Georgian Technical University, Kostava str. 77, Tbilisi, Georgia
[2] Institute of Micro and Nanoelectronics, Ilia Chavchavadze Ave. 13, Tbilisi, Georgia
[a]bakhtiari.habib@gmail.com

Today, modern life on the Earth is correlated to semiconductors. Silicon abundance on the Earth and its nontoxic properties make it the most favorite material in semiconductor industries. But, its physical properties are restricted, then its efficiency is limited. The application of material science is essential in efforts to increase the efficiency. In this regards, Graphene Thin-Film on Silicon is a significant method for efficiency improvement.

Each atom in a graphene Thin-Film is connected to its three nearest neighbors by a σ-bond, and contributes one electron to a conduction band that extends over the whole sheet. These conduction bands make graphene a semimetal with unusual electronic properties. Hence, Graphene nanolayer (Thin-Film) that is deposited on the Silicon improve its physical properties such as thermal and electrical conductivity as well as magnetic properties.

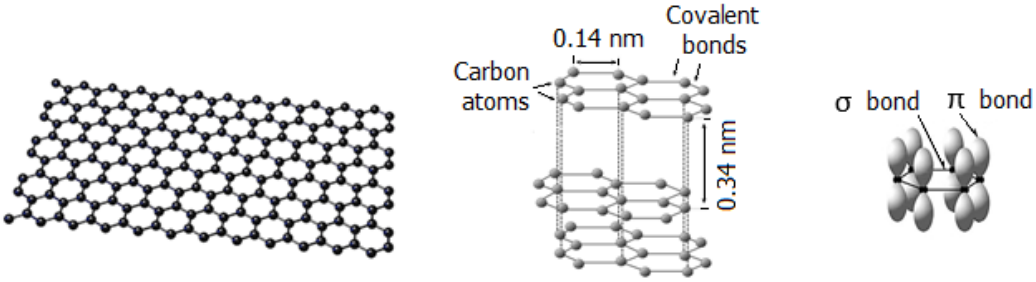

In this work first, Silicon physical properties improvement by Graphene Thin-Film is studied generally. However, there are different Silicon physical properties that could be improved by Graphene Thin-Film, but the authors current experimental investigation focused on electrical properties improvement. Therefore, the novel Thin-Film methodology (CWLD) and related results will be discussed secondly [1,2].

References:

[1] Kervalishvili P., Bakhtiari A., Berberashvili T. Phototransforming Device, Georgian Intellectual Properties Center, Patent No: P 2020 7134 B, 2018
[2] Bakhtiari A., Kervalishvili P. Dynamic Fractal Doctrine as Nonlinear Systems Model, American Journal of Condensed Matter Physics 2021, 11(1): 1-6, DOI: 10.5923/j.ajcmp.20211101.01

EXPERIMENTAL DEVICE FOR 2D MATERIALS PREPARATION BY LASER-PLASMA METHOD

A. Bakhtiari[1], W. Maier[2], P. Kervalishvili[1]

[1] *Georgian Technical University, Kostava str. 77, Tbilisi, Georgia*
[2] *AE Solar GmbH, Messerschmittring 54, Konigsbrunn, Germany*
bakhtiari.habib@gmail.com

Two-dimensional (2D) materials have attracted enormous research interest due to their predominant quantum effects and fascinating materials properties, that potentially lead to different important applications. 2D materials physical properties such as the other materials come out their structure quality. On the other hand, refer to their critical Nano sizes, manufacturing requires very accurate methodology. Hence, Thin-Film methodology is significant.

However, there are various methods, but they categorized in 2 Thin-Film methodologies as *Physical Vapor Deposition* (PLD) and *Chemical Vapor Deposition* (CVD). Thin-Film methodologies assessment are correlated to the final product quality and production cost. Therefore, the methodology flexibility and feasibility are the main factors.

In the presenting work, a novel and patented method as Thin-Film preparation by Laser-Plasma (CWLD) is introduced [1,2]. Also, the method is comprised to the other common methods and its flexibility and feasibility will be investigated.

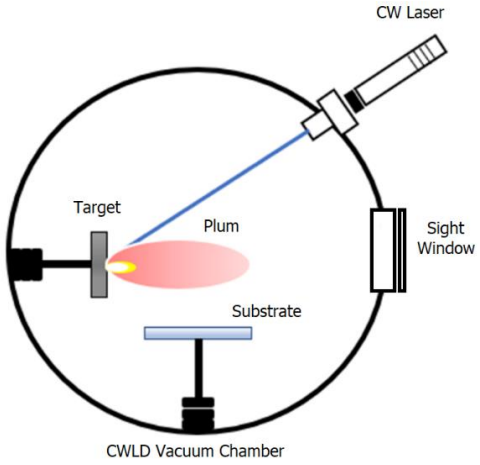

References

[1] Bakhtiari A., Maier W., Kervalishvili P. Device for obtaining solid-state films by laser-plasma method Georgian Intellectual Properties Center,Patent applied 2021 (Case No. 15728/1)
[2] Bakhtiari A., Berberashvili T., Kervalishvili P. Preparation of Graphene Structures by Continuous Wavelength Laser Deposition Method, American Journal of Condensed Matter Physics 2022

PRODUCTION OF HOMOGENEOUS COMPOSITE PRESS-POWDERS BASED ON ZRB_2 AND SIC FOR UHTCS

G. Bokuchava[1], E. Sanaia[1], Z. Mestvirishvili[1,a], N. Jalagonia, T. Prikhna[2], T. Kuchukhidze, N. Darakhvelidze

[1] Ilia Vekua Sukhumi Institute of Physics and Technology. 7 Mindeli Str., Tbilisi, Georgia
[2] V.Bakul Institute for Superhard materials, 2, Avtozavodskaya Str., Kiev, Ukraina
[a]zviad.mst@gmail.com

Abstract. The aim of the research was to obtain superfine homogeneous composite powders, which, due to their unique composition and morphology, will be used to obtain ceramics with improved properties for the thermal protection of supersonic aircraft. The novelty of research was microstructure refining methods, selection of sintering additives/dopants and their combining action. As regards sintering additives and dopants, B_4C and graphite powder, carbon black and graphene structures were used. The use of the latter individually and in combination sintering additives was one of the innovations of the research.

1. Introduction

Materials working in the extreme environment are subject to permanent research. The extreme environment is the joint impact of temperature, chemically reactivity, mechanical stress, wear, etc. Such an environment is formed on the nose cone, wing leading edges and the propulsion system components of the hypersonic space vehicle (HSSV), generally during the HSSV's atmospheric re-entry and rocket propulsion. Already in its early reports, NASA underlined the necessity for rocket nozzles and thermal protection systems (TPSs) [1-3]. A particular attention was paid to the conditions associated with the entry into atmosphere, the rocket engine and the requirements to the materials of the leading edges and propulsion system of vehicles. A whole series of recommendations contained in the reports are still being prioritized for modern research. Studying the properties of refractory borides and carbides for hypersonic aerospace vehicles is a part of research carried out in the U.S.A. A great impact in the NASA reports was made in the definition of Ultra-High Temperature Ceramics (UHTCs), where zirconium and hafnium borides are the main candidates for HSSV. Based on the properties of zirconium boride ceramics, the ZrB_2-based UHTCs are rather promising in the TPS materials. Of special interest is the ZrB_2-SiC composite ceramics, on which a major part of the ZrB_2 research falls.

2. Experimental procedure

Milling and mixing of the powders were carried out in the tungsten carbide jar with zirconium oxide milling balls by the planetary micro mill PULVERISETTE 7 (FRITSCH, Germany). Zirconium oxide balls eliminated contamination of the powders with new elements. A novelty was the production of a multiphase mixture with equally distributed phases of different size and inhibitors, using ultrasonic, the planetary milling machine and granulator. Ultrasonic homogenizer TF-1000N and Granulator SD-1000 was also used. Production of ZrB_2 fine powders were carried out by carbo/borothermal reduction at 1500-1650°C in the high-temperature vacuum furnace FR210-30T-A-200-EVC (OXY-GON, USA) according to the following reaction: $2ZrO_2 + B_4C + 3C \rightarrow 2ZrB_2 + 4CO\uparrow$. In parallel, graphene structures were synthesized using modified Hummer's method; thereafter, reduction of the produced graphene oxide were carried out by chemical reagents, using ultrasonic and a microwave oven. Because graphene structures are characterized by the ability to aggregate, which prevent its homogeneous distribution in the matrix and have an affect the mechanical properties of the final product, graphene was prepared in the form of stable suspensions, for which an organic solvent was selected, where we placed graphene and treated by ultrasound for 1-2 hours. Graphene structures obtained in this way are ideal for use as additives in composites. A composite powder (mixture) with different stoichiometry - $ZrB_2 + SiC + B_4C(C)$ were produced. At first, we carried out powder milling and mechanic activation for production homogeneous mixtures of composite powders ($ZrB_2 + SiC + B_4C(C)$).

Next step was production of press-powders using sintering additives/dopants by nano mill, ultrasonic, and a granulator.

3. Results and discussions

In Fig. 1 the results of X-Ray, PSD and scanning microscopy of the ZB_2-powder are presented. The XRD shows a small amount of ZrC along with the ZrB_2, which was expected because carbon black was taken in excess. PSD da Scan indicate the superfine size of the powder.

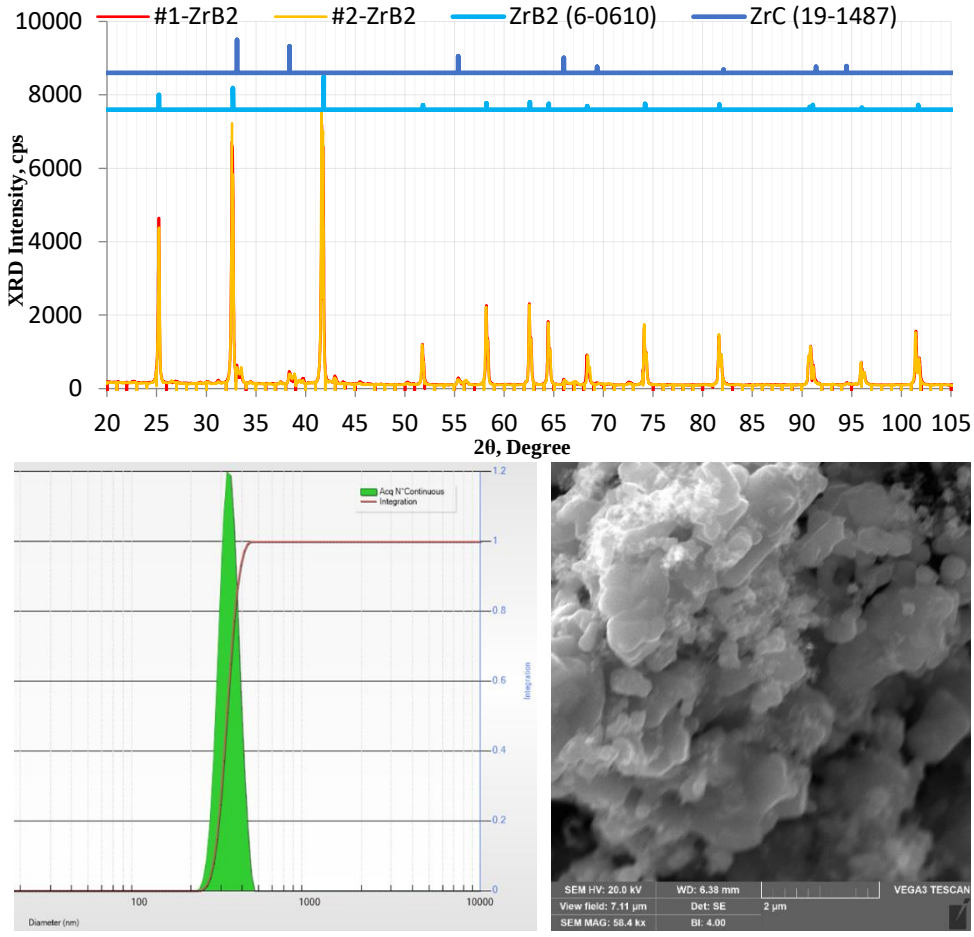

Fig.1. The results of X-Ray, PSD, and scanning microscopy of the ZB_2-powder

Conclusions:

A method has been developed of production of the superfine homogeneous composite press-powders based on ZrB_2 and SiC. For this, both methods of mechanical processing of powders and selection of sintering additives/dopants and their combining action were used. The method of obtaining super fine ZrB_2 powder is also developed, where, by adjusting the stoichiometry, the powder of the desired chemical composition is obtained.

Acknowledgement:

This work was supported by Shota Rustaveli National Science Foundation of Georgia (SRNSFG) [# FR-21-1603, Graphene structure-reinforced composite for thermal protection of hypersonic space vehicles].

References:

[1] Jaffe H.A. Development and testing of superior nozzle materials. National Aeronautics and Space Administration Final Report for Project NASw-67. Washington, DC: National Aeronautics and Space Administration; April 1961.

[2] Freeman J.W., Cross H.C. Notes on heat-resistant materials in Britain from technical mission October 13 to November 30, 1950. National Advisory Committee for Aeronautics Technical Memorandum RM51D23. Washington, DC: National Advisory Committee for Aeronautics (NACA); May 14, 1951.

[3] U.S. Air Force and National Aeronautics and Space Administration Joint Conference on Manned Hypervelocity and Reentry Vehicles: A Compilation of Papers Presented; NASATMX-67563; April 11–12, 1960; Langley Research Center, Langley Field, VA.

FUNCTIONAL SUPERCONDUCTOR-FERROMAGNET NANOSTRUCTURES FOR SUPERCONDUCTING ELECTRONICS

A. S. Sidorenko[1,a], V. Boian[1,b], E.I. Antropov[1,c], Yu. B. Savva[2,d], A.A. Lomakin[2,e], A.V. Vakhrushev[3,f]

[1]Institute of Electronic Engineering and Nanotechnologies named after D. Ghitu, Moldova, MD-2028, Chisinau, Academiei 3/3, [a]sidorenko.anatoli@gmail.com, [b]boianvladimir@gmail.com, [c] aidjek@gmail.com

[2]Orel State University named after I.S. Turgenev, Russia, 302026, Orel, Komsomolskaya, 95, [d]su_fio@mail.ru, [e] lomakin@gmail.com

[3]Udmurt Federal Research Center, Ural Branch of the Russian Academy of Sciences, ul. T. Baramzina, 34 [f]vakhrushev-a@yandex.ru

Abstract. The work is devoted to the study of the processes of formation and analysis of the parameters of a functional nanostructure - a superconducting spin valve, which is a multilayer structure consisting of ferromagnetic cobalt nanofilms separated by niobium superconductor films. The studies were carried out using molecular dynamics simulations and vacuum deposition of the modelled nanostructures. The atomic structure of individual nanolayers of the system is considered. Particular attention is paid to the analysis of the atomic structure of the contact regions, since the quality of the interface between the layers plays a decisive role in creating of a microelectronic devices. The obtained results can be used both in the development and optimization of technologies for the formation of spin valves and other functional elements of spintronics.

1. Introduction

The development of nanotechnologies led to the emergence of a special section of quantum electronics - spintronics [1]. The systems in spintronics are based on heterostructures consisting of ferromagnets, superconductors and normal metals [2], which implies the creation of multilayer nanocomposites formed by nanofilms. The aim of this study is to analyze the processes of formation and microstructure of a multilayer nanostructure: superconductor (niobium)-ferromagnet (cobalt).

2. Experimental procedure and sample preparation

The samples are fabricated by vacuum deposition in the magnetron sputtering system LEYBOLD Z400 of the film material on Si (111) substrates. In the general case, the nanosystem contains more than 20 layers, but the processes of their formation, as well as their structural features, are similar.

3. Mathematical model and problem statement

The study of the contact layer between superconducting and ferromagnetic materials was carried out by the method of molecular dynamics, while considering both the process of formation of nanolayers and the resulting structure formed by atoms inside a multilayer nanocomposite. The basis of the method of molecular dynamics is Newton's equation of motion, which is solved for each elementary particle:

$$m_i \frac{d^2\vec{r}}{dt^2} = -\frac{\partial U(\vec{r})}{\partial \vec{r}_i} + \vec{F}_{ex}, \vec{r}_i(t_0) = \vec{r}_{i0}, \frac{dr_i(t_0)}{dt} = \vec{V}_{i0}, i = 1, \dots N \quad (1)$$

where N is the total number of atoms in the nanosystem; m_i is the mass of the i-th atom; $\vec{r}_{i0}, \vec{r}_i(t)$ are the initial and current radius vectors of the i-th atom, respectively; $U(\vec{r})$ - potential energy or potential of the system, depends on the relative position of all particles; $\vec{V}_{i0}, \vec{V}_i(t)$ are the velocity vectors at the initial and current moment; $\vec{r}(t) = \{\vec{r}_1(t), \vec{r}_2(t), .., \vec{r}_K(t)\}$ - generalizing variable, indicates dependence on all coordinates of atoms; $\vec{F}_{ex}$ - the strength of the external environment, it also serves to maintain a constant temperature. For the definiteness of the solution of the equation of molecular dynamics, it is necessary to have clarifying conditions, which in (1) are the indication of the initial coordinates and velocities for all atoms.

4. Results and their analysis

Figure 1 illustrates the layer-by-layer analysis of the Nb/Co heterostructures composition.

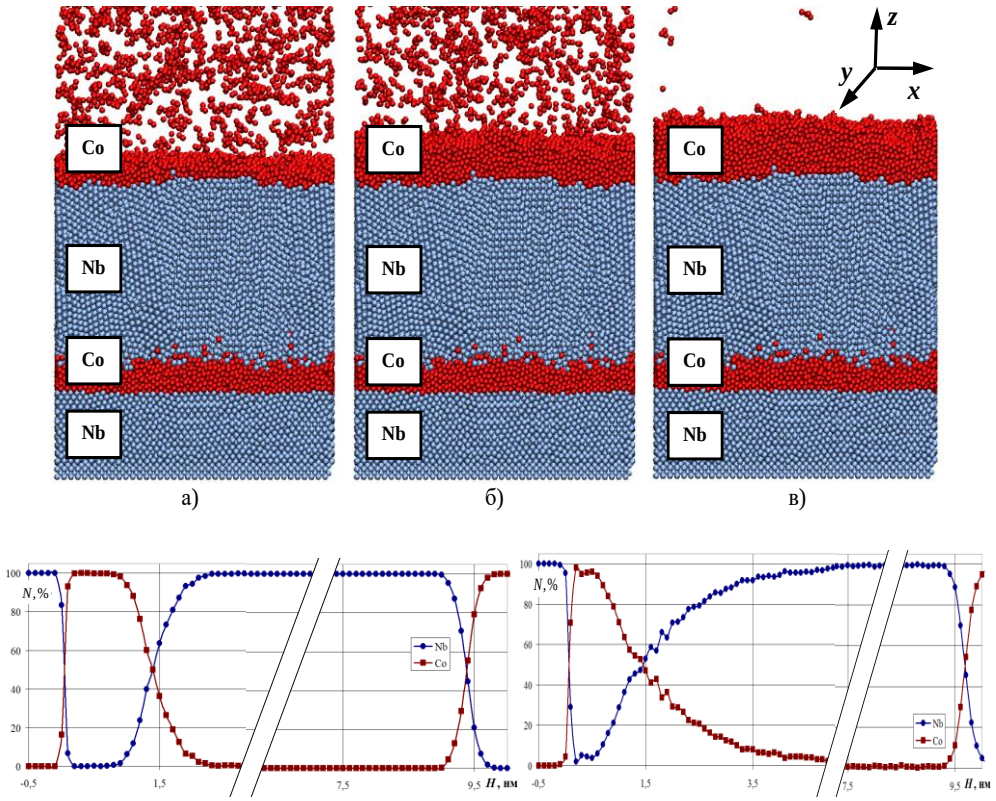

Fig.1. Deposition of a heterostructure from niobium and cobalt (upper panel) at temperature of 300 K, deposition time a) 0.1 ns, b) 0.2 ns and c) 0.4 ns (top panel). Percentage composition of a multilayer Nb/Co nanocomposite formed at 300 K (bottom panel, left) and at 800 K (bottom panel, right)

The deposition of layers corresponding to alternating elements, Nb and Co, led to the formation of contact layers in the niobium/cobalt interfaces. The contact areas are characterized by a change in the structure and the presence of a mixed composition (bottom panels in Fig1). An analysis of the structure of these layers also shows that niobium is formed by crystalline regions of different directions. Cobalt nanofilms are characterized by a structure close to amorphous one.

Conclusions:

Several series of computational and vacuum deposition experiments were carried out in the work, in which the formation of heterostructures at high temperatures (300, 500 and 800 K) were studied. The results obtained indicate a significant dependence of the processes of formation of multilayer nanocomposites, their contact areas, as well as the composition and structure of the layers on the temperature at which the formation of a multilayer nanosystem occurs.

This work was done in frame of the project Nr. 20.80009.5007.11 of the Moldova State Program (samples fabrication and investigation) and the grant RSF No. 20-62-47009 (theory development, nanostructures modelling).

References:

[1] Krupa M.M. Advantage Engineering Technologies. 2007. V. 2, 1 (2007).
[2] Sidorenko A.S. Fizika Nizkikh Temperatur. V.43, 962 (2017).

POSTERS

INTEGRATING IOT INTO AGRICULTURAL OPERATIONS TOWARDS THE INDUSTRY 4.0 AND SUSTAINABILITY

E. Symeonaki[1,a], H.C. Leligou[1,b], D. Tseles[1,c], T. Ganetsos[1,d], C. Drosos[1,e]

[1]*Dept. of Industrial Design and Production Engineering, University of West Attica, Greece*
aesimeon@uniwa.gr, be.leligkou@uniwa.gr, cdtsel@uniwa.gr, dganetsos@uniwa.gr, edrososx@uniwa.gr

Abstract. Industry 4.0 is a trend that is expected to have major impact on the transformation of all industrial sectors. Since agriculture is probably the most essential sector of the primary industry, facing the challenge of ensuring food security with regard to sustainability, it is significant to integrate the technological advancements that emerged in the context of Industry 4.0 within the agricultural operations. This paper presents an approach of facilitating agricultural operations by employing an IoT based system, capable of delivering a variety of operational services.

1. Introduction

The Industry 4.0 concept, which was originally introduced by the German National Academy of Science and Engineering [1], represents a prominent trend expected to significantly affect the modernization of all industrial sectors [2] by promoting a framework for the integration of the entire production process into a "smart" digitalized environment. In this sense, since agriculture is a major sector of the primary industry, it is essential to launch the Industry 4.0 technological advancements into agricultural operations, in order to address the excessive challenge of ensuring food security for the constantly increasing world population with regard to the climate change effects and the imperative necessity for long-term sustainable usage of environmental resources.

Provided that the Industry 4.0 concept is considered to be a "collective" term through the establishment of a digitalized environment wherein physical and virtual objects can interconnect and interact autonomously along the entire value chain [3], it is strongly tied to the technology of the Internet of Things (IoT). In all industrial sectors, among which is agriculture, the IoT integrates the concepts of "Internet" and "thing" offering some key features such as heterogeneity, interoperability, high scalability, interconnectivity, object-related services as well as dynamic changes [4].

This paper is keen to present an approach of employing a responsive and adaptive IoT based system, capable of delivering a wide variety of services in order to facilitate agricultural operations. To this end, the proposed approach adopts a layered hierarchical structure consisting of a farming facility at the lower level and two higher levels involving cloud components. It is considered that such an approach constitutes an alternative solution for overcoming computational and storage challenges by using the resources offered into the cloud in order to facilitate the process, analysis and storage of sizeable amounts of raw data acquired remotely in multiple agricultural environments, and support the control of infrastructures as well as the making of critical decisions related to the optimization of agricultural production. In such manner the framework acts in the backend as a DSS providing finally intelligent services which optimize agricultural production, minimize the cost and assist all agricultural stakeholders in making decisions for the benefit of sustainability.

2. Operational Overview of the System

According to the suggested IoT operational framework, the raw data, which are acquired by the sensors of a Wireless Sensor and Actuator Network (WSAN) located in a farming facility, are transmitted to a context-aware middleware cloud wherein they are modified accordingly to context. These generated contextual data are additionally managed inside the middleware cloud, along with incoming rules that are provided by the services cloud, so as to result in monitoring information, control actions and services. Subsequently, the context-aware middleware cloud responds back to the actuator nodes of the farming facility's WSAN triggering the proper equipment infrastructures in order to perform the required agricultural operations. Additionally, end-users, such as farmers, agronomist engineers and food commodities merchants, are provided with real-time monitoring information and context-aware services, mostly but not exclusively via suitable mobile apps, so as to undertake further assistive actions. In this sense, end-users can manage agricultural operations remotely by means of the cloud services. It is worth noting that that this framework, may be easilyapplied to more than one farming facilities. Within the proposed system, the IoT serves as the

enabling technology for efficient farm management ensuring maximum agricultural output of optimum quality and increase the profitability of various agricultural production schemes.

3. Implementation and Performance Evaluation

In order to study the functionality of the operational framework, a model was developed by employing the Python programming language for prototyping and a cloud platform for computing infrastructure and services. The performance of the system has been validated by conducting a number of trials both in simulated and actual conditions in a farming facility in Greece.

Testing the system allowed its proper analysis and evaluation in terms of health, operation, and performance. In general, according to the outcomes provided by the metrics obtained during the tests, the system performs fairly satisfactory for controlling one agricultural facility environment since sensory data could be adequately acquired, processed, stored in the knowledge base, retrieved and disseminated to the applications of interest, resulting consequently into the proper actions. Nevertheless, the performance of the system is intended to be more thoroughly tested by evaluating additional parameters and integrating multiple agricultural environments for various cultivations and in distinct locations as part of future research.

Conclusions:

In conclusion, it is strongly believed that the proposed system framework may support the integration of agricultural operations toward the Industry 4.0 concept. It is in that regard that the introduced approach, based on the integration of WSANs into the IoT, has the benefit of being effortlessly adaptable, modifiable, and extendable for any application in any agricultural system environment no matter how complex it is.

Future work on the subject is intended to include an in-depth performance evaluation of the model through the integration of multiple agricultural facility environments with various cultivations and in distinct locations, in order to improve the interoperability and standardization of the proposed framework. For what is more, since the involvement of smart mobile devices and social networking was not taken into much consideration, these features are going to be included as part of the ongoing work.

References:

[1] Kagermann H., Wahlster W., Helbig J. (2013) Recommendations for Implementing the Strategic Initiative Industrie 4.0 - Securing the Future of German Manufacturing Industry; AcatechNational Academy of Science and Engineering: Munich, Germany. Available online: http://forschungsunion.de/pdf/ industrie_4_0_final_report.pdf [Accessed March 01, 2023]

[2] Xu L.D., Xu E.L., Li L. (2018) Industry 4.0: state of the art and future trends. International Journal of Production Research, 56(8), pp.2941–2962.

[3] Pfeiffer S. (2017) The Vision of "Industrie 4.0" in the Making—a Case of Future Told, Tamed, and Traded. NanoEthics, 11(1), pp.107–121

[4] Talavera J.M., Tobón L.E., Gómez J.A., Culman M.A., Aranda J.M., Parra D.T., Quiroz L.A., Hoyos A., Garreta L.E. (2017) Review of IoT applications in agro-industrial and environmental fields. Computers and Electronics in Agriculture, 142, pp.283–297

DEVELOPMENT AND CHARACTERISTICS OF METAL-POLYMER LAMINATES

G. Baliashvili[1], T. Iashvili[1,a], S. Kvinikadze[1,c], D. Tsverava[1,d] , G. Abashidze[1,e] , A. Vanishvili[1,g]

[1]LEPL Grigol Tsulukidze Mining Institute., 7, E. Mindeli Str., 0186, Tbilisi, Georgia
[a]g.baliashvili@yahoo.com, [b]Tamuna123iashvili@gmail.com, [s]sophi.kvinikadze@gmail.com,
[d]datotsverava@gmail.com, [e]guramiabashidze@yahoo.com, [g]alexandre.vanishvili@gmail.com

Abstract: For the last 20 years, research about impact-resistant polymeric materials is going intensively. The issue is a modern actual scientific and technical problem. Such material includes Metal-Polymer laminates. Metal-Polymer laminates are hybrid composite materials that consist of conventional fiber reinforced plastics with the addition of a metal component, typically a foil or mesh layers. While a range of potential advantages and applications have been discussed for such materials, the primary application to date has been for aircraft structures. Nowadays, laminates find its use in construction. Aim of Research is developing of metal-polymer laminate type materials with improved mechanical properties which will have a wide range of applications. Such kind of materials were obtained by the scientists at the Grigol Tsulukidze Mining Institute. In terms of the development of polymer chemistry, it is possible to produce such composites with targeted properties and use of synthetic fiber reinforced materials, that would satisfy wide–specter exploitation conditions, namely, the conditions of dynamic loads on material. The advantage of the proposed technology for making metal-polymer laminate compared to other technologies are lower costs of electricity (30-40% less), the possibility of receiving large-sized products/details and 40-50% lower cost of labor.

Acknowledgment:

This work was supported by Shota Rustaveli National Science Foundation of Georgia (SRNSFG) – Grant # AR–22–1445: Production of multifunctional metal-polymer laminate with high mechanical characteristics and determination of technological parameters.

ZrO_2 NANOPOWDERS AS FILLERS OF EPOXY POLYMERS

T. Hryhorenko[a], Y. Kochergin, X. Meng

Harbin Institute of Technology, China
[a]grigorencot@outlook.com

The effect of ZrO_2 nanopowders on the deformation-strength, adhesion, tribological and thermophysical properties of epoxy polymers in a wide range of concentrations has been studied. Zirconium oxide with various heat treatment, differing particle sizes and specific surface area, phase composition and the presence of an alloying additive – Y_2O_3 were used as nanopowders.

The preparation of ZrO_2 nanopowder was carried out by precipitation of hydroxide from a solution of nitric acid salt with an aqueous solution of ammonia. In order to obtain particles of different sizes, zirconium oxide was calcined at 500 and 700°C.

When using ZrO_2 nanopowders as a filler of epoxy polymers, it is possible to achieve an increase in tensile strength, elastic modulus and the work of destruction of the material by more than 100, 80 and 200%, respectively, compared with an unfilled sample.

The dependence of the complex of properties on the calcination temperature of the injected powder is established. Higher values of strength characteristics, modulus of elasticity, fracture work and abrasion resistance when using nanopowders with a calcination temperature of 500°C are associated with a smaller particle size and a larger specific surface area compared to powders obtained at 700°C. The alloying of zirconium dioxide powder with yttrium oxide provides an increase in the modulus of elasticity and compressive strength.

Interesting results were obtained in the study of the effect of the thickness of the samples on their deformation and strength characteristics. It is established that the values of tensile strength and elastic modulus initially increase with increasing sample thickness, reaching a maximum at a sample thickness of ~ 0.4 mm, and then monotonically decrease with increasing sample thickness. At the same time, the thinnest sample has the lowest strength in the entire thickness range, and the thickest has the smallest modulus of elasticity.

The deformation at break at small thicknesses increases almost linearly with increasing sample thickness, reaches a maximum at a sample thickness of 1.5 mm, and then decreases. At the same time, the difference between the maximum and minimum values of tensile strength, modulus of elasticity and deformation at break is 1.45; 4.0 and 1.7 times, respectively. It is revealed that the microhardness index also depends on the geometric dimensions of the sample.

ON THE CONVERGENCE OF THE SOLUTION OF SCHRODINGER EQUATION FOR FINITE DIFFERENCE METHOD

D. Kobaidze[1,a], T. Gagnidze [1], T. Tchelidze [1], T. Davitashvili [1], H. Meladze [2]

[1]Ivane Javakhishvili Tbilisi State University, Tbilisi, Georgia, [a]daviti.kobaidze708@ens.tsu.edu.ge
[2]Muskhelishvili Institute of Computational Mathematics

Abstract. In the present paper we investigate the convergence of solution of the Schrodinger equation for potential energy of particular conditions. The issue is crucial for application of numerical techniques, such as finite difference method.
Keywords: Schrodinger equation, Finite difference method

1. Introduction

Quantum mechanical processes and dynamics of quantum particles are described by Schrodinger equation [1]. It is well known, that Schrodinger equation has exact, analytical solutions (wave functions and energy spectrum),only in few cases. There are a lot of interesting from practical and theoretical point of view potentials, for which it is unable to write down exact solutions. Therefore, it is of great importance to proceed numerical calculations. One of the most important and practically usable way to solve the equation is the finite difference method [2]. The problem is that when we solve the equation numerically, firstly it must be known if the solution is convergent. One of our main purpose is to show that the solution of Schrodinger type equation converges when we use finite difference method to solve it.

2. Theoretical framework

Let's discuss the following equation:

$$L(u) = u''(x) - p(x)u(x) = -f(x), \qquad x \in [0, X]; \tag{1}$$

$$u(0) = a, \quad u(X) = b\,. \tag{2}$$

On $[0, X]$ segment, let's define regular grid with the step $h = \frac{X}{N}$. Denote this grid by $\overline{\omega_h}$. On this grid we change the equation (1) by the finite difference equation, which reads as follows:

$$l(y_n) = \frac{y_{n+1} - 2y_n + y_{n-1}}{h^2} - p_n y_n = -f_n\,, \quad n = 1,2,3, \dots, N-1 \tag{3}$$

In this case boundary conditions will be:

$$y_0 = a, \quad y_N = b\,. \tag{4}$$

It can be proven, that if $p(x) \geq 0$, than problems (3), (4) have unique solution which converges.

We also estimate the expected error of the method, which turns out to be satisfactory.

Acknowledgment:
The work is supported by Shota Rustaveli National Science Foundation of Georgia, Grant Number STEM-22-188.

References:

[1] David J. Griffiths, Introduntion to Quantum Mechanics, Prentice Hall, 1995
[2] Randall J. LeVeque, Finite Difference Methods for Differential Equations, 2004

PARTICLE IN A MULTI-STEP QUANTUM WELL

N. Basharuli[a], T. Tchelidze

Ivane Javakhishvili Tbilisi State University, Tbilisi, Georgia, [a]nikabasharuli907@ens.tsu.edu.ge

Abstract. We developed the method of solving the Schrodinger equation for multi-step quantum well, with arbitrary step number. The solution very useful for modeling of semiconductor hetero-structures of varying composition.

1. Introduction

Semiconductor quantum structures - quantum wells, quantum wires, quantum dots are very important for modern electronics and optoelectronics. As in quantum structures additional parameters for controlling electrical and optical properties, such as size, shape and material distribution, appear. In the presented paper we investigate multistep quantum wells; particularly we find eigen functions and eigen values of particle (electron, hole) confined in it.

2. Theoretical framework

We model our physical potential with the following potential

$$V(x) = \begin{cases} V_N & |x| < L_N \\ V_{N-1} & L_N < |x| < L_{N-1} \\ \vdots & \\ V_2 & L_3 < |x| < L_2 \\ 0 & L_1 < |x| \end{cases} \tag{1}$$

where the depth and the width of each successive well is arbitrary

$$V_N < V_{N-1} < \ldots < V_1 < 0 \qquad \text{and} \qquad 0 < L_N < L_{N-1} < \ldots < L_1$$

If a particle is located in this potential and it's energy is $V_m < E < V_{m-1}$ then its wavefunction (odd and even) will be of this form:

$$\phi(x) = \begin{cases} Ae^{-\alpha_0 x} & x > L_1 \\ B_1 \cosh(\alpha_1 x) + C_1 \sinh(\alpha_1 x) & L_1 > x > L_2 \\ \vdots & \\ B_{m-1} \cosh(\alpha_{m-1} x) + C_{m-1} \sinh(\alpha_{m-1} x) & L_{m-1} > x > L_m \\ B_m \cos(a_m x) + C_m \sin(\alpha_m x) & L_m > x > L_{m-1} \\ \vdots & \\ B_{N-1} \cos(a_{N-1} x) + C_{N-1} \sin(\alpha_{N-1} x) & L_{N-1} > x > L_N \\ D \sin(\alpha_N x) \text{ or } D \cos(\alpha_N x) & L_N > x > 0 \end{cases} \tag{2}$$

expansion to x < 0 will have the same coefficients just with the different signs. Then these coefficients can be expressed as:

$$\begin{bmatrix} B_n \\ C_n \end{bmatrix} = T(n)^{-1}_{n,n} \left(\prod_{j=1}^{n-1} T(j)_{j+1,j} T(j)^{-1}_{j,j} \right) \Gamma \begin{bmatrix} A \\ 0 \end{bmatrix} \tag{3}$$

For the even case:

$$\begin{bmatrix} D \\ 0 \end{bmatrix} = T(N)^{-1}_{N,N} \left(\prod_{j=1}^{N-1} T(j)_{j+1,j} T(j)^{-1}_{j,j} \right) \Gamma \begin{bmatrix} A \\ 0 \end{bmatrix} \quad (4)$$

and for the odd case:

$$\begin{bmatrix} 0 \\ D \end{bmatrix} = T(N)^{-1}_{N,N} \left(\prod_{j=1}^{N-1} T(j)_{j+1,j} T(j)^{-1}_{j,j} \right) \Gamma \begin{bmatrix} A \\ 0 \end{bmatrix} \quad (5)$$

Here the terms $T(j)_{n,m}$ are some 2x2 matrices that depend on j,n,m. Equating the right hand side of the (4), (5) equating to 0 we obtain from the first component the energy spectrum for the odd wavefunction and from the second component - energy spectrum for the even wavefunction. However the equations are difficult to solve since the L's and V 's were taken arbitrary, nevertheless it may be possible to regularize the choice of those quantities in a way to get solvable equations for the energy spectrum

Acknowledgment:
The work is supported by Shota Rustaveli National Science Foundation of Georgia, Grant Number STEM-22-188.

MODELING AND OPTIMIZATION OF PROPERTIES OF GA2O3-BASED QUANTUM STRUCTURES IN ORDER TO ACHIEVE HOLE CONDUCTIVITY

T. Gagnidze[1,2,3,a*], D. Kobaidze[1], L. Burdiladze[1], N. Basharuli[1], E. Chikoidze[4], T. Davitashvili[1], H. Meladze[5], T. Tchelidze[1]

[1]*Ivane Javakhishvili Tbilisi State University, Tbilisi, Georgia*
[2]*AndronikaShvili Institute of Physics, Tbilisi, Georgia*
[3]*Chavchanidze Institute of Cybernetics, Tbilisi, Georgia*
[4]*Groupe d'Etude de la Matiere Condensee (GEMaC), Universite de Versailles Saint Quentin en Y.-CNRS, Universite Paris-Saclay, 45 Av. des Etats-Unis, 78035, Versailles Cedex, France*
[5]*Muskhelishvili Institute of Computational Mathematics, Tbilisi, Georgia*
[a]*tornike.gagnidze@tsu.ge*

Abstract: In this project, we investigate the properties of Ga_2O_3-based quantum structure with the aim of improving hole conductivity in the oxide. Ga_2O_3 is a promising material for electronic and optoelectronic applications due to its ultra-wide band gap and high breakdown voltage. However, its low hole mobility and concentration limit its performance in some applications. Recent studies have shown that Ga_2O_3 thin films can exhibit surface p-type conductivity under certain growth conditions. In this work, we use the finite-element method to model the electronic properties of Ga_2O_3 quantum well with triangular potential barrier. Our results provide insights into the design and optimization of Ga_2O_3-based quantum structures for improved hole conductivity in the oxide.

1. Introduction:

Gallium oxide is a ultra-wide band gap semiconductor material that has attracted increasing attention for its potential use in electronic and optoelectronic devices due to its high breakdown voltage and optical transparency in the visible to ultraviolet region. However, its low hole mobility and concentration limit its performance in certain applications. Recently, surface p-type conductivity has been observed in Ga_2O_3 thin films grown under specific conditions, which provides a promising pathway to improve its hole conductivity[1,2].

In this project, we use the finite-element method to model the electronic properties of Ga_2O_3-based quantum structures with triangular confinement potential. The triangular potential well is a widely adopted geometry due to its similarity to the potential profile observed in quantum heterojunctions, for instance the modulation-doped AlGaAs-GaAs heterojunction, for electrons confined within GaAs[3]. Our investigation aims to understand the impact of this confinement potential on the electronic structure of Ga_2O_3-based quantum structures, and how it can be optimized to enhance their hole-concentration and mobility.

In our study, we solved the Schrödinger equation with triangular potential using the WKB (Wentzel-Kramers-Brillouin) approximation, which is a method used to obtain approximate solutions to quantum mechanical problems [4]. Additionally, we developed a finite-element method to tackle the triangular barrier with a finite wall, which is a more challenging problem. Additional, we take into account the presence of impurities, which are known to affect the electronic properties of semiconductor materials.

By employing these methods, we were able to gain insights into the electronic properties of quantum structures with triangular confinement potentials. Our findings can guide the experimental efforts towards developing high-performance electronic and optoelectronic devices based on Ga_2O_3.

Acknowledgment:
The work is supported by Shota Rustaveli National Science Foundation of Georgia, Grant Number STEM-22-188.

References:

[1] Chikoidze E., et al., J. Vac. Sci. Technol. A. 40, 043401 (2022)
[2] Chikoidze E., et al., Mater. Today Phys. 3, 118 (2017)
[3] Tsui D.C., et al., Phys, Rev. Lett. 48, 22 (1982)
[4] Barnham K., Vvedensky D. Low-dimensional semiconductor structures: Fundamentals and device applications: Cambridge university press (2008)

PROPOSAL OF A 3-D STEREOLITHOGRAPHY SYSTEM INCORPORATING MAGNETIC LEVITATION TECHNIQUE

T. Ohji[1,a], K. Nishi[1], J. Yui[1], K. Amei[1]

[1] *Faculty of Engineering, University of Toyama, 3190 Gofuku, Toyama 930-8555, Japan*
[a] *ohji@eng.u-toyama.ac.jp*

Abstract. This paper proposes a novel stereolithography (SLA) system for forming designed models by photocuring and stacking magnetically levitated special fluid. A drawback of stereolithography, one of the 3-dimensional printing techniques, is the post-processing of burrs and wasted support materials. The proposed method repeats photocuring while magnetically levitating magnetic photocurable resin (mPCR) fluid. Therefore, burrs and support materials are unnecessary, saving both time and money. The system has two main structural requirements; one is to generate an upward attractive force so that the mPCR fluid and its formed object do not droop under gravity, and the other is to irradiate the laser beam while reliably tracking the apex of the mPCR fluid cone that is magnetically supported and manipulated. This paper briefly introduces the prototype machine, designed to align a laser beam path, the controlled electromagnet with a through-hole, and the apex of magnetically levitated mPCR fluid.

1. Introduction

One of the additive manufacturing (AM) technologies is the stereolithography apparatus (SLA) [1], which uses photocurable resin liquid. SLA is a higher-resolution fabrication method than fused deposition modeling (FDM) with filament materials. Figure 1 shows the basic principle of SLA. A Z stage exists in a container (reservoir) filled with photocurable resin liquid. A laser beam is scanned in the *x*- and *y*- directions using Galvano mirrors. The resin liquid on the Z stage surface is cured only where the beam is irradiated. In the stacking process, support legs other than the modeled object are also layered, and the portions are removed after completion. The support legs cause extra material, printing time, removal process, and deburring.

We have developed a magnetic levitation (maglev) device that is easy to use for levitating a magnetic fluid droplet at room temperature and in the atmosphere [2]. Figure 2 is a photo of a magnetic fluid cone with its apex position controlled. When the controlled electromagnet installed above moves in the *x*- and *y*- directions, it has been confirmed that the apex of the fluid cone follows while maintaining the positioning control state. Utilizing this know-how, we propose a new stereolithography incorporating a maglev technique that uses magnetic photocurable resin (mPCR) fluid and has no support leg and burr to the limit.

2. Concept

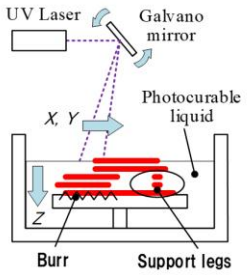

Fig. 1

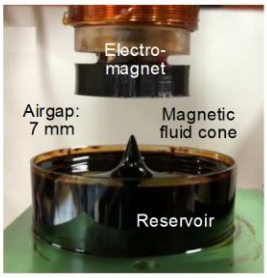

Fig. 2

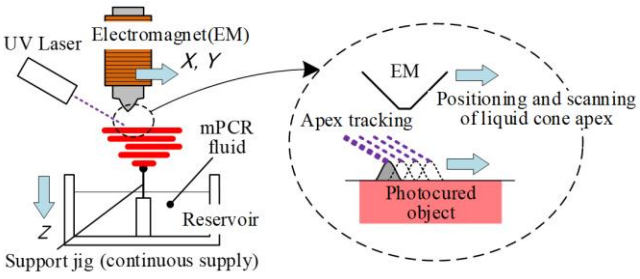

Fig. 3

Fig. 1. Basic principle of SLA. Fig. 2. Photo of a positioning-controlled magnetic fluid cone. Fig. 3. Conceptual diagram of a new SLA system with maglev functions

Figure 3 is a conceptual diagram of the proposed SLA system. The system consists of an electromagnet, a displacement sensor, control equipment, a laser light source, an mPCR fluid reservoir, and a support jig. The mPCR fluid belongs to suspensions. It consists of 10 wt% triiron tetroxide (Fe_3O_4) powder (average particle size is around 1.0 um) dispersed uniformly in an acrylate prepolymer resin solution. It responds well to magnetic fields and UV light with a wavelength of 405 nm. First, a controlled attractive force from the electromagnet pulls up the mPCR fluid from the reservoir to the tip of the support jig. Next, the laser beam photocures the top of magnetically levitated mPCR fluid. Furthermore, additive manufacturing would be possible by moving the electromagnet in the *x*- and *y*- directions and the reservoir in the *z*-direction,

simultaneously scanning the laser beam to track the apex of the fluid cone.

3. Configuration of a prototype machine

Figure 4 shows a prototype machine based on the concept of Fig. 3. The main requirements for the proposed SLA system are as follows:

- The attractive force from the electromagnet can pull up mPCR fluid from the reservoir to a desired position along the surface of the support jig;
- The pulled-up mPCR fluid can be fixed with photocuring at the top of the support jig;
- The attractive force can move the mPCR fluid cone in the *x*-, *y*-, and *z*- directions while controlling the apex position of the cone;
- The laser beam can always track the apex of the cone; and
- Vibrations from moving parts should not affect forming quality.

When the electromagnet, suspended from a linear stage fixed to the aluminum frame, was moved left and right, housing vibration occurred due to the movement, and the laser beam could not track the apex of the fluid cone. To solve these issues of vibration and misalignment, in the prototype machine shown in Fig. 4, a laser beam path, the controlled electromagnet with a through-hole on the central axis, and the apex of a fluid cone are aligned center vertically, and the reservoir is placed on the XYZ stage. As a result, the tip of the support jig set in the reservoir moves three-dimensionally, thereby advancing the stereolithography process.

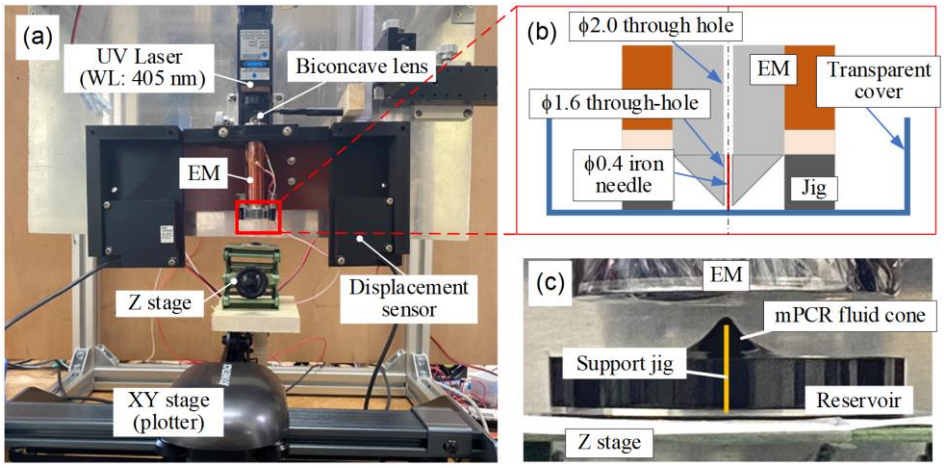

Fig. 4 A prototype machine of SLA with maglev functions: (a) overall structure; (b) cross section of the electromagnet tip; and (c) positioning control test for the apex of mPCR fluid cone

Acknowledgement:

This research is supported by JSPS KAKENHI Grant Number JP21H01308.

Conclusions:

This research has just started to develop the 3-dimensional stereolithography system with maglev functions. Pulling up and positioning control of mPCR fluid (see Fig. 4c) and photocuring at the top of the support jig have been achieved.

References:

[1] US Patent, No. 4575330, Apparatus for production of three-dimensional objects by stereo-lithography, 1986.

[2] Ohji T., Yamaguchi S., Amei K., Kiyota K. Magnetic Levitation of a Ferrofluid Droplet in Mid-Air, AIP Advances (Vol.10, Issue 1), 015037, 2020.

TO THE PROPERTIES OF LASER-INDUCED PLASMA

D.Jakobia[1,a*], P.Kervalishvili[2,b], N.Gomidze[1,c]

[1]Batumi Shota Rustaveli State University, 6010 Batumi, Georgia, [a]david.935335@gmail.com, [c]gomidze@bsu.edu.ge

[2]Georgian Technical University, Kostava str. 77, Tbilisi, Georgia
[b]paata.kervalishvili@gtu.ge

Abstract: Laser-induced breakdown spectroscopy (LIBS) is an analytical technique that uses a laser-induced plasma to perform elemental analysis of a sample. It is a versatile and non-destructive method that can be applied to various materials, including solids, liquids, and gases.

1. Introduction:

LIBS offers several advantages as an analytical technique. It is rapid, often requiring only a few seconds to analyze a sample. It is also non-contact and non-destructive, which means it can be used to analyze samples in their natural state without requiring any sample preparation. Additionally, LIBS can be performed remotely, making it suitable for applications such as space exploration or hazardous environments.

The basic principle of LIBS involves focusing a laser pulse onto the surface of a sample, causing rapid heating and vaporization of the material. This creates a high-temperature plasma plume consisting of ions, atoms, and electrons. The plasma emits characteristic radiation in the form of atomic and molecular emission lines when the excited species return to their ground state. These emission lines correspond to the elemental composition of the sample.

The emitted radiation is collected and passed through a spectrometer, which disperses the light into its constituent wavelengths. A detector then measures the intensity of the emitted light at specific wavelengths, allowing identification and quantification of the elements present in the sample. The resulting spectrum provides information about the elemental composition and concentration of the sample.

2. Challenges and limitations of LIBS:

While LIBS has numerous applications and advantages, it also presents certain challenges and limitations:

Plasma Instabilities: Laser-induced plasma can exhibit instabilities, such as filamentation or irregular plasma shapes. These instabilities can affect the consistency and reliability of experimental results. Careful control of laser parameters is required to minimize these instabilities

Heating and Damage: High-power laser pulses used to generate plasma can cause heating and damage to the target material or surrounding environment. Excessive heating can alter the sample's properties or even lead to its destruction. Proper selection of laser parameters and appropriate cooling techniques are essential to mitigate these issues.

Spectral Interferences: In spectroscopic applications, spectral interferences can occur when the emitted radiation from the plasma overlaps with other emission lines or background noise. This hinders accurate identification and quantification of elements. Careful calibration and advanced data analysis techniques are required to address spectral interferences.

Matrix Effects: In analytical applications, the matrix effect refers to the influence of the sample composition on the plasma generation and emission characteristics. Different sample matrices can affect the plasma temperature, electron density, and particle composition, leading to variations in the measured signals. Compensating for matrix effects requires proper calibration strategies and reference materials.

"The matrix effect makes the preparation of high-quality standards important," said Steven J. Rehse, an associate professor in the Department of Physics at the University of Windsor, "It also makes it more difficult to sample highly heterogeneous samples like complex minerals or complicated powders like dirt or soil." [1]

Quantitation and Reproducibility: Achieving consistent and reproducible results with laser-induced plasma can be challenging due to the complexity of plasma dynamics and various experimental parameters. Careful control of laser parameters, sample preparation, and experimental conditions is crucial to ensure reproducibility.

Before LIBS can become available on a large scale we have to solve issue with same sample groups having variation in spectral signal. Resulting in Laser Induced plasma Spectroscopy spectra for the same experiment on different instruments having nonidentical results.

For this issue, an assistant professor at Johns Hopkins University, Ishan Barman, suggested to move from reproducibility issue and try to use LIBS only as a "robust screening tool". As a screening tool, the relative variations-due to laser fluctuations, environmental and matrix effects, and self-absorption-would cease to have as much of an impact [1].

Improving Equipment: development of new compact, accurate device for LIBS experiments. This will improve resulting accuracy and time needed for process. Currently we posses Porta-Libs-2000 device, which consists of laser emitter, sample frame-box and spectrometer that is connected to terminal with installed software to view results.

Signal-to-Noise Ratio: Laser-induced plasma signals can be relatively weak, especially for trace element analysis or when detecting low-concentration species. The signal-to-noise ratio can limit the sensitivity and detection limits of the technique. Advanced detection systems and signal processing methods are employed to enhance the signal-to-noise ratio.

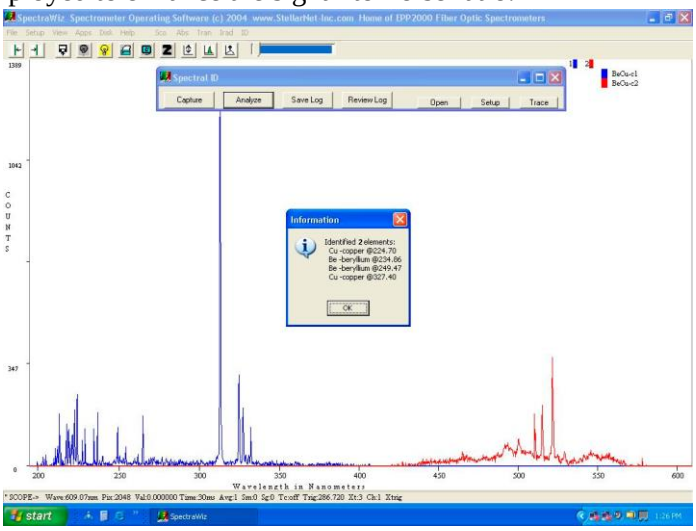

Theoretically, we can improve received results with introducing better calculations methods, improving software and creation of standardized data library. Such methods wont's require improving hardware (CCD detectors, optical transfer cables, laser emitter) that would lead to much higher price and unavailability to reserchers.

Conclusion:

Addressing these problems requires a combination of experimental optimization, advanced instrumentation, and data analysis techniques. Despite these challenges, laser-induced plasma remains a valuable tool in various scientific fields and continues to be an active area of research and development.

References:

[1] Analysis of the State of the Art: LIBS, **Spectroscopy-06-01-2015,** Volume 30, Issue 6, https://www.spectroscopyonline.com/view/analysis-state-art-libs

CREATION 3D FLUORESCENCE SPECTRA OF WINE

M.Khajishvili[*1, a], N.Gomidze[1, b], I.Jabnidze[1, c], K.Makharadze[1, d], L.Kalandadze[1, e], O.Nakashidze[1, f]

[1]*Batumi Shota Rustaveli State University, 6010 Batumi, Georgia*
miranda.khajishvili@bsu.edu.ge

Abstract: Our research provides for the analysis of different types of Georgian wine based on 3D fluorescence spectroscopy (3DF) using the Black Comet (200-950 nm) spectrometer manufactured by StellarNet. In this method, the 3D fluorescence signal is divided into a fixed number of statistical components. For each type of wine, a 3D database is strictly defined, which we conventionally call references. The etalon describe the excitation/emission spectra in detail. The advantage of the 3DF method compared to other statistical methods, such as peak component analysis (PCA), lies in the uniqueness of the unfolding of the spectra. The fluorescence spectra of the wine will be further analyzed by peak component analysis (PCA). After performing the PCA analysis, in order to reduce the number of tolerant etalon, we used the tolerant etalon sample (TES) comparison analysis, thus determining how tolerant the researched wine sample is to this or that specific etalon.

Keywords: 3D fluorescence spectroscopy, peak component analysis, wine analysis, Georgian wine, Tolerant etalon sample

1. Introduction

The combination of 3D fluorescence spectroscopy (3DF) and peak component analysis (PCA) has been used in various fields, including chemistry, biology, environmental science, and food analysis.

The combination of 3D fluorescence spectroscopy (3DF) and peak component analysis (PCA) presents a powerful tool for quality control and authentication in the wine industry, particularly for Georgian wine.

The algorithm for processing the fluorescence excitation-emission matrix for the classification of Argentine white wine is presented in [1]. The effectiveness of using the TES method in wine classification lies in the fact [2] that the types of molecules (such as polyphenols, vitamins, amino acids) and the amount depend on the specific type and maturity of the wine, as well as the wine technology [3].

The study includes fluorescence spectroscopy excitation/emission matrix (AEM) analysis, peak component analysis (PCA) and tolerance etalon sample (TES) comparison analysis method development and modeling according to wine product variety and origin. About 100 samples of four types of white Georgian wine were taken. The methodology chosen by us is based on the one hand on the hardware complex, which was gradually modernized by our group [4,5,6], on the other hand on the development of new analytical approaches [7] that are quite acceptable to be used in typical laboratory control of food products and beverages.

For analyses 3D spectra it is known techniques that are specifically designed for spectroscopic data analysis, such as Multivariate Curve Resolution (MCR), Parallel Factor Analysis (PARAFAC), or Multivariate Analysis of Variance (MANOVA).

2. Experiment

Fluorescence spectra were recorded using a Black Comet (200-950 nm) spectrometer manufactured by StellarNet. LED lamps of different frequencies were used as light sources. A wine sample of 100 µl is placed in a quartz cuvette and the spectra are recorded at room temperature. The number of scans is determined from the same experimental measurement to exclude drift effects on the sample. At the beginning of each experiment, the standard is calibrated. The excitation wavelength range is between 250-500 nm, and the emission wavelength is between 275-600 nm. Measurements are performed at different excitation wavelengths with a 5 nm bias. The total time to scan a sample is approximately 10 minutes. Measurements were performed over a short period of time (10-15 days), thereby minimizing the influence of atmospheric effects and instrumental fluctuations (eg. lamp intensity fluctuations).

PCA was performed for descriptive analysis of spectral features and TES modeling of analog classes will be used to classify these data. SpectraWiz and LAbView software were used for graphical visualization of the spectra. Data recording and processing were performed in MS Excel and MySQL.

3. Results and Conclusion

With PCA analysis, we will build tables and graphs for the sample of a specific group. Figure 1a shows the generation of 2D data with non-linear correlation and the execution of PCA to reduce the dimensionality to 1D. We visualize data points in a reduced one-dimensional space. Figure 1b shows a 2D plot that visualizes the original 2D data and the first principal component vector obtained from PCA. In Figure 1b visualized the

original 2D data as scattered points and plot the first principal component vector obtained from PCA as a red arrow. The arrow represents the direction of maximum variance in the data, which corresponds to the first principal component. The plot also includes a label indicating that it represents the principal component.

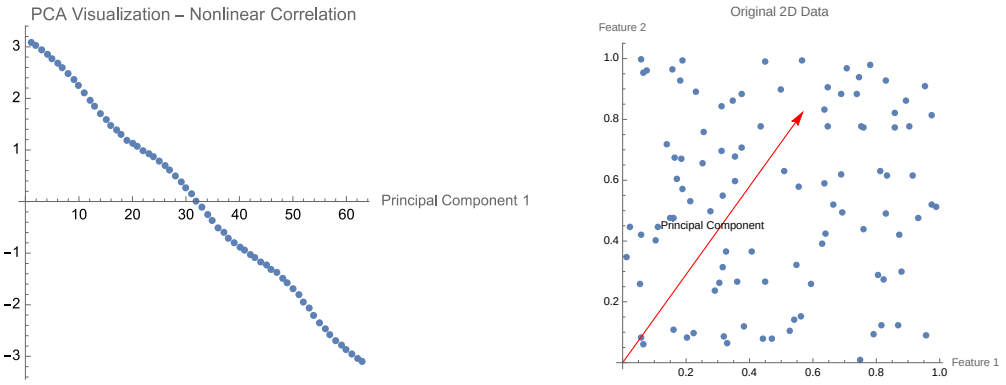

a) b)

Fig.1. a) 2D data with non-linear correlation and the execution of PCA to reduce the dimensionality to 1D, b) 2D plot that visualizes the original 2D data and the first principal component vector obtained from PCA

In Figure 2 given 3D plot to visualize the original 3D data, the principal component vectors obtained from PCA, and the data points projected onto the principal component subspace. In this 3D plot, we visualize the original 3D data as scattered points, plot the first two principal component vectors obtained from PCA. The data points projected onto the principal component subspace as green points.

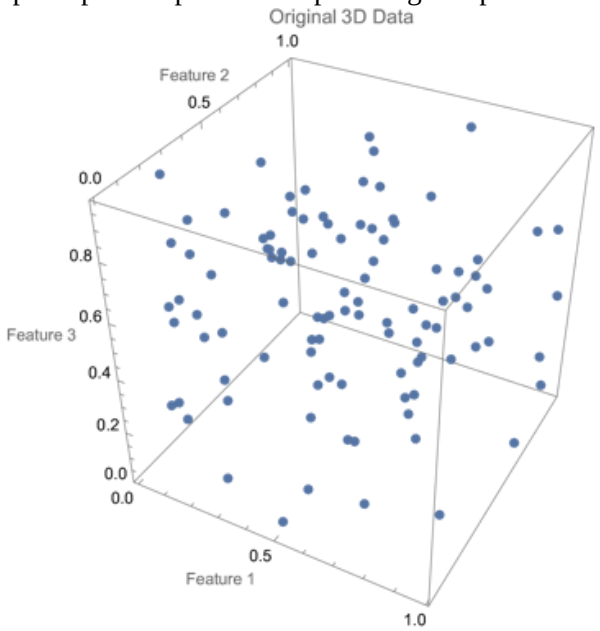

Fig.2 3D plot to visualize the original 3D data, the principal component vectors obtained from PCA

Conclusion:

The combination of 3DF and PCA allows for a detailed assessment of the unique fluorescence patterns present in different types of Georgian wine. This can be used as a reliable method for quality control and authentication, helping to identify any adulteration or counterfeit products in the market. By comparing the fluorescence spectra of a given wine sample with the well-defined references (etalons), we can verify its authenticity and origin.

The fluorescence spectra of wine can be influenced by factors such as grape variety, soil composition, and climate conditions. The 3DF method, combined with PCA and etalon references, can potentially be used to establish a link between the fluorescence patterns and the geographical origin of the wine. This could be valuable for wine producers aiming to protect and promote wines with specific geographical indications.

Different vintages of the same wine type can exhibit variations in their fluorescence properties due to varying environmental conditions and winemaking processes. The 3DF analysis, along with PCA and etalon

references, might help discern these subtle differences and aid in distinguishing between wines from different years.

Some wines are known for their unique characteristics and premium quality, which are often reflected in their distinct fluorescence profiles. Utilizing the 3DF method with PCA analysis can help classify wines into different quality grades based on their fluorescence patterns. This information can be valuable for consumers, sommeliers, and wine enthusiasts when making purchasing decisions.

Understanding the fluorescence properties of different wines can provide insights into the chemical composition and structural changes during the winemaking process. This knowledge may assist winemakers in optimizing their production techniques and ensuring consistent quality in the final product.

The 3DF technique can provide a wealth of data on the complex chemical composition of wines. Researchers can use this information to study the presence of various compounds and their interactions, contributing to a deeper understanding of wine chemistry and its influence on wine characteristics.

Overall, the combination of 3DF, PCA, and etalon references in the analysis of Georgian wine offers a powerful and sophisticated approach to gain valuable insights into the unique fluorescence properties of different wine types. As this technology evolves and becomes more established, it has the potential to revolutionize the field of wine analysis and enhance various aspects of the wine industry.

Acknowledgement:

Work was supported by the 2023 Competition for Targeted Scientific Research Projects On the Development of the Fluorescence Excitation-Emission Etalon Matrix Algorithm of Wine". Batumi Shota Rustaveli State University (2023), project manager PhD of Physics Miranda Khajishvili

References:

[1] Azcarate S. M. *et al*. (2015). Modeling excitation–emission fluorescence matrices with pattern recognition algorithms for classification of Argentine white wines according grape variety. *Food Chem.* **184**, 214–219.

[2] Wold S. (1976). Pattern recognition by means of disjoint principal components models. *Pattern Recognit.* **8**, 127–139.

[3] Urbano M., Luque de Castro, M. D., Pérez, P. M., García – Olmo, J. & Gómez – Nieyo, M. A. (2006). Ultraviolet – visible spectroscopy and pattern recognition methods for differentiation and classification of wines. *Food Chem.* **97**(1), 166–175.

[4] Gomidze N., Jabnidze I., Makharadze K., Khajishvili M., Shashikadze Z., Surmanidze Z., Surmanidze I. (2012). Numerical Analyses of Fluorescence Characteristics of Watery Media via Laser Spectroscopy *Method. Journal of Advanced Materials Research. Vol. 590*, pp. 206-211. www.scientific.net/AMR.590.201

[5] Gomidze N.Kh., Makharadze K.A., Khajishvili M.R., Jabnidze I.N., Shashikadze Z.Kh. (2014). Some Issues of Fluorescence Characteristics Aqueous Media via Diagnosis of Laser Spectroscopy Method. *International Journal of Engineering, Science and Innovative Technology*. ISSN No: 2319-5967 (ISO 9001:2008 Certified, Impact Factor of IJESIT is 1.753), №3, issue 3, pp.142-152. http://www.ijesit.com/Volume%203/Issue%203/IJESIT201403_17.pdf

[6] Gomidze N.Kh., Jabnidze I.N., Surmanidze Z.J. (2016). Stroboscopic Method of Fluorescence Analyses of Optically Solid Media. *2016 IEEE 7th International Conference on Advanced Optoelectronics and Lasers (CAOL)*. September 12-15, Odessa, Ukraine, pp. 34-36.

[7] Khajisvili M.R., Gomidze N.Kh, Shainidze J.J. (2021). 3D Fluorescence Spectroscopy of Liquid media via internal reference method. *INTER-ACADEMIA 2021: Research and Education: Traditions and Innovations*, Part of the Lecture Notes in Networks and Systems book series (LNNS, volume 422, pp.59-71). DOI: 10.1007/978-981-19-0379-3_7. 3D Fluorescence Spectroscopy of Liquid Media via Internal Reference Method | SpringerLink

STRUCTURAL PROPERTIES OF III-NITRIDES RECEIVED BY UV STIMULATED TECHNOLOGY

Z. Kushitashvili[1,a], A. Bibilashvili[1,2,b], R. Guliaevi[1,c], A. Kurtanidze[4,d]

[1]*LEPL Institute of Micro and Nanoelectronics, Chavchavadze ave.13, 0179 Tbilisi, Georgia*
[2]*LEPL Institute of Micro and Nanoelectronics, Chavchavadze ave.13, 0179 Tbilisi, Georgia*
[3]*LEPL Institute of Micro and Nanoelectronics, Chavchavadze ave.13, 0179 Tbilisi, Georgia*
[4]*Ivane Javakhishvili Tbilisi State University, Chavchavadze ave.1, 0179 Tbilisi, Georgia*
[a]*zurab.kushitashvili@ens.tsu.edu.ge*, [b]*amiran.bibilashvili@tsu.ge*, [c]*rezo.guliaev@gmail.com*,
[d]*ana.kurtanidze854@ens.tsu.edu.ge*

Abstract. In terms of structural studies, X-ray diffraction (XRD) studies are discussed in this paper. Based on the experimental results, X-ray diffraction graphs of III nitrides obtained with and without UV irradiation are shown and is evaluated the role of UV stimulation in magnetron sputtering technology.

Key words: 2θ degree, intensity, FWHM.

1. Introduction

The presented paper discusses the structural analysis of III nitrides (GaN, AlN, InN). These nitrides are obtained by reactive magnetron sputtering technology stimulated by ultraviolet radiation [1,2,3]. This technology has been the leading technology for many decades to obtain thin metallic, semiconductor and dielectric films. With this technology, it is possible to obtain not only individual elements, but also their compounds. Such compounds are represented by wide-bandgap semiconductors gallium nitride (GaN), aluminum nitride (AlN) and indium nitride (InN). For this purpose, magnetron sputtering takes place in the presence of the reagent gas whose chemical compound we want to obtain. In our case, such a reagent gas is nitrogen (N2). An important factor in obtaining clean and high quality materials along with technological processes is the use of clean precursor materials. These materials include the material to be sputtered from the magnetron, in our case gallium, aluminum and indium, and the purity of the reagent gas. The purity of the metals used in the experiments was 99.95%, and in the case of the reagent gas nitrogen - 99.9999%.

Novelty and innovation in the technology of obtaining III-nitrides is the use of ultraviolet (UV) radiation [4,5,6] directly in the process of obtaining nitrides. UV radiation (365 nm wavelength) falls directly on the surface on which the nitrides are grown. Its intense absorption by the deposited first monoatomic layers helps to change the mutual arrangement of atoms and by this way prevents the formation of defects, since the formation and growth of the crystal in any crystallographic direction depends on the structure of the first monoatomic layers. Since III-nitrides are obtained on sapphire plates, it becomes even more important in the technology to eliminate defects at the boundary separating the two environments. Because it is known that in relation to sapphire, III nitrides have a large lattice mismatch. Therefore, introducing an additional stimulating component and reducing defects is a priority in these studies.

2. Experiment

To obtain III nitrides, reactive magnetron sputtering technology is used, which is performed on a „УВН-2М-1'' vacuum unit. This device is equipped with a two-stage vacuum system - a mechanical pump and a turbomolecular pump. By their action, the vacuum system can obtain a vacuum of $1 \cdot 10^{-6}$ torr. Vacuum measuring instruments and mass spectrometer (RGA 200) for residual gas analysis are attached to the vacuum chamber (Fig. 1).

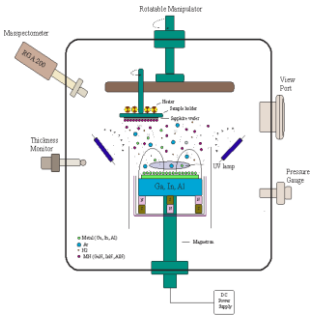

Fig.1 magnetron sputtering system

3. Results and disscutions

One of the important places in the research of III nitrides was determining the influence of UV radiation in the growth process of nitrides. As can be seen from Table 1, in the process of obtaining gallium nitride, UV stimulation accelerates the process and the deposition rate in the case of

GaN-37s and GaN-38s increases from 10.6 nm/min to 12.3 nm/min, while GaN-39s and GaN-40s increases from 17.2 Nm/min to 18.5 Nm/min. In the first case, the stimulation result is 16%, and in the second case is about 7%. The relatively low (7%) stimulation result is due to temperature and deposition current differences. In the case of a 16% increase, the average temperature is 650^0C and the deposition current is 100 mA, and in the second case the average temperature is 70^0C and the deposition current is 150 mA.

It is clear from the data that the structural parameters of GaN-38s are better (2θ=32.08; FWHM=828 sec) than those of GaN-27s. Also, the thickness of the sample obtained with UV (1511 nm) exceeds the thickness of GaN-27s (1272 nm). Which means that UV stimulation increases the deposition rate, and in the case of these two samples, the rate increased from 10.6 nm/min to 12.3 nm/min. Below are the X-ray graphs of GaN-27s and GaN-38s (Fig.2 and Fig.3).

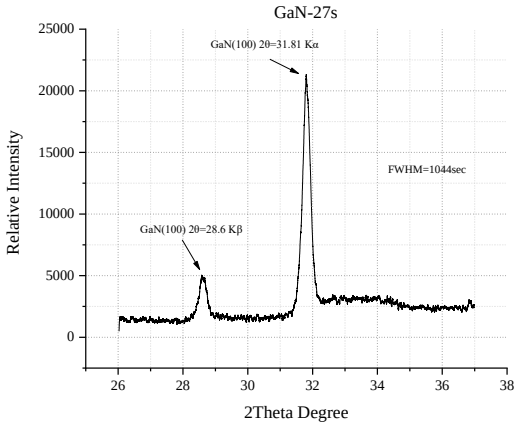

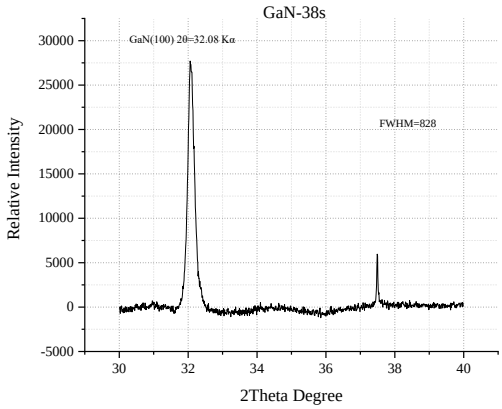

Fig.2 GaN XRD pattern for specimen GaN-27s **Fig.3 GaN XRD pattern for specimen GaN-38s**

Let's compare GaN-39s and GaN-40s samples obtained at low temperature. GaN-39s obtained without UV and GaN-40s obtained with UV. Thay have all other parameters the same. The same result is recorded here as in the case of the previous two samples. The structural parameters are better for the sample obtained by technological processes with UV, than for the sample obtained without UV. Here too, UV radiation stimulates the technological process and increases the deposition speed from 17.2 nm/min to 18.5 nm/min. It should be noted that the effect of UV stimulation in the case of these two samples is less pronounced than the previous two samples, both in terms of structure and deposition rate increase. which is mainly due to the low temperatures of growing GaN films.

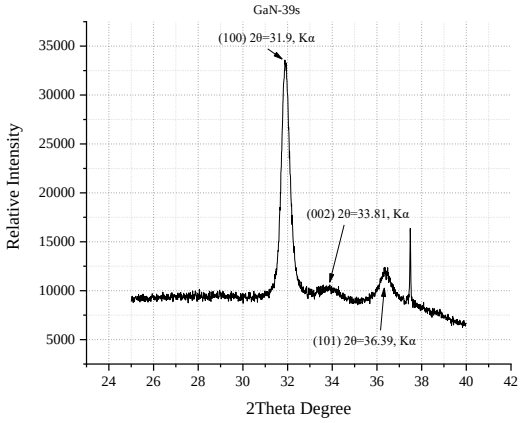

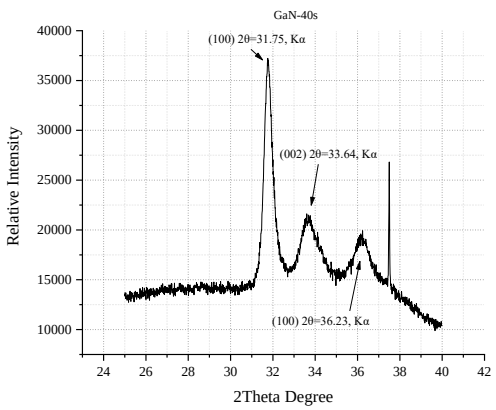

Fig.4 GaN XRD pattern for specimen GaN-39s **Fig.5 GaN XRD pattern for specimen GaN-40s**

4. Conclusion

Research outcomes have shown that stimulation with UV irradiation increases the deposition rate by up to 16%, and most importantly, the results of these studies show that UV exposure improves the structural properties of the deposited material. This was well demonstrated in the case of gallium nitride, when samples obtained at the same temperature, performed better those irradiated with UV rays.

Thus, multifaceted studies have shown that the properties of gallium nitride can be improved using technical and technological innovations. In particular, the inclusion of UV stimulation in reactive magnetron sputtering technology improves the properties of gallium nitride. For other III nitrides materials - aluminum nitride and indium nitride, the improvement of their parameters was not affected by UV exposure.

Acknowledgement:

The work is implemented under the #YS-21-488 project of Shota Rustaveli National Science Foundation of Georgia.

References:

[1] Kushitashvili Z., Bibilashvili A. Mechanism of Processes Stimulated by Ultraviolet Radiation. 6th World Multidisciplinary Earth Sciences Symposium, IOP Conf. Series: Earth and Environmental Science **609** (2020) 012051, doi:10.1088/1755-1315/609/1/012051

[2] Kushitashvili Z., Bibilashvili A., Biyikli N. Properties of Hafnium Oxide Received by Ultra Violet Stimulated Plasma Anodizing. IEEE Transactions on Device and Materials Reliability, Vol. 17, Issue: 4, pp. 667 – 671, December, 2017. DOI: 10.1109/TDMR.2017.2751078

[3] Bibilashvili A., Kushitashvili Z., Skhiladze G. Electrical, Optical and Structural Properties of Titanium Dioxide Dielectric Films Formed by DC Magnetron Sputtering. Nano Studies 2014, Vol. 9, pp.111-114, Decmber, 2014.

[4] Bibilashvili A., Kushitashvili Z. Low Temperature Oxidation of GaAs by UV Stimulated Plasma Anodizing. IOP Conf. Series: Earth and Environmental Science 44 (2016) 032002. DOI: 10.1088/1755-1315/44/3/032002

[5] Bibilashvili A., Kushitashvili Z. C-V Measurement of HfO2 Dielectric Layer Received by UV Stimulated Plasma Anodizing. IOP Conf. Series: Earth and Environmental Science 44 (2016) 052008. DOI: 10.1088/1755-1315/44/5/052008

[6] Kushitashvili Z., Bibilashvili A., Borisenko V. C-V Characterization and Electric Parameters of ZrO2 Received by UV Stimulated Plasma Anodizing. IOP Conf. Series: Earth and Environmental Science. 2019

SMART ENERGY MANAGEMENT IN THE CONTEXT OF INDUSTRY 4.0

N. Kyrtsilas[a], E. Symeonaki[b], D. Tseles[c], M. Papoutsidakis[d], C. Drosos[e]

Dept. of Industrial Design and Production Engineering, University of West Attica, Greece
[a]nkyrtsilas@uniwa.gr, [b]esimeon@uniwa.gr, [c]dtsel@uniwa.gr, [d]mipapou@uniwa.gr, [e]drososx@uniwa.gr,

Abstract. In view of the energy crisis, which is also strongly affected by recent geopolitical developments, energy security and sustainability are more significant than ever. To this end, the Industry 4.0 approach along with cutting-edge technological trends which advance in its context are expected to transform energy management for energy consumption in more efficient and sustainable ways. This paper overviews these Industry 4.0 technological trends which can enable smart energy management and identifies some of the corresponding challenges regarding this issue.

1. Introduction

Energy is a critical factor which considerably defines several elements of human activity and globally affects the economic and social development in general [1]. Taking into account that economic growth is strongly tied to energy consumption [2], the rising economic development in recent decades has led to an exponential demand in energy, which is expected to further increase in the near future, leading to major concerns regarding energy and environmental security [3]. In this context, governments, corporations, and other organizations are urged to prioritize agendas regarding energy security and sustainability in order to bring the energy crisis to a halt. The fourth industrial revolution, known as Industry 4.0 (I4.0), is considered to impact the energy potency through the establishment of digitalized infrastructures. Hence, by adopting the cuttingedge technologies which advance in the context of I4.0, energy management is expected to be transformed into "smart" by effectively metering the power and predicting the demand as well as regulating the distribution and consequently optimizing the grid [4]. This approach enhances consequently energy security with regard to sustainable policies. The main scope of this paper is to overview these I4.0 technological trends of which the integration into the energy sector enables smart energy management and identify some of the corresponding challenges regarding this issue.

2. Smart Energy Management towards the Industry 4.0

Deficiencies in conventional power grids, such as inability to predict the demand, lack in efficiently managing the energy distribution, delay in detection of failures, have urged the advance of smart grids (SG) [5]. The primary goal of the SG is the energy supply through the usage of advanced digital technologies offering a variety of advantages toward reliable, cost-effective, and environmentally safe prospects. In this context, the I4.0 digital technologies enable all SG actors to control their energy needs, consumptions, and costs in real-time [6].

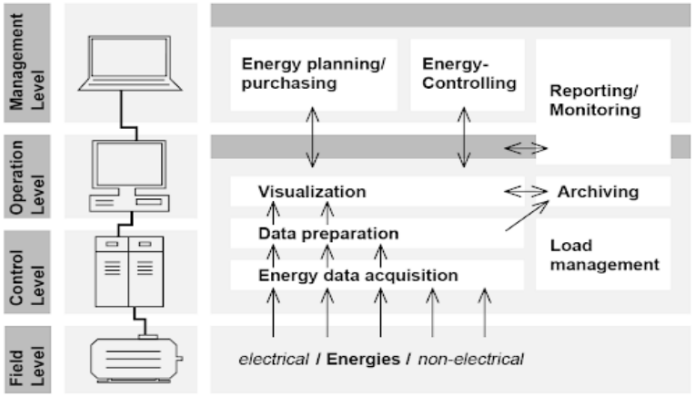

Fig. 1 Smart Energy Management System Architecture [7]

For the implementation of such a corporate policy a multi-level Smart Energy Management System is best to be incorporated, as indicatively shown in Fig. 1 [7]. This results into an energyaware system which through the incorporation of I4.0 technologies is capable of integrating raw energy data into the corresponding industrial processes, performing energy effective and flexible production planning, improving the energy supply and consequently optimizing energy efficiency [8].

3. Industry 4.0 Key Technologies for Smart Energy Management

The key technological trends that are particularly significant for Smart Energy Management, according

to the guidelines for the operative implementation of the Industry 4.0, along with their respective capabilities and probable challenges in the context of sustainability policies, are overviewed as follows:

- *Industrial Internet of Things (IIoT):* The Industrial Internet of Things (IIot) paradigm is considered to be the fundamental enabling technology for effective Smart Energy Management while it is currently associated with the development of the smart grid. In particular, the integration of the IIoT into Smart Energy Management allows the overall supervision and regulation of the smart grid with regard to actual energy and production costs permitting the drawing of directions for further optimization. Nevertheless, the IIoT nfrastructure's growing number of connections among smart devices poses significant challenges towards privacy and security, heterogeneity and data standards, reliable communication protocols, tracking and monitoring as well as performance evaluation, maintenance and optimization.
- *Big Data Analytics*: Big data technologies support data model assessment and enhance data management. Given the growing number of data sources in the smart grid due to the widespread integration of smart interconnected devices, the usage of powerful analytics tools capable of interpreting the accumulated data into useful information are an imperative necessity for successful Smart Energy Management. However, challenges impose regarding a) the identification of unexpected correlations, hidden consumption, market trends, and other useful information, b) reliable storage and retrieval of vast amounts of data with regard to the priority of applications and c) the dependability and safety of intelligent decision-making at the appropriate moment for the appropriate purpose.
- *Blockchain:* The integration of blockchain with the smart grid demonstrates its effectiveness in addressing concerns regarding security and privacy, rewarding and disciplinary systems, as well as standardization. Given that it may be used to create more transparent and secure energy systems that benefit both consumers and producers, the integration of blockchain technology in the smart grid is still a hot research area. Although the blockchain is already being used in industry to organize diversified supplies of renewable energy without the involvement of intermediaries, there are several challenges that need to be addressed, turning this technology a hot spot for both academic research and practical applications in Smart Energy Management.
- *Artificial Intelligence (AI) and Machine Learning (ML):* Approaches that provide advanced solutions for Smart Energy Management, refer to incentive-based demand response models, allowing variable involvement levels depending on the load, utilization of deep learning and reinforcement learning techniques to build a real-time incentive mechanism for the smart grid as well as various incentive mechanisms that can be used for smart energy systems.

Conclusions:

It can be concluded, that a combination of the Industry 4.0 technologies is most significant in order to achieve a high degree of real energy efficiency while maintaining high productivity. As a next step, more particular recommendations for suitable strategies depending on specific system characteristics and influencing parameters should be conducted. As the overviewed technological trends embody various characteristics for efficient energy management systems, future work should also examine the economic and environmental consequences of presented energy flexibility strategies.

References:

[1] Glavič P. (2021). Evolution and current challenges of sustainable consumption and production. Sustainability, 13(16), 9379.
[2] Li F., Song Z., Liu W. China′s energy consumption under the global economic crisi: decomposition and sectoral analysis Energy Policy, 64 (2014), pp. 193-202 3
[3] Kaygusuz K., Bilgen S. Energy related environmental policies in Turkey Energy Sources Part B, 3 (2008), pp. 396-410
[4] Dileep G. A survey on smart grid technologies and applications. Renew. Energy 2020, 146, 2589–2625.
[5] Triantafyllou A., Jimenez J.A.P., Torres, A.D.R., Lagkas T., Rantos K., Sarigiannidis P. The challenges of privacy and access control as key perspectives for the future electric smart grid. IEEE Open J. Commun. Soc. 2020, 1, 1934–1960
[6] Sittón-Candanedo I., Alonso R.S., García Ó., Muñoz L., Rodríguez-González S. Edge computing, IoT and social computing in smart energy scenarios Sensors, 19 (15) (2019), p. 3353
[7] Smart EAM. Energy management according to Industry 4.0 principles. ttps://smarteam.com/news/jenergomenedzhment-po-principam-industry-4-0/
[8] Wu Z., Yang K., Yang J., Cao Y., Gan Y. Energy-efficiency-oriented scheduling in smart manufacturing J. Ambient Intelligence Humanized Comput., 10 (3) (2019), pp. 969-978

ON THE EFFECTIVE DIELECTRIC PERMITTIVITY OF NANOCOMPOSITE STRUCTURES

O. Nakashidze[a], L. Kalandadze[b], N. Gomidze[c], I. Jabnidze[d]

Department of Physics, Batumi Shota Rustaveli State University, Georgia
[a]omar.nakashidze@bsu.edu.ge, [b] lali.kalandadze@bsu.edu.ge, [c]gomidze@bsu.edu.ge,
[d]izolda.jabnidze@bsu.edu.ge

Effective medium methods [1] are widely used to describe the optical properties of nanocomposite structures [2-6]. A nanodispersed structure can be considered as a new homogeneous medium with an effective permittivity ε_{ef}, which has the same optical properties as the given nanodispersed structure. Since the size of nanoparticles and the distance between them is less than the wavelength of light in the medium, it is sufficient to restrict ourselves to the electrostatic approximation to calculate the effective permittivity ε_{ef} of such a medium.

This article considers a multicomponent nanodispersed structure consisting of randomly oriented ellipsoidal nanoparticles in a matrix with a permittivity ε_m.

If the particles have the same ellipsoidal shape and are oriented in the one direction, and the external field E is directed along the direction of one of the main axes of the ellipsoids $i = a, b, c$, then the particles will have the same polarization [2], and the particle polarization coefficient is determined by the formula:

$$\alpha_i = \frac{1}{4\pi}\frac{\varepsilon - \varepsilon_m}{\varepsilon_m + f_i(\varepsilon - \varepsilon_m)}. \tag{1}$$

Where, f_i is the shape factor of the ellipsoid in the direction of one of its principal axes. The formula for calculating the effective permittivity of the medium is written as follows

$$\frac{\varepsilon_{ef} - \varepsilon_m}{\varepsilon_m + f_i(\varepsilon_{ef} - \varepsilon_m)} = \sum q_i \cdot \frac{\varepsilon_i - \varepsilon_m}{\varepsilon_m + f_i(\varepsilon_i - \varepsilon_m)} \tag{2}$$

Formula (2) is a generalized formula for the Maxwell-Garnett effective medium model for a multicomponent nanodispersed medium with anisotropic (ellipsoidal) particles. f_i depends on the ratio of the principal axes of the ellipsoid and is calculated by the integral [4]

$$f_i = \frac{abc}{2}\int_0^\infty \frac{ds}{(s+i^2)\left((s+a^2)(s+b^2)(s+c^2)\right)^{1/2}} \tag{3}$$

The depolarization factors f_a, f_b and f_c satisfy the condition: $f_a + f_b + f_c = 1$. Also, if $a < b < c$, then $f_a > f_b > f_c$.

In the case of a spheroid, $b = c \neq a$ and therefore $f_b = f_c \neq f_a$.

If the nanocomposite medium is an ensemble of nanoparticles with dielectric permittivity ε, in the matrix of permittivity ε_m, then in formula (2) $\varepsilon_i = \varepsilon$, $q_i = q$, therefore, with simple transformations, we obtain the following formula for calculating the effective permittivity:

$$\varepsilon_{ef} = \varepsilon_m\left(1 + \frac{q(\varepsilon - \varepsilon_m)}{\varepsilon_m + f_i(1-q)(\varepsilon - \varepsilon_m)}\right) \tag{4}$$

In the case of randomly oriented ellipsoidal particles, we use the average value of the ellipsoidal polarization in the direction of the principal axes.

$$\bar{\alpha} = \frac{1}{3}\sum \alpha_i = \frac{1}{12\pi}\sum \frac{\varepsilon - \varepsilon_m}{\varepsilon_m + f_i(\varepsilon - \varepsilon_m)} \tag{5}$$

It can be shown that the determination of the average value of the polarization of an ellipsoid is reduced to the introduction of the effective form factor f_{ef}. In this case, the value of f_{ef} must be placed in the interval [0;1] and the relation must be satisfied:

$$\bar{\alpha_i} = \frac{1}{4\pi}\frac{\varepsilon - \varepsilon_m}{\varepsilon_m + f_{ef}(\varepsilon - \varepsilon_m)} = \frac{1}{12\pi}\sum \frac{\varepsilon - \varepsilon_m}{\varepsilon_m + f_i(\varepsilon - \varepsilon_m)} \tag{6}$$

In the case of a spheroidal shape of the particles, from eq. (6) is determined:

$$f_{ef} = \frac{1}{\xi - 1} \cdot \left(\frac{3 \cdot (1 + (\xi - 1)f_a)(1 + (\xi - 1)f_b)}{3 + (\xi - 1)(2f_a + f_b)} - 1 \right) \quad (7)$$

The effective form factor is determined by the relative permittivity of the particle and the medium around the particle $\xi = \boldsymbol{\varepsilon}/\boldsymbol{\varepsilon_m}$ and depends on the ratio of the principal axes of the spheroid $\boldsymbol{\vartheta} = \frac{\boldsymbol{a}}{\boldsymbol{b}}$.

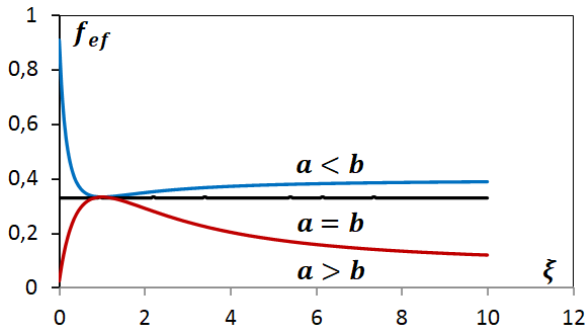

Fig.1. Dependencies of the f_{ef} on the ξ with different ϑ

Fig.1 shows the dependences of the f_{ef} on the ξ with different ϑ: $a > b$, $a = b$ and $a < b$. It can be seen that the value of the effective depolarization factor is always in the range 0-1. This makes it possible to prove that an ensemble of anisotropic nanoparticles can be replaced by an ensemble of nanoparticles with a depolarization coefficient f_{ef} uniformly oriented with respect to the external electric field.

Taking into account the effective depolarization factor, formula (4) is written in the following form:

$$\varepsilon_{ef} = \varepsilon_m \left(1 + \frac{q(\varepsilon - \varepsilon_m)}{\varepsilon_m + f_{ef}(1 - q)(\varepsilon - \varepsilon_m)} \right) \quad (8)$$

From formula (8) for given values of the parameters q, ε and ε_m, when f_{ef} =0, we obtain

$$\varepsilon_{ef} = q\varepsilon + (1 - q)\varepsilon_m, \quad (9)$$

and when $f_{ef} = 1$ we get

$$\frac{1}{\varepsilon_{ef}} = \frac{q}{\varepsilon} + \frac{1 - q}{\varepsilon_m} \quad (10)$$

For any configuration of nanocomposite structures, formulas (9) and (10) determine the minimum and maximum values of the effective dielectric permittivity.

References

[1] Maxwell Garnett, J.C. Colours in metal glasses and in metallic films. Phil. Trans. R. Soc. Lond. A 203 (1904) 385–420.

[2] Petrov Yu.I. Physics of small particles, M., Nauka, 1982, p.360 (in Russian)

[3] Kalandadze L., Nakashidze O. Influence of the size, shape and concentration of magnetic particles on the optical properties of nano-dispersive structures, Journal of Magnetism and Magnetic Materials, V. 500, (2020) https://doi.org/10.1016/j.jmmm.2019.166355

[4] Yunos N.,Khairi T., Khairuddin A.,Shafie S.,Ahmad T., Lionheart W. The depolarization factors for ellipsoids and some of their properties. MJFAS, Malaysian Journal of Fundamental and Applied Sciences Vol. 15, No. 6 (2019) 784-789.

[5] Kalandadze L., Nakashidze O., Gomidze N., Jabnidze I. Influence of the size, shape and concentration of magnetic particles on the optical properties of nano nickel films, J. Nanotechnology Perceptions, V,17 No.3 (2021) 197-203 http://nano-ntp.com/index.php/nano/issue/view/48

[6] Fan D., Tan R., Wei B., Chen P., Zhou J. Broadband microwave absorption performance and theoretical dielectric properties model of hollow porous carbon spheres/expanded polypropylene composite foams, Polymer, Vo. 234, (2021); https://doi.org/10.1016/j.polymer.2021.124262